National Library of Canada
Canadian Theses Service
Ottawa, Canada
K1A 0N4

Bibliothèque nationale du Canada
Service des thèses canadiennes

NOTICE

The quality of this microform is heavily dependent upon the quality of the original thesis submitted for microfilming. Every effort has been made to ensure the highest quality of reproduction possible.

If pages are missing, contact the university which granted the degree.

Some pages may have indistinct print especially if the original pages were typed with a poor typewriter ribbon or if the university sent us an inferior photocopy.

Reproduction in full or in part of this microform is governed by the Canadian Copyright Act, R.S.C. 1970, c. C-30, and subsequent amendments.

AVIS

La qualité de cette microforme dépend grandement de la qualité de la thèse soumise au microfilmage. Nous avons tout fait pour assurer une qualité supérieure de reproduction.

S'il manque des pages, veuillez communiquer avec l'université qui a conféré le grade.

La qualité d'impression de certaines pages peut laisser à désirer, surtout si les pages originales ont été dactylographiées à l'aide d'un ruban usé ou si l'université nous a fait parvenir une photocopie de qualité inférieure.

La reproduction, même partielle, de cette microforme est soumise à la Loi canadienne sur le droit d'auteur, SRC 1970, c. C-30, et ses amendements subséquents.

NL-339 (r. 88/04) c

Canada

Long-Term Deflections Analysis of Reinforced Concrete Flat Plates Under Construction Loads

by

Abdel-Hafid Boussouf

A thesis submitted to
the School of Graduate Studies
in partial fulfillment of the requirements for the
degree of Master of Applied Science
in
Civil Engineering

DEPARTMENT OF CIVIL ENGINEERING
UNIVERSITY OF OTTAWA

© Abdel-Hafid Boussouf, Ottawa, Canada, 1990

National Library of Canada
Bibliothèque nationale du Canada

Canadian Theses Service
Service des thèses canadiennes

Ottawa, Canada
K1A 0N4

The author has granted an irrevocable non-exclusive licence allowing the National Library of Canada to reproduce, loan, distribute or sell copies of his/her thesis by any means and in any form or format, making this thesis available to interested persons.

The author retains ownership of the copyright in his/her thesis. Neither the thesis nor substantial extracts from it may be printed or otherwise reproduced without his/her permission.

L'auteur a accordé une licence irrévocable et non exclusive permettant à la Bibliothèque nationale du Canada de reproduire, prêter, distribuer ou vendre des copies de sa thèse de quelque manière et sous quelque forme que ce soit pour mettre des exemplaires de cette thèse à la disposition des personnes intéressées.

L'auteur conserve la propriété du droit d'auteur qui protège sa thèse. Ni la thèse ni des extraits substantiels de celle-ci ne doivent être imprimés ou autrement reproduits sans son autorisation.

ISBN 0-315-60021-7

Canada

UNIVERSITÉ D'OTTAWA
UNIVERSITY OF OTTAWA

TO MY PARENTS

Abstract

Relatively large construction loads applied to immature slabs with their low elastic moduli will cause large initial elastic deflections. The high applied stress/developed strength ratio will cause significant creep, resulting in large long-term deflections. Shrinkage, while not related to construction loads, also contributes to long-term deflections. Studies reported by many investigators showed that the long-term deflections cannot be ignored in the design process and that the contribution of the effects of the construction loads cannot be ignored. The influence of the construction loads on the long-term deflection serviceability means that the construction process cannot be independent of the design considerations. However, ACI 318 and CSA A23.3, specify maximum span thickness ratios for which deflections need not be considered.

A computer investigation of the long-term deflections for flat plates, of typical dimensions, was effected using a finite element analysis program for several possible load histories. The study indicated that the present span thickness recommendations of ACI 318 and CSA A23.3 would not necessarily prevent excessive deflections. The study also indicates that, in most cases, the code requirement of total deflection not to exceed $l/240$ was critical and could not be met.

Acknowledgements

My thanks are extented to the individuals who made this work possible. My deepest thanks go to my supervisor, Professor N.J. Gardner for his helpful guidance, advice, understanding and encouragement during the preparation of this thesis.

I also wish to acknowledge the efforts of several professors of the Civil Engineering Department for the help, information, and instructions during the course work.

In addition I should like to thank my father, my mother, and my whole family for their incessant encouragement and their great support, as I pursued yet another degree.

The author is thankful to the government of Algeria for providing financial assistance in carrying out this research.

Contents

List of Tables

List of Figures

List of Symbols

A	Triangular element area
A_s	Area of tension steel
A'_s	Area of compression steel
$[B]$	Strain-displacement matrix
c/l	Column width to span ratio
$[C]$	Stress-strain matrix
C_t	Creep coefficient
CF_{SL}	Correction factor for slump of the concrete mix
CF_{SZ}	Size correction factor
CF_{RH}	Correction factor for relative humidity
$[D]$	Stress-strain matrix
f'_c	Compressive strength of concrete
f'_t	Tensile strength of concrete
f_y	Yield stress of the reinforcing steel
$\{F\}_B$	Vector of nadal forces due to body forces
$\{F\}_s$	Vector of nadal forces due to surface tractions
$\{F\}_{\varepsilon_0}$	Vector of nodal forces due to initial strains
$\{F\}_{\sigma_0}$	Vector of nodal forces due to initial stresses
$\{\Delta F\}$	Vector of incremental loads
h	Overall thickness of the slab
I_e	Average effective moment of inertia
$[k]$	Structural stiffness matrix
K_{sh}	Shrinkage deflection coefficient
l	Span length
l_n	Clear span length
l/d	Span to depth ratio
$[N]$	Shape function matrix

$[R]$	Applied nodal forces vector
S	Surface of the finite element
t_s	Smeared thickness
U_e	Strain energy
u, v, w	Displacements in cartesian coordinates
x, y, z	Cartesian coordinates
V	Volume of the finite element
W	Potential energy of the applied loads
β	Ratio of long to short clear spans
β_s	Ratio of length of continuous edges to total perimeter of slab panel
$\{\delta\}$	Displacement field
Δ_{cp}	Additional deflection due to creep
Δ_{cs}	Additional deflection due to creep and shrinkage
Δ_{ic}	Initial deflection based on cracked sections
Δ_{sh}	Additional deflection due to shrinkage
Δ_t	Additional long-time deflection
$\{\epsilon\}$	Strain vector
$\{\epsilon\}_0$	Initial strain vector
ϵ_{sh}	Shrinkage strain at any time t
$(\epsilon_{sh})_u$	Ultimate shrinkage strain
λ_t	Long-term multiplier
λ_c	Immediate + creep multiplier
λ_{sh}	Shrinkage multiplier
ν	Poisson's ratio
$\{\sigma\}$	Stress vector
$\{\sigma_0\}$	Initial stress vector
Π	Total potential energy

Chapter 1

INTRODUCTION

1.1 General

Flat slabs are generally constructed using flying forms and reshores which is a very rapid high quality repetitive construction process. The common construction procedure is to cast concrete onto forms which are, in turn, supported on one or more previously cast floors. As a result, the construction loads in the supporting slabs may appreciably exceed the loads under service conditions. Such loads are dependent on the number of forms, number of reshores, and the sequence of stripping the forms and reshores and cannot be determined by inspection. The order of magnitude of the maximum construction loads has been previously given as 2 to 2.5 times the average self-weight of the slab plus formwork [1,2].

Relatively large construction loads applied to immature slabs with their low elastic moduli and tensile strength will cause extensive flexural cracking and large immediate deflections. The high applied stress/developed strength ra-

tio will cause significant creep, generally non-recoverable, resulting in large long-term deflections. Shrinkage, while not related to construction loads, also contributes to long-term deflections. Due to these excessive deflections, serviceability problems such as cracked partitions, jamming doors and windows, and uneven placement of furniture are a source of concern to owners and other parties involved. In some cases, the visual impact of sagging floors may cause concern for the safety of the structure even if it has adequate strength.

Present procedures contained in the CSA A23.3 M84 [3] and ACI 318-83 [4] codes provide two alternative methods for the control of deflections of two-way slab systems. Deflections may be calculated directly and the magnitudes compared with specified deflection limits. The code requires that deflection computations take into account size and shape of panel, conditions of support, and nature of restraints at panel edges. Alternatively, both CSA A23.3 M84 and ACI 318-83 imply that deflections need not be computed if the slab thickness is greater than a minimum specified value. The selection of the minimum thickness as specified in Section 9.5.3.1 of the American code does not guarantee serviceability and does not give the designer any idea of the magnitude of the final deflection [5]. Gilbert [5] stated that an equation for slab thickness which does not include an allowance for the actual load limit can not insure adequate deflection control. Similar criticism has been voiced by others [6]. Scanlon [7] on the other hand, reported that the code minimum thickness equations are compatible with the maximum permissible deflections using the code criteria for deflection computations.

1.2 Problem Statement

Slabs constructed through shoring procedures in multistory structures are subjected to loads that may exceed the total design service load. Application of these loads often occurs before the slab has reached the specified design strength. The combination of early age loading and reduced concrete material properties may lead to increased cracking and loss of slab stiffness. As a direct result, immediate, as well long-term deflections will increase. The ability to predict these increased long-term deflections including early age loads is required.

1.3 Objective and scope

The main objectives of the present research may be summarized as follows:

1. To study the effects of early age construction loading on flat slab deflections.
2. To identify and evaluate deflections associated with the construction of multistory structures.
3. Evaluate CSA. A23.3 M84 minimum thickness provisions.
4. Recommend changes in the provisions if required.

The present study was confined to the analysis of flat plates. Ten different structures in terms of thickness, span, live load to dead load ratio, and aspect ratio were selected and were loaded under different loading histories to simulate the loads which result from the construction schedule. The

analysis was conducted using an existing finite element computer program called NOPARC (NOnlinear Analysis of Prestressed And Reinforced Concrete structures) to predict the behaviour of the reinforced concrete flat plates.

The scope of the work undertaken in this study consisted of the following:

Chapter 2 describes the different methods of analysis of construction process and the resulting construction loads imposed on slab of multistory structures.

Chapter 3, reviews existing methods dealing with the calculation of the immediate, as well as, the long-term deflections of two-way slab systems with an emphasis on long-term deflections calculation methods.

The finite elements method used for the present study is described in Chapter 4. Chapter 4 also comprises a brief review of the general method of the finite elements, a description of the material models used to derive the constitutive relationships for concrete and steel, and gives a description of the selected finite element along with the general solution algorithm, the solution procedure for time-dependent effects, and the computer program.

The description of the present analysis is given in Chapter 5. In the beginning of Chapter 5, some remarks concerning the tensile strength of the concrete and the methods for shrinkage prediction are given. Alternative expressions for both the tensile strength and shrinkage of th concrete are presented. The second step consists of the validation of the computer program by comparing experimental results with those given by the computer program. Finally, a description of the geometrical and the material properties of the slabs used in this investigation is given.

Chapter 6 presents and discusses the computer simulation results of the analyzed slabs.

Based on the computer simulation results, conclusions and recommendations are given in Chapter 7.

Chapter 2

CONSTRUCTION LOADS ON FLAT SLAB SYSTEMS

2.1 General

The basic objective of the design of a reinforced concrete structure is to ensure that the loads imposed on it are carried safely not only during service but also during the construction process. Uncertainty about the magnitude of floor loads imposed during the period of construction has always concerned designers, especially with recent trends toward shallower members and longer spans and more rapid construction.

A survey by Meyer and Rusch [8] indicates that more buildings collapse during construction than under service loads. As an example, on March 2, 1972, portions of the Skyline Plaza Apartment building in Fairfax County, Va., during construction collapsed resulting in 14 deaths and 34 injured. In a recently published review of this catastrophe, Carino et al.[9] concluded

that the collapse was due to:

- Premature removal of shores,
- Low strength of the unshored concrete floors, and
- Colder than anticipated ambient temperature, which reduced the rate of strength gain of the concrete.

During the construction of multistory flat slab structures fresh slabs are usually supported by several previously cast slabs through a series of forms, shores and reshores known as the supporting assembly. Shoring consists of a system of vertical posts and horizontal longitudinal and transverse members providing uniform support for the formwork and the newly cast slab. Reshores, usually tubular screw props are substituted for shores to free formwork for use at other levels. Removing the shores allows the slab to deflect and carry its own self weight. In Canada, prefabricated flying forms are usually used as the casting surface.

Attention has been given in the last three decades to different ways of determining the load history during construction. Several analytical methods have been developed to estimate construction loads transferred to slabs in the supporting assembly. Some of these methods will be briefly reviewed in this chapter.

2.2 Grundy and Kabaila, 1963

Grundy and Kabaila [1] developed a simplified analytical method to determine the loads imposed on the forms and on the individual slabs in any

systems of forms during construction process. The following assumptions were made:

1. The shores are infinitely rigid in comparison with the slabs in vertical displacement.
2. The shores are spaced close enough to consider the shore reactions as a distributed load.
3. A load applied to the shoring system is distributed between the slabs in proportion to their relative flexural stiffnesses.
4. The effects of creep and shrinkage may be ignored.
5. The foundation is infinitely rigid compared to the stiffness of the slabs.

The analytical results indicated that the maximum load ratios obtained with constant E_c and variable E_c are very close, and hence the error introduced by not modifying the stiffness of each slab in the supporting assembly to account for their different ages is not appreciable.

The loads calculated by the Grundy and Kabaila method carried by the shores and the slabs with three levels of shores, constant elastic modulus for all floors and a construction cycle of 7 days are shown in Fig. 2.1. The maximum load ratio calculated is 2.36, at 42 days (3 cycles), and a converged value of 2.00 for a typical floor. From this analysis, Grundy and Kabaila showed also that, the absolute maximum load ratio actually increases with an increasing number of the shored levels. However, the age of the slab at which these maxima occur also increases. For 2, 3 and 4 levels of shores, the absolute maximum factors were 2.25 at 14 days (2 cycles), 2.36 at 42 days (3 cycles), and 2.43 at 28 days (4 cycles) respectively. In each case, the loads converge on a cycle in which the bottom slab of the shored

system has a load ratio of 2.00. The slab with the absolute maximum loads is always the last slab supported directly from the ground.

2.3 Taylor, 1967

To reduce the loads imposed on a slab during construction, Taylor [10] employed a technique of stripping formwork by slackening and tightening adjustable shores before each new slab is cast. With this method, all shores at one level must be slackened simultaneously, thus requiring greater supervision and inspection.

Using the same assumptions adopted by Grundy and Kabaila, Taylor reported that the maximum load ratio is reduced from 2.35 to a value of 1.44.

In his consideration of the behavior of flat slabs and plates, Taylor showed that cracking of concrete of these structural systems affects slightly the deflection of a floor. Consequently, the stiffness at an early age is dependent mainly on the elastic modulus of the concrete, therefore Taylor endorsed variable values for E.

2.4 Marosszeky, 1972

Marosszeky [11] presented an analytical method for the shoring and reshoring of floors during the construction stage. Basically, the method consists of completely releasing a floor at time (T-1) days after pouring and immediately reshoring it. At this time, the floor carries its self weight plus the weight of the superimposed formwork while all loads imposed during the

construction of the next level are distributed.

It was shown that construction loads using such a system, are considerably less severe than those using undistributed shores and consequently in most cases the structure may be designed for normal working loads. In this analysis, Marosszeky derived a formula to estimate the critical load on a typical floor and can be defined as (1+1/n)D at age T, where n indicates the number of sets of shores used.

In addition to the above method, a rational basis for the evaluation of the severity factor was presented too and a severity factor F was derived at any time T:

$$F = \frac{construction\ load/total\ service\ load}{f_{ct}\ at\ time\ of\ loading/f_{ct}\ at\ 28\ days} \tag{2.1}$$

$$F = \frac{load\ ratio}{tensile\ strength\ ratio} \tag{2.2}$$

where f_{ct} is the concrete tensile strength.

2.5 Agarwal and Gardner, 1974

Form and reshores loads were measured by Agarwal and Gardner [2] over a complete construction cycle for two high-rise flat slab buildings in 1971, to determine the actual load ratios applied to the slabs and shores-reshores during the various construction stages. The field measurements agreed within acceptable accuracy with those predicted by the simplified theory of Grundy and Kabaila and confirmed that, the lower supporting slabs in a shore-reshore construction schedule can be subjected to loads often greater than the design loads of the structure.

Design tables [2,12] were given to determine the permissible shoring schedules for various live load to dead load ratio, rates of construction, types of cement, and ambient temperatures. As reshoring is effective in reducing the maximum loads experienced by the supporting slabs, and that the greater the number of shores, the greater the construction loads applied to the slabs, one level of forms plus reshores was recommended by Agarwal and Gardner.

From the field investigation, an expression was derived by Gardner to estimate load during construction, the following relation was proposed:

$$U_{construction} = 1.1 \times 1.1 \times 1.4 \times LR \times D + \frac{D}{N} \qquad (2.3)$$

where D denotes the slab dead load, LR the load ratio, and N the number of levels of supports-shores and reshores.

This investigation overlapped in time with that of Marosszeky and the theoretical methods are identical.

2.6 Chan, 1984

Chan [13] used the Strudl computer program to calculate the load history which would occur during construction using the preshoring process (Cantor and Rizzi). Cantor and Rizzi [13] proposed a schedule in which the reshores are placed before the shores are removed in an effort to reduce slab deflections. Based on simplified assumptions, Chan carried out a two-dimensional analysis . The shores and forms system considered was a 'flying form' system as shown in Fig. 2.2b and the preshoring practice was adopted in the analysis. The essential stages involved in this analysis are presented in Figs. 2.2a-I through 2.2a-IV.

Fig. 2.3 shows the third floor slab load history using Grundy and Kabaila's shoring system, Gardner's reshoring system and the preshoring method. The load history of slabs constructed using the preshore method lies between the all form system and 1 form plus reshore schedule and does not fulfill the claims of the proposes.

2.7 Sbarounis, 1984

Sbarounis [14] reports that when incorporating the effects of cracking into the load distribution factors for the supporting slabs reduces the previously established maximum load ratios by approximately 10 percent. Both Agarwal and Gardner [2] and Sbarounis account for the construction live load effect by increasing the maximum load carried by the lowest slab in the supporting assembly. Sbarounis recommended additional loads, due to $50\ psf(2394\ Pa)$ live load, of $55/N\ psf(2633/N\ Pa)$ and $35/N\ psf(1676/N\ Pa)$ for uncracked and cracked slabs respectively; where N represents the total number of levels in the supporting assembly.

Sbarounis also recommended the use of the following expressions to estimate the maximum construction dead load:

$$W_n = 2[W_{ss} + \sum W_f(N+1)] \tag{2.4}$$

$$W_L = 50/N\ psf(2394/N\ Pa) \tag{2.5}$$

Or, by an adequate estimation:

$$W_n = 2[W_{SS} + 10\ psf(479\ Pa)] \tag{2.6}$$

where W_{SS} is the weight of one slab, $\sum W_f$ is the sum of the weights of the falsework and W_L is the portion of the construction live load resisted by the lowest slab.

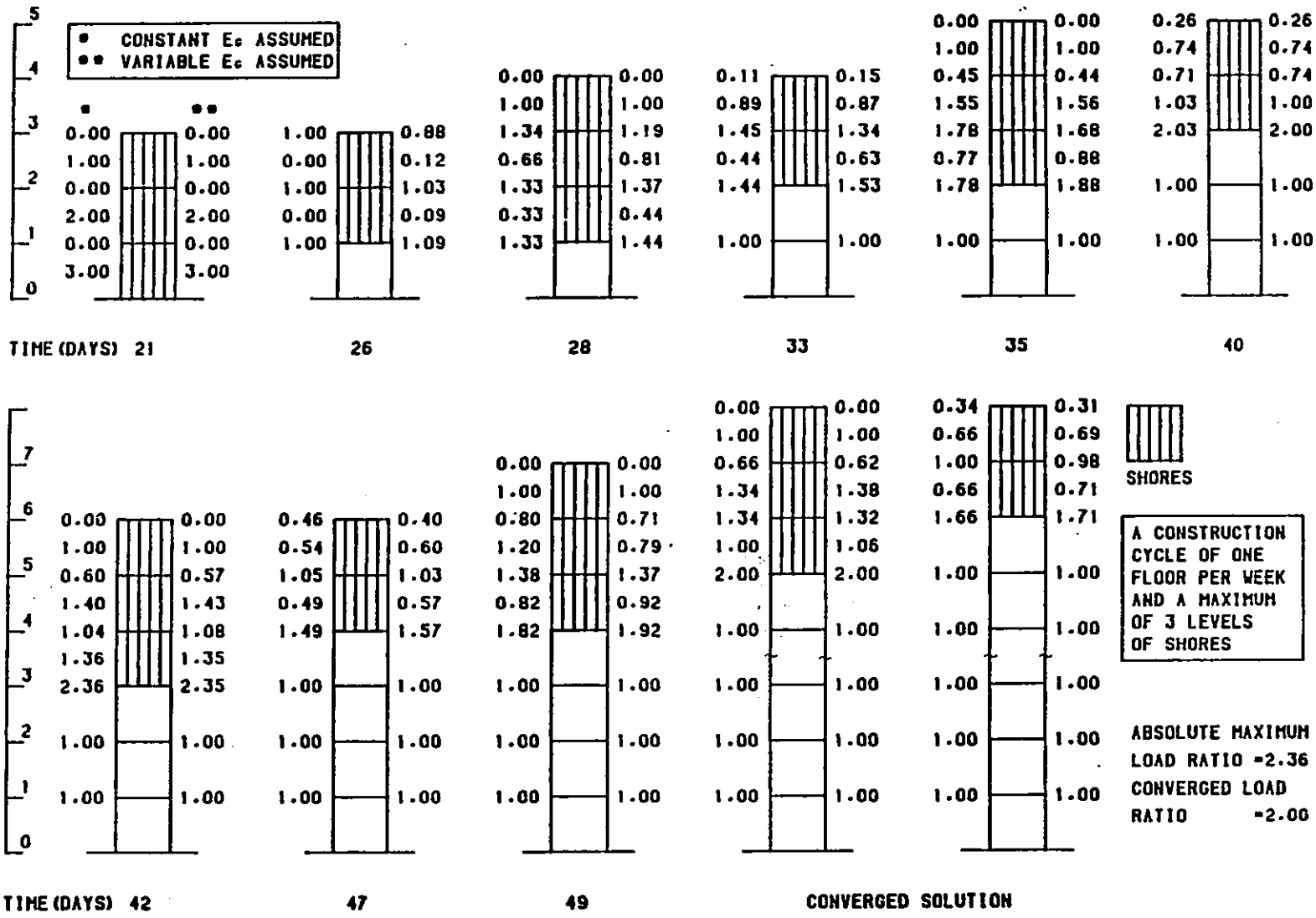

Figure 2.1: Construction Loads with 3 Levels of Shores [1]

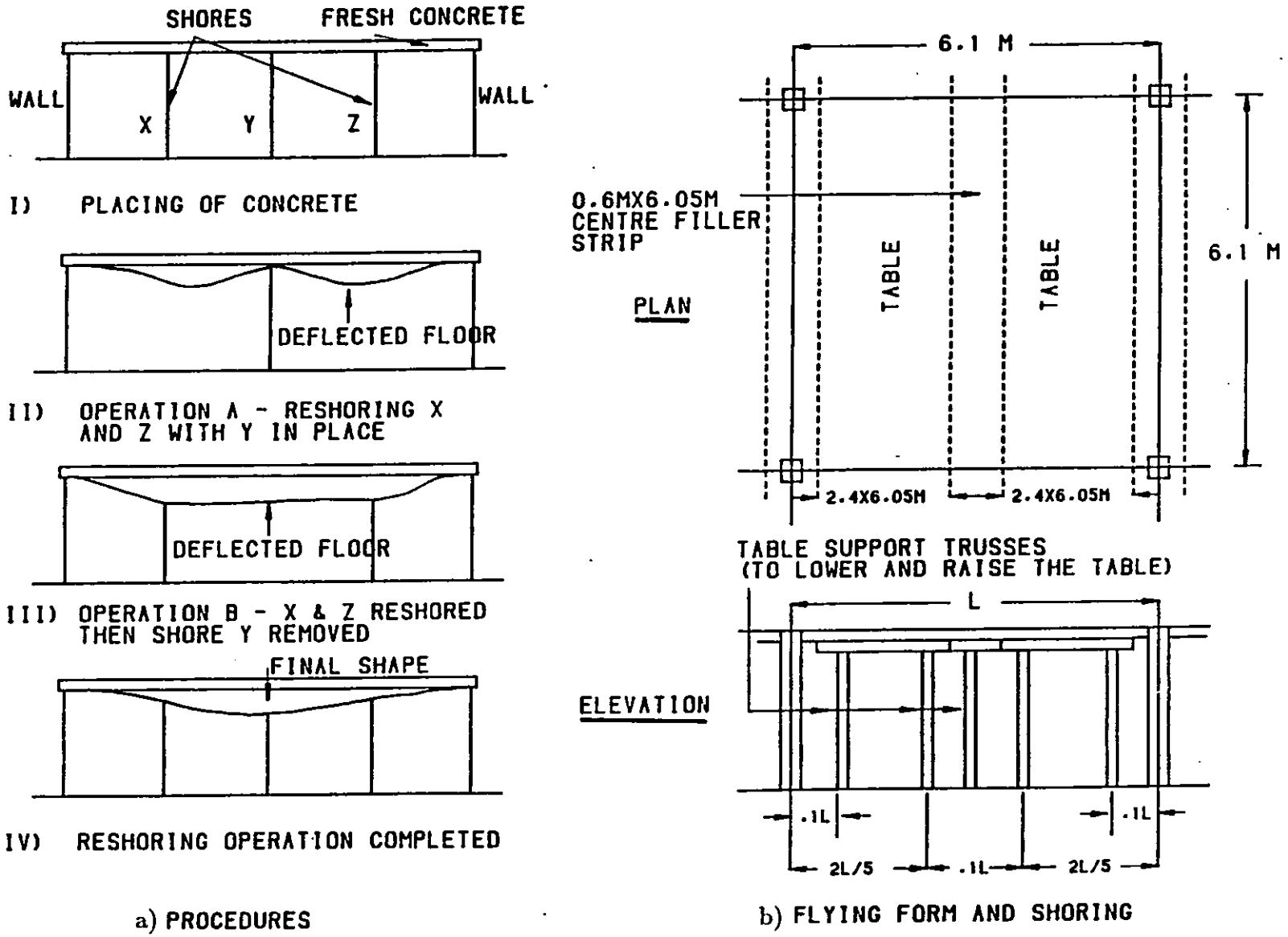

Figure 2.2: Preshoring Technique Representation [13]

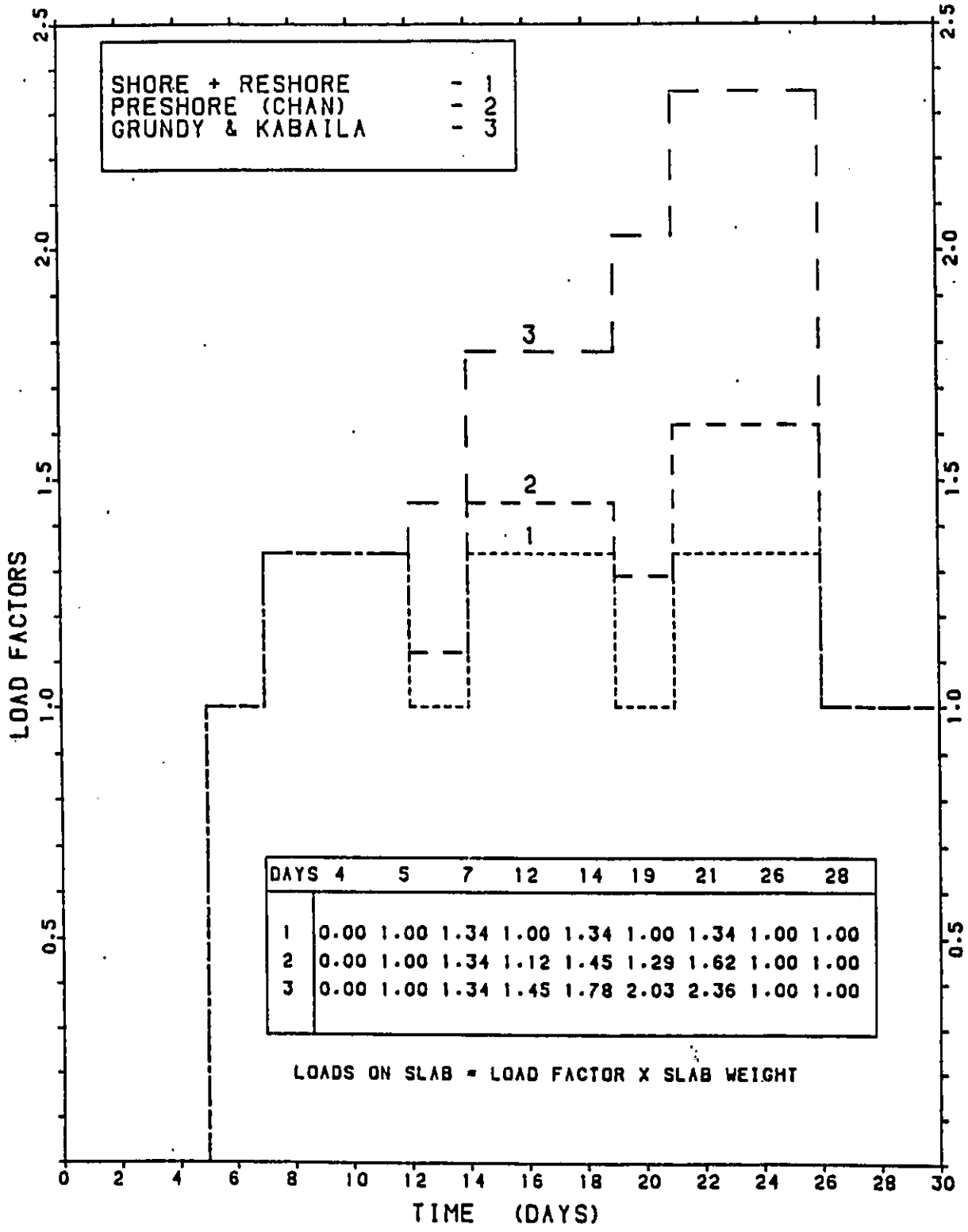

Figure 2.3: Loading Histories on Flat Slab Structures

Chapter 3

DEFLECTIONS OF TWO-WAY REINFORCED CONCRETE SLAB SYSTEMS

Calculation of two-way slab deflections is complicated by the three-dimensional nature of the problem; the less well defined influence of cracking and tension stiffening, and the development of biaxial creep and shrinkage strains create additional difficulties. The following gives a review of available deflection calculation methods. Long-time deflections will be reviewed extensively since the present study is mainly concerned with this type of deflections.

3.1 Immediate Deflections

Both classical and numerical methods can be used to calculate the deflections of a flat plate carrying distributed or concentrated loads. A comprehensive review of the response of slabs with various support conditions and loads is given by Timoshenko and Woinowsky- Krieger [15].
The deflection of a thin, rectangular plate of uniform thickness at a point (X, Y) can be expressed by the following equation:

$$\frac{\partial^4 W}{\partial X^4} + 2\frac{\partial^4 W}{\partial X^2 \partial Y^2} + \frac{\partial^4 W}{\partial Y^4} = \frac{q}{D} \tag{3.1}$$

where,

W = deflection at point (X,Y)
q = transverse load
D = flexural plate rigidity
$= Eh^3/12(1-\nu^2)$
h = plate thickness
ν = Poisson's ratio
E = modulus of elasticity

Theoretical methods of finding solutions to plate problems can be grouped into the following:

- Closed form
- Infinite series
- Energy methods
- Finite differences

- Moment distribution
- Finite element method

One of the greatest difficulties in attempting to determine the deflection of a reinforced concrete slab using Eq. 3.1 is that it is a nonhomogenous structure of two materials which experiences cracking. The problem can be classified as an inelastic, nonlinear analysis of a nonhomogenous anisotropic body. An analysis to determine slab deflections by a direct application of elastic theory is essentially impossible. However, some progress has been made in the development of analytical models for these structures based on finite elements methods.

The basis of the finite element method is the representation of a body or a structure by an assemblage of subdivisions called finite elements. These elements are considered interconnected at joints called nodes. Simple functions called displacement functions are chosen to approximate the distribution or variation of the actual displacements within each finite element. The unknown magnitudes of the displacement functions are the displacements (or the derivatives of the displacements) at the nodal points. Hence, the final solution will yield the approximate displacements at the nodal points.

The complexity of the theoretical methods of analyses of plates has led various investigators to attempt to formulate simple methods of analyses. Some of the popular methods of analyses are described briefly below.

The equivalent frame method is a standard method of two-way slab design in both the CSA A23.3 M84 [3] and ACI 318.83 [4] codes. The structure is divided into continuous frames centered on the column lines in each direction. Each frame is composed of a column strip including any column line beam, and a broad band of slab between panel centerlines.

A method to calculate deflections based on an equivalent frame approach is described by Vanderbilt, Sozen, and Siess [16]. Deflection at the midpanel of an equivalent frame is found as the sum of the centerline deflection of the slab-beam plus the deflection of the beam edge with respect to the centerline plus the additional deflection of the center-panel element.

A more direct application of the equivalent frame method was proposed by Nilson and Walters [17]. This method considers the deflections of a typical panel in one direction at a time, then uses superposition to obtain the final midpanel deflections. Kripanarayanan and Branson [18] extended the method to include the effects of cracking. In calculating deflections, the equivalent frame stiffness is modified by using an average of the effective moments of inertia of the negative and positive moment regions.

More recently, Rangan [19] proposed calculating the midpanel deflection of a flat plate as the sum of the midspan deflections of the column-beam strip (in the long direction) and middle-beam strip (in the short direction). Each strip is considered as a separate beam carrying a uniformly distributed load and applied end moments. Scanlon and Murray [20] proposed a similar procedure, but used an equivalent uniform strip load and actual beam end moments in the deflection calculation. The moments were obtained from an equivalent frame analysis or from the ACI Code direct design method.

The finite element method (FEM) which will be described in section 4.2 provides a more general approach and a more powerful tool for the analysis of reinforced concrete slab systems than the methods mentioned above.

The main problem of the application of the FEM to reinforced concrete is the derivation of a suitable set of constitutive relations to model the slab

behavior under various loading conditions. The response is generally not linearly elastic under all loading conditions. The majority of existing finite elements programs apply only to linear elastic analyses. However Jofriet and McNeice [21], Scanlon [22], and Scanlon and Murray [23] considered the inelastic range by modifying the element stiffness matrices to account for flexural concrete cracking. This approach is known as the "modified EI" approach in which an overall moment-curvature relation reflecting the various stages of material behavior is assumed. Another approach used in the analysis of reinforced concrete slabs is the layer approach which is based on the basic nonlinear stress-strain law and the finite element is divided into imaginary concrete layers. This approach was applied by Hand et al.[24] and Van Greunen [25]. The reinforced concrete section is modelled as a layered system of concrete and "equivalent smeared" steel layers. Perfect bond is assumed to exist between the concrete and bonded steel layers. The stiffness properties of an element are then obtained by integrating the contribution from all the layers in the section. The latter approach is used in the finite element computer program used in the present analysis.

3.2 Long-Time Deflections

Under sustained loads, the deflection of concrete members continue to increase with time, due principally to the effects of creep and shrinkage. The additional long-time deflection may be many times greater than the elastic immediate deflection. The creep and shrinkage deflections are related to structural details, reinforcement ratio, the developed concrete strength, and hence temperature and humidity, and load history.

Fu and Gardner [26] reviewed the literature reporting measured long-term deflections and the results of a detailed laboratory study. Table 3.1 presents

a summary of the published ratios of measured long-term deflection to initial deflection. The summary shows that the long-term deflections are significant and cannot be ignored in the design process and the work of Sbarounis [27], Fu and Gardner [26], and Graham and Scanlon [28] indicates that the contribution of the effects of the construction loads on long-term deflections have to be accounted for when doing time-dependent analysis of slabs. The long-term deflection of a concrete member will include a deflection due to shrinkage of the concrete and the immediate deflections caused by the various dead and live loads plus creep deflections. Long-term deflections may be further increased by temperature differences through the thickness of the slab.

3.2.1 Creep Deflection

Deflection due to creep depends upon the creep characteristics of the concrete, the amount of compressive reinforcement and the amount of cracking that has taken place. As a result of creep under sustained stresses, the compressive strain in the concrete at the extreme fiber increases with time as shown in Fig. 3.1 while the strain in the tension fiber increases only marginally. The creep strains causes an increase in curvature which causes additional deflection of the member.

ACI 209 proposed the following empirical equation for calculating the additional deflection due to creep :

$$\Delta_{cp} = k_r \, C_t \, \Delta_i \tag{3.2}$$

$$k_r = 0.85 - 0.45 \, \frac{A_S'}{A_S} \tag{3.3}$$

where,

Δ_i = immediate deflection

C_t = creep coefficient (Section 4.3.4)

k_r = factor to account for compression steel and neutral axis shift

3.2.2 Deflection due to Shrinkage

In an unrestrained reinforced concrete member, shrinkage causes shortening of the member which is resisted by the reinforcement. When the reinforcement is symmetrically placed in the section, shrinkage does not cause any curvature of the member. However, when the reinforcement is not symmetric, shortening of the reinforced face is far less than that of the unreinforced face (Fig. 3.2). This differential shrinkage causes a curvature of the member. For thin slabs, where compression steel is not usually provided, the differential shrinkage strains magnify considerably the deflections.

Branson and Christianson [29] proposed that the long-term deflection due to shrinkage could be calculated from the following expression:

$$\Delta_{sh} = K_W \phi_{sh} L^2 \tag{3.4}$$

where K_W is a coefficient depending on the boundary restraints, ϕ_{sh} is the shrinkage curvature, and L is the span length.

$$\phi_{sh} = 0.7 \frac{\epsilon_{sh}}{h} (p - p')^{\frac{1}{3}} \sqrt{\frac{p - p'}{p}} \tag{3.5}$$

for $(p - p') \leq 3$ percent

$$\phi_{sh} = \frac{\epsilon_{sh}}{h} \tag{3.6}$$

for $(p - p') > 3$ percent

where,

p = percentage of tension steel
p' = percentage of compression steel
h = slab thickness
ϵ_{sh} = shrinkage strain (section 4.3.3)

In the following, a literature review of the determination of long-term deflections of reinforced concrete slab systems will be given.

3.2.3 Analytical studies

Taylor, 1970

The two methods proposed by Taylor to determine the long-term deflection of flat plates were based on a computed initial elastic deflection, together with a procedure recommended by Branson [30] or a simple multiplier according to Taylor [31].

In the calculation for this plate it has been assumed that the final state of the column strip will be 100% cracked, the cantilever element will be 50% cracked, and the simply- supported plate element will be 50% cracked.

The first method considered creep and shrinkage effects separately. The shrinkage deflection was determined using Branson's procedure (Equations 3.2 and 3.3) and the deflection due to creep was equal to the initial deflection multiplied by a creep factor C_{ct}.

The alternative method proposed by Taylor considered creep and shrinkage

effects together, using multipliers and the following equations presented by Branson:

$$\Delta_t = \Delta_{ic} + \Delta_{cs} \tag{3.7}$$

$$\Delta_{cs} = k_r C_t . \Delta_{ic} \tag{3.8}$$

where $k_r = 1 - 0.6(A'_s/A_s)$ and the value of C_t depends on the average relative humidity and the age of the concrete when loaded.

Scanlon and Murray, 1974

Scanlon and Murray [23] presented a finite element model coupled with a time integration procedure to simulate the behavior of reinforced concrete slabs at working loads, including the effects of nonuniform reinforcement, tensile cracking, shrinkage, and creep.

A rigorious approach to the computation of slab deflections requires a formulation which includes coupling between the membrane and flexural behavior of the plate. However, the analysis developed by Scanlon and Murray considers only flexural behavior and disregarded the requirements of in-plane compatibility.

The model considered the plate to be subdivided into a set of layers, each of which had an instantaneous linear elastic orthotropic constitutive relationship.

A parametric study was carried out to illustrate the application of the proposed method of analysis. The study was restricted to a square interior panel of a flat plate floor system and the effects of the following parameters were considered,

- concrete properties
- loading history
- span to depth (l/d) ratio
- column width to span (c/l) ratio
- reinforcement layout

For an 8-in. thick interior flat plate panel designed in accordance with the direct method of ACI 318-71 Building code and for a (c/l) ratio of 0.1 and a sustained load equal to the design live load, an average ratio of final deflection after 800 days to the initial deflection at 7 days was estimated to be in the range of 3.5 [22].

Rangan, 1976

By considering the deflection at the midpoint of a rectangular panel of a flat plate as the sum of the deflections of a column-beam strip in the long direction and a middle-beam strip in the short direction; Rangan [19], proposed a simple procedure to predict long-term deflections of flat plates and slabs. In the long-term deflection prediction, the column-beam strip is considered to be fully cracked and the middle-beam strip is only partially cracked. Based on Branson's [32] procedure for computing creep and shrinkage deflection and using $C_t = 2.35$ as recommended by ACI Committee 209 [33], the long-term deflection of a flat plate was computed and compared to Taylor's experimental result of a flat plate.

The measured initial and long-term deflections after 850 days of Taylor's

flat plate were 0.11 in. (2.8 mm) and 0.72 in. (18.3mm), giving a final to initial deflection ratio of 6.5. Rangan found the initial deflection to be 0.20 in. (5.0 mm) and the total one to be 0.67 in. (170.0 mm), giving a final to initial deflection ratio of 3.35.

Sbarounis, 1984

Sbarounis [27] proposed a simple procedure to calculate the long-term deflection of multistory flat plate buildings equal to the immediate secant service dead load deflection, δ_{sd} times a simple multiplier:

$$\delta_{Long-term} = \delta_{sd} \times \ Multiplier \tag{3.9}$$

δ_{sd} is given by:

$$\delta_{sd} = \delta'_{max}(\frac{W_{sd}}{W_{max}}) \tag{3.10}$$

$$Multiplier = 1 + 2.8(\frac{C_u}{2.35}) + 1.2(\frac{\epsilon_{shu}}{800}) \tag{3.11}$$

where δ'_{max} is the deflection due to the maximum construction load (W_{max}) when applied as a single increment and W_{sd} is the total service dead load. The quantity δ_{sd} is variable and depends on the maximum construction load and the concrete strength at the time of loading.

The multiplier for creep will range from 1.5 to 4.9 and for shrinkage from 0.6 to 1.6 according to the variation of C_u and ϵ_{shu}. The multipliers and the procedure developed herein are applicable only to multistory structures constructed by supporting the fresh slabs on previously cast floors.

Scanlon and Graham, 1986

Scanlon and Graham [28] used a finite element program SAPIV to perform a parametric study of the deflections in flat slabs including load history and recommended a set of factors to convert immediate deflections to long-term deflections. A reduced modulus of rupture was specified to account for cracking due to shrinkage restraint.

Creep deflection due to incremental loading was calculated using ACI Committee 209 procedures. Total instantaneous plus creep deflection at time t due to the load increments was obtained by summing each individual load increment deflection. To account for irrecoverable creep, the creep deflection due to unloading was multiplied by a factor less than one. Shrinkage deflection was also calculated using ACI Committee 209 recommendations and added to the total instantaneous plus creep deflection.

Based on the parametric study, an alternative simplified method was proposed for design purposes. The procedure involves calculating a maximum deflection Δ_{max} due to construction loads, scaling the deflection down to the sustained load deflection Δ_{sl} by a factor λ_t to obtain the net deflection Δ_t at time t. The recommended multipliers are based on Standard ACI 209 creep and shrinkage values. For any different conditions, the long-term multiplier can be modified using the following equation:

$$\lambda_t = 1 + \lambda_c\left(\frac{C_u}{2.35}\right) + \lambda_{sh}\left(\frac{\epsilon_{sh}}{780 \times 10^{-10}}\right) \tag{3.12}$$

where $\lambda_c = \lambda_{ic} - 1$, λ_{ic} is the immediate plus creep component and λ_{sh} is the shrinkage component.

Based on their investigation and the subsequent parameter study, Scanlon and Graham recommended a set of long-term deflection multipliers, given in Table 3.2.

3.2.4 Measured Deflections

Documentation of field-measured two-way slabs deflection is not extensive. Most recorded data relates to flat slabs and plates constructed in Australia. Although construction materials and procedures may differ from those in North America, these case studies still indicate the extent of two-way slab deflection problems.

ACI Committee 435 prepared a report on observed deflections of reinforced concrete slab systems, and causes of large deflections [34]. The report comprised two distinct parts.

The first part is a summary of published studies on slab deflections. The summary focused on construction practices and materials quality. Comparison of deflections calculated by various methods with actual long-term deflections was made in some cases.

The second part summarized several construction problems and material deficiencies which can contribute to large long-term deflections. A brief review of these case studies will be given herein.

Blakey, 1961

Blakey [35] reported on an experimental lightweight concrete flat plate structure. After a period of 200 days, the ratio of the total deflection to the initial dead load deflections was seven for the center of an interior panel. In a separate investigation, Blakey [36] in 1963 described deflections for an experimental 3.5 in. thick lightweight concrete flat plate, spanning three bays of 9 ft in one direction and three bays of 12 ft in the other, with

cantilevers of 4.5 ft in the long direction. In eight months, loaded only by self weight, the deflections at the center of the interior panel increased by twelve times the initial elastic deflections. Of this measured deflection, 20% was attributed to differential column settlements, 40% to cracking and to local bond slip, and 40% to creep.

The slab was constructed of expanded shale concrete and built outdoors in the summer. It was noted that the slab underwent fluctuating conditions of temperature and relative humidity, and was exposed to direct sunlight during the construction and observation periods.

Taylor,1970

Taylor [31] described long-time deflections for a reinforced concrete flat plate constructed in Sydney, Australia. The longer span-to-depth ratio was 31.0. Ratios of initial (three-day) deflection measurements to those taken 2.5 years later indicate increases of 6.5 to 10 for deflections at the center of four interior panels. It was thought a partial reason for the large multipliers was the high creep and shrinkage characteristics of the concrete used.

Comparison with calculated long-time deflections indicated best results were obtained when creep and shrinkage deflections were considered separately using Branson's procedure [37], thus allowing for cracking in the slab.

Heiman, 1974

The deflections of flexural members in four different buildings in Australia were reported by Heiman [34]. These slab systems consisted of:

1. a flat plate roof in two-story commercial building ($l/h = 31$)
2. a flat slab in a three-story unenclosed car park ($l/h = 36$)
3. a flat plate in a four-story motel and car park ($l/h = 31$)
4. a tapered beam and slab construction in a fifty-story circular high-rise building ($l/h = 21$ for beams)

Deflections measurements were recorded for periods ranging from 2.5 to 8 years.

The first two systems had negligible construction loads as the slabs were propped directly to the ground below or supported on upper level slabs. For system (1) the long-time to initial deflection ratio was 8.7, while for system (2) the ratio ranged from 5.1 to 6.3. Shrinkage deflections were thought to be a major factor in both these structures.

The latter two systems were subjected to heavy construction loads from the subsequent slabs cast above. In addition, the props bearing directly onto the ground in system (3) settled during construction causing additional slab loading and deformation.

Jenkins, 1974

Tests were carried out by Jenkins [38] on a panel on the fourth level of a building comprising five levels of flat plate floor, four bays wide and seven bays long. The column grid was 21 ft 3 $in.$ × 18 ft 10 $in.$ with columns 22 $in.$ × 22 $in.$ and the thickness of the slab was 9 inches. The ratio of one-year dead load deflection to the initial (ten-day) deflection was approximately four. The slab supported heavy construction loads from the above

floor slab and storage of bricks for partition construction which acted as preload.

Sbarounis, 1984

Slab deflections were recorded by Sbarounis [39] in a multistory flat plate building at 175 bays on 13 floors of the upper part of the structure one year after casting. Lateral force resistance of the flat plate was assured by shear walls and a stiff system of beams and closely spaced wide columns. The center-to-center slab spans were 21.6 and 22.4 ft (6.6 to 6.8 m) and an average thickness of 7.25 in. (184 mm).

The net measured one-year deflections on the 13 alternating floors, ranged from 0.53 to 2.16 in. (13.5 to 54.9 m). They averaged 1.35 in. (34.3 mm) with a standard deviation of 0.29 in. (7.4 mm) and a coefficient of variation of 12%. In 90% of the cases deflections exceeded 1 in. (25.4 mm) and in 10% of the case exceeded 1.72 in. (43.7 mm).

The calculated deflection for the 7.25 in. (184 mm) slab loaded to the service dead loads of 87 psf (4166 Pa) at a 28-day strength of 4000 psi was 0.21 in. (5.3 mm).

Long-time deflections were calculated using the procedures developed previously and assuming a one-year multiplier of 4.2 [27] and were in good agreement with averaged measured one-year deflections.

Fu and Gardner, 1985

Five nominally identical simple span one-way slabs were tested by Fu and Gardner [26]. The slabs were subjected to different load histories and the resulting deflections measured. The load histories were modelled to represent different construction methods. All slabs were designed for a live load/dead load ratio of 0.5. All the slabs had a width of 8 in. (203 mm), were 2.5 in. (63.5 mm) deep and spanned 77 in. (1960 mm).

Only the mid-span deflections of the tested slabs were measured under load. After the formwork was stripped, measurements were made every day for the first month and then weekly afterwards. The time-dependent deflections were significant and of the order of 5 to 7 times the immediate deflections.

Based on their experimental investigation, Fu and Gardner derived a method to determine the total long-term deflection of one-way slabs in terms of the peak construction load relative to the slab strength. The multipliers obtained were similar but larger than those given by Sbarounis [27].

3.3 Effects of Concrete Cracking

The deflection of reinforced concrete slabs is influenced greatly by the degree and distribution of cracking. Cracking may occur in slab members due to restraint of shrinkage as well as flexure resulting from the applied loads.

The effect of cracking in slabs, as in beams, is to reduce the flexural stiffness of the member and thus to increase the deflection. Although most cracking occurs around panel supports, extensive cracking may also develop in the

midpanel regions. Prior to cracking, deflections are computed using the moment of inertia of the gross concrete cross section. At the cracks, the moment of inertia is reduced, but the concrete between cracks continues to have a stiffening influence, and use of the cracked transformed moment of inertia overestimates the computed slab deflections.

For simple-span beams, Branson [30] recommended use of an average effective moment of inertia for the entire length of a span:

$$I_e = (\frac{M_{cr}}{M_a})^3 I_g + [1 - (\frac{M_{cr}}{M_a})^3] I_{cr} \leq I_g \tag{3.13}$$

where,

I_g = gross moment of inertia
I_{cr} = fully cracked moment of inertia
M_{cr} = cracking moment
M_a = maximum bending moment in the span

Although Eq. 3.13 was derived on the basis of tests on simple and continous rectangular beams and simple T-beams, its use for two-way slab systems is permitted under the ACI code specifications [4].

3.4 Code Requirements for Deflections

The present Code limitations for deflections of two-way slabs are based on minimum thickness requirements. Both CSA A23.3 M84 and ACI 318-83 Codes provide similar minimum thickness equations that take into account

the size and shape of the panel, the conditions of support, the nature of restraints at the panel edges, and grade of reinforcement. For slabs without beams, the controlling minimum thickness relation is a function of only clear span and reinforcement grade.

If a slab meets the minimum thickness requirements, then deflections need not be computed. For smaller slab thickness, computed deflections must not exceed specified limits. These limits pertain to immediate live load deflection and long-time deflection occuring after the attachment of non-structural elements due to all sustained loads, plus immediate deflection due to any additional live load.

There are no separate provisions concerning the effects of construction loads at early age. Maximum construction loads may be higher than the total service loads that are used to check the serviceability limits specified in the code. This may lead to unsatisfactory deflections in slabs otherwise meeting code requirements.

Table 3.1: Summary of Long-term Deflection Terms [26]

Source	Year	Age of initial deflection	Age of final deflection	Long-term to short-term deflection ratio
Washa	1947	28 days	5 years	3.9
CSIRO	1961	10 days	8 months	12
Taylor and Heiman	1970	14 days	2.5 years	6 - 8
Taylor	1971	56 days	1 year	3.9
			3.5 years	6.3
			8 years	6.7
Heiman and Taylor	1972	17 days	610 days	2.2
			3.5 years	2.5
Jenkins	1972	10 days	1 year	2.6
Yamamato	1982	1-28 days	112 days	4.4 - 6.4
Sbarounis	1984		1 year	4.2 - 6.4
Jokinen and Scanlon	1987	7 days	1 year	2.5

Table 3.2: Recommended one-year and ultimate multiplier [28]

Assumed modulus of rupture for calculation of immediate deflection	One-year multipliers			Ultimate multipliers		
	λ_{ic}	λ_{sh}	λ_t	λ_{ic}	λ_{sh}	λ_t
$f_r = 0.6\sqrt{f'_c}$ Mpa						
- full creep recovery	2.05	1.65	3.70	2.25	1.75	4.00
- one-half creep recovery	2.60	1.65	4.25	3.00	1.75	4.75
$f_r = 0.32\sqrt{f'_c}$ Mpa						
- full creep recovery	1.80	0.70	2.50	2.00	0.75	2.75
- one-half creep recovery	2.30	0.70	3.00	2.50	0.75	3.25

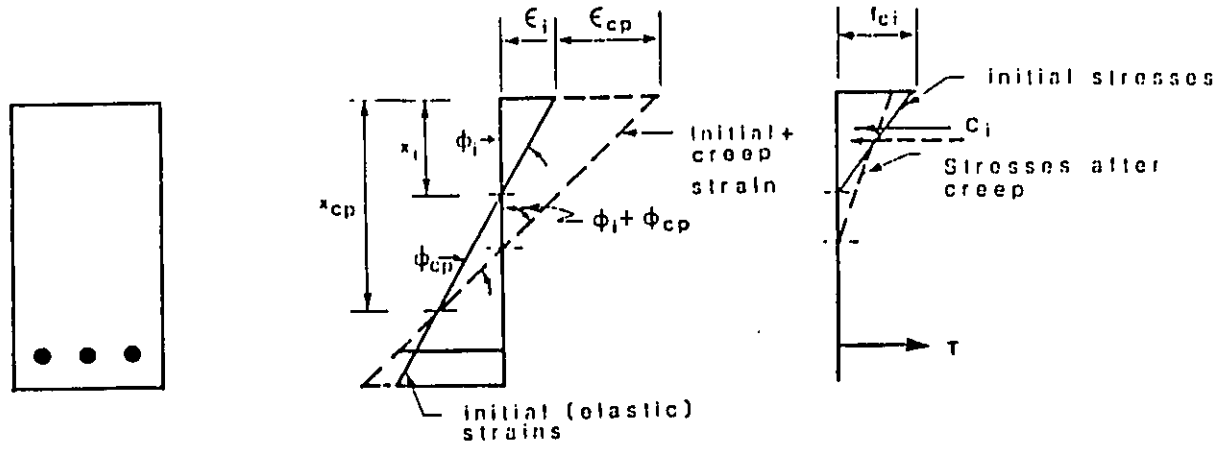

(a) Section (b) Strains (b) Stresses

Figure 3.1: Creep Strain and Curvature

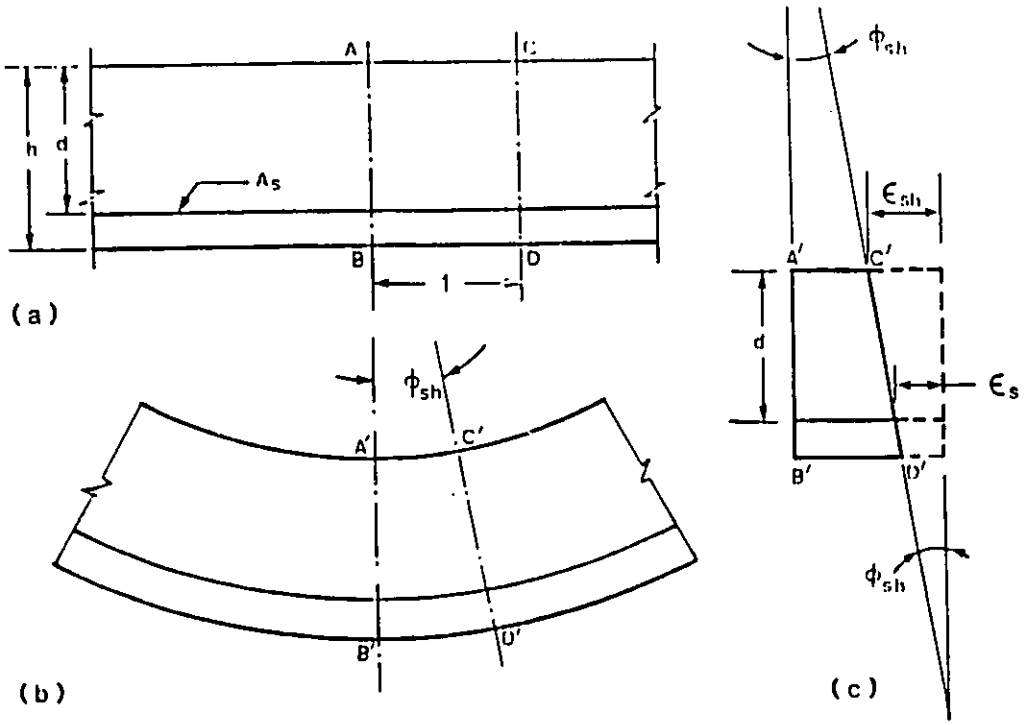

Figure 3.2: Shrinkage Curvature

Chapter 4

FINITE ELEMENT ANALYSIS

4.1 General

The finite element method (FEM) is a numerical procedure for solving a continuum mechanics problem with an accuracy acceptable to engineers. The FEM has gained universal acceptance and is today the most important and versatile method available for the analysis of structures. Several texts [40,41] have been written about the method, therefore only a highlighting description will be given here along with a brief review of the FEM used to perform the present analysis and the development of the computer program.

4.2 Description of the Method

The concept of the FEM stems from the idea of discretization and numerical approximation. The FEM is a technique for analyzing complicated structures by dividing the continuum into a number of small elements. These elements are considered interconnected at joints which are called nodes or nodal points, this is the first approximation. The second approximation is that the elements are deemed to be able to represent the general behavior of the structure between the nodal points.

4.2.1 Basic Equations

To accomplish the second approximation mentioned above, the displacement field u within an element is approximated by a set of shape functions N, which are choosen to reflect the deformation patterns within an element as follows:

$$\{u\} = [N]\{\delta\} \tag{4.1}$$

where $\{\delta\}$ is the elements nodal displacements vector.
The strain displacement relationship can be expressed as follows:

$$\{\epsilon\} = [L]\{u\} \tag{4.2}$$

where $[L]$ is a suitable linear operator.
Substituting Eq. 4.1 into Eq. 4.2 yields

$$\{\epsilon\} = [B]\{\delta\} \tag{4.3}$$

where $[B] = [L][N]$ represents the strain-displacement matrix.
The stresses at the nodes are related to the strains at the nodes by the stress-strain matrix $[D]$ known as the constitutive matrix as:

$$\{\sigma\} = [D](\{\epsilon\} - \{\epsilon_0\}) + \{\sigma_0\} \tag{4.4}$$

where,

$\{\epsilon_0\}$ = initial strain vector

$\{\sigma_0\}$ = initial stress vector

The total potential energy of an elastic system, can be written as:

$$\Pi = U_e + W \tag{4.5}$$

where U_e is the strain energy and W is the potential energy of the applied loads.

The strain energy stored in the body is given by:

$$U_e = \frac{1}{2}\int_V \epsilon^T \sigma \, dV \tag{4.6}$$

The work done by the applied loads which is the negative of their potential energy can be separated into three parts: that which is due to the concentrated loads, R, that which results from surface tractions, T, and that which is done by the body forces, P.

Therefore, Eq. 4.5 can be rewritten as:

$$\Pi = \frac{1}{2}\int_V \epsilon^T \sigma \, dV - \int_V u^T P dV - \int_S u^T T dS - \{\delta\}^T \{R\} \tag{4.7}$$

The combination of Eqs. 4.3 and 4.4 and the minimization of the total potential energy by using Ritz procedure ($\partial\Pi/\partial\{\delta\} = 0$) yield:

$$[K]\{\delta\} = \{F\}_S + \{F\}_B + \{F\}_{\epsilon_0} + \{F\}_{\sigma_0} + \{R\} \tag{4.8}$$

where,

$$
\begin{aligned}
[K] &= \textstyle\sum_e \int_V [B]^T [D][B] dV \\
&= \text{structural stiffness matrix} \\
\{F\}_S &= \textstyle\sum_e \int_S [N]^T \{T\} dS \\
&= \text{nodal force vector due to surface tractions} \\
\{F\}_B &= \textstyle\sum_e \int_V [N]^T \{P\} dV \\
&= \text{nodal force vector due to body forces} \\
\{F\}_{\epsilon_0} &= \textstyle\sum_e \int_V [B]^T [D] \{\epsilon_0\} dV \\
&= \text{nodal force vector due to initial strains} \\
\{F\}_{\sigma_0} &= \textstyle\sum_e \int_V [B]^T \{\sigma_0\} dV \\
&= \text{nodal force vector due to initial stresses} \\
\{R\} &= \text{applied nodal force vector}
\end{aligned}
$$

In the above P and T represent the vectors of body forces and surface tractions respectively.

4.2.2 Element Types

A structure can be modelled by using one-, two-, or three-dimensional elements or a combination of these elements.

One-dimensional Elements

A one-dimensional element may be represented by a straight line whose ends are nodal points. This type of element is used for structures that can be idealized by line drawings, such as trusses and frames. Fig. 4.1a shows a bar element which can take only axial tension or compression, therefore it has one degree of freedom at each node. Fig. 4.1b shows a beam element,

it possesses bending strength as well as axial strength, hence it has 6 DOF per node.

Two-Dimensional Elements

Two-dimensional elements connect three or more nonlinear nodes. If the nodes are allowed to have only displacements in their plane, the element is termed a membrane element. It has 2 DOF (u, v) at each node, as shown in Fig. 4.2a. Alternatively, the element may be used to simulate plate bending action by specifying 3 DOF (w, θ_x, θ_y) at each node as shown in Fig. 4.2b. Membrane actions and flexural actions can be combined to obtain a flat shell element with 5 DOF at each node as shown in Fig. 4.2c. The common types of two-dimensional elements are the triangular and rectangular shapes.

Three-Dimensional Elements

Three-dimensional solid elements connect four or more nodes. Typical solid elements can be grouped under tetrahedron, triangular prism and hexahedron family elements and they are shown in Fig. 4.3. This type of elements is used to solve practical problems where three-dimensional stress analysis is required such as openings in pressure vessels, pipe intersections, stress distribution in soils and rocks, concrete dams etc..

4.3 Material Modelling

4.3.1 General

Concrete exhibits a pronounced nonlinear behaviour at high stress levels, and its response differs markedly to compression and tension. The low tensile strength and cracking of concrete is one of the major factors causing nonlinear behavior of the reinforced concrete composite. In addition to this nonlinearity, concrete properties also depend on its age and enviromental factors like ambient humidity and temperature. This leads to creep and shrinkage of concrete which can in some cases be of major importance in assessing the behavior of a structure over its lifetime. Reinforcing steel can be considered homogeneous material with well defined properties which can be modelled satisfactorily with simple models.

4.3.2 Concrete

In a detailed review of concrete subjected to biaxial stress states Kupfer et al.[42] presented experimental data for a complete range of stress combinations. These investigators concluded that the strength of concrete subjected to biaxial compression may be as much as 27 % higher than the uniaxial strength. The concrete ductility at maximum compressive strength also increases as shown in Fig. 4.4. In Figs. 4.5 to 4.7 stress-strain curves for specimen tested at different constant principal stress ratios are shown.

Based on these experimental results, it has been established that concrete behaves as an orthotropic material in the two principal stress directions,

and this is the assumption made for the concrete model. For an orthotropic material, the incremental constitutive relationship referred to the principal axes 1 and 2 can be written as:

$$\begin{Bmatrix} d\sigma_1 \\ d\sigma_2 \\ d\tau_{12} \end{Bmatrix} = \frac{1}{(1-\nu^2)} \begin{bmatrix} E_1 & \nu\sqrt{E_1 E_2} & 0 \\ \nu\sqrt{E_1 E_2} & E_2 & 0 \\ 0 & 0 & (1-\nu^2)G' \end{bmatrix} \begin{Bmatrix} d\epsilon_1 \\ d\epsilon_2 \\ d\gamma_{12} \end{Bmatrix} \quad (4.9)$$

where G' is the shear modulus under plane stress, and ν is the effective Poisson's ratio under biaxial stress.

While no experimental work has successfully determined the value of the shear modulus under a state of biaxial stress, the following value for G' has been proposed [43]:

$$G' = \frac{1}{4(1-\nu^2)}(E_1 + E_2 - 2\nu\sqrt{E_1 E_2}) \quad (4.10)$$

The value of ν is obtained from experiments and varies from 0.15 to 0.2 below the elastic limit. At a stress level higher than 80% of the ultimate stress an increase in values is observed.

The tangent moduli, E_1 and E_2, are determined from curves similar to the uniaxial stress-strain curve for plain concrete and a concept of "equivalent uniaxial strain" was developed . The technique involves the separation of the Poisson effect from those facets of the stress-strain behavior of concrete that may be attributed to the biaxial strength envelope shown in Fig. 4.8.

A typical equivalent uniaxial stress-strain relation based on an equation suggested by Saenz [44] is shown in Fig. 4.9. The constitutive relationship for the compression part of the curve is given by:

$$\sigma_i = \frac{E_0 \epsilon_{iu}}{1 + (E_0/E_s - 2)\epsilon_{iu}/\epsilon_{ic} + (\epsilon_{iu}/\epsilon_{ic})^2} \quad (4.11)$$

in which E_0 is the initial tangent modulus; $E_s = \sigma_{ic}/\epsilon_{ic}$ is the secant modulus at the point of maximum compressive stress σ_{ic}; and ϵ_{ic} and ϵ_{iu} are the equivalent uniaxial strains at the maximum compressive stress and in the principal direction i respectively.

For tension the relationship is:

$$\sigma_i = E_0 \epsilon_{iu} \qquad for\ \sigma_i \leq \sigma_{it} \tag{4.12}$$

where σ_{it} is the tensile strength of the concrete in the principal stress direction.

Detailed information on how the equivalent uniaxial stress-strain curves are constructed, and subsequently the stress-strain curve after peak stress and the way in which stress reversals are handled is given in [25]. Five material properties of concrete are needed to construct the equivalent uniaxial stress-strain curves. These are (1) uniaxial initial tangent modulus, E_0; (2) uniaxial compressive strength, f_c'; (3) strain corresponding to f_c', ϵ_c; (4) uniaxial tensile strength, f_t'; and (5) Poisson's ratio, ν.

All these parameters can be obtained from uniaxial load tests on concrete. In cases where experimental data are not available, one can use the expressions recommended by different ACI Committees.

Assuming moist-cured concrete (normal or lightweight) using typeI cement, ACI Committee 209 [33] recommends the following expressions at any time t:

$$f_c'(t) = \frac{t}{4.0 + 0.85t} f_c'(28) \tag{4.13}$$

$$f_t'(t) = 0.65\sqrt{W f_c'(t)} \tag{4.14}$$

$$E_0(t) = 33.0 W^{1.5} \sqrt{f_c'(t)} \tag{4.15}$$

where,

$f_c'(28)$ = 28 day uniaxial compressive strength in psi
$f_c'(t)$ = uniaxial compressive strength in psi
$f_t'(t)$ = tensile strength in psi (represented by the modulus of rupture)
$E_0(t)$ = initial uniaxial tangent modulus in psi
W = unit weight of concrete in pcf
t = time in days since casting

The strain corresponding to peak uniaxial compressive stress is given by Hognestad:

$$\epsilon_c(t) = \frac{2f_c'(t)}{E_0(t)} \tag{4.16}$$

Poisson's ratio for concrete is taken to be 0.15, although at a stress level higher than $0.8f_c'$, higher values are observed [42].

Unloading in Concrete

Unloading or stress reversal occurs during the time-dependent analysis due to the effects of creep and shrinkage or load history. Darwin et al.[43] proposed the use of the initial tangent modulus E_0 for unloading before reaching the maximum compressive stress. The unloading in concrete model adopted in this study is based on this assumption. Extensive details on how this approach is used are given in [25].

Cracking and Tension Stiffening

The tensile weakness of concrete and the resulting cracking is a major factor contributing to the nonlinear behavior of reinforced concrete elements. When it is subjected to a net tensile stress, concrete behaves as a linear elastic-brittle material.

When a principal stress exceeds the uniaxial tensile strength of concrete, it is assumed that a crack is formed perpendicular to this principal direction (direction 1 for instance). The modulus of elasticity in that direction is set to zero and the constitutive relationship in Eq. 4.9 reduces to:

$$\begin{Bmatrix} d\sigma_1 \\ d\sigma_2 \\ d\tau_{12} \end{Bmatrix} = \frac{1}{(1-\nu^2)} \begin{bmatrix} 0 & 0 & 0 \\ 0 & E_2/(1-\nu^2) & 0 \\ 0 & 0 & \beta G' \end{bmatrix} \begin{Bmatrix} d\epsilon_1 \\ d\epsilon_2 \\ d\gamma_{12} \end{Bmatrix} \qquad (4.17)$$

where $\beta\,(0.0 \leq \beta \leq 1.0)$ is a cracked shear constant introduced by Lin [45] to provide a way of estimating the effective shear modulus after cracking. The physical situation in the vicinity of a crack is illustrated in Fig. 4.10. As the concrete reaches its tensile strength, primary cracks form. The full load is transferred over the crack by the reinforcement. The concrete between the cracks, however, still carries some tensile stress due to the bond between the concrete and the steel. This is called the tension stiffening effect. As the load increases the bond between the steel and the concrete will deteriorate and the tensile stress will drop.

The tension stiffening has been represented by using two procedures. In one case, the tension portion of the concrete stress-strain curve has been given a descending branch. This has been introduced in different ways by Scanlon [22] and Lin [45] as shown in Fig. 4.11. The second method is to ignore the concrete between the cracks and use an increased stiffness for the steel. The relative effects of different representations for tension stiffening

have been studied by Van Greunen [25].

4.3.3 Shrinkage

Shrinkage of concrete is defined as the volume changes which occur independently of externally applied stresses and of temperature changes. Shrinkage may lead to increased cracking which is very difficult to prevent in some cases. In order to predict whether shrinkage cracking will occur, and how to adopt a thorough design to prevent it from happening, it is necessary to understand the mechanism of shrinkage.

Shrinkage arises mainly from two causes: loss of water on drying and volume changes due to carbonation. The latter phenomenon is a physico-chemical reaction involving cement hydration in presence of atmospheric carbon dioxide and of moisture. Carbonation shrinkage is not separated from drying shrinkage and most experimental data on drying shrinkage includes this effect. Drying shrinkage occurs due to the loss of water from the concrete to the surrounding unsaturated air. A part of this movement is irreversible and should be distinguished from the reversible part (moisture movement). The surface dries more rapidly than the interior causing nonuniform distribution of shrinkage through the volume, this is known as differential shrinkage.

The factors which influence shrinkage are generally taken to be the water content, relative humidity, size of the member and aggregate content. Shrinkage increases with the increase in water content, while it decreases for any increase in the ambient relative humidity, the size of the member and the aggregate content.

The shrinkage strain at any time t can be found from experimental curves or from ACI Committee 209 [33] recommendations.

According to ACI Committee 209, shrinkage at time t, measured from the start of drying t_0, is expressed as follows:

$$\epsilon_{sh}(t) = K_s K_h K_H \frac{(t-t_0)^e}{f+(t-t_0)^e} \epsilon_{shu} \tag{4.18}$$

where,

ϵ_{shu} = ultimate shrinkage strain
f, e = constants, determined from experiments
K_s = correction factor for slump of the concrete mix
K_h = correction factor for the size of the concrete member
K_H = correction factor for relative humidity

The ranges for c, f and ϵ_{shu} for normal or lightweight concrete and for moist or steam curing have been found to be:

ϵ_{shu} = 415×10^{-6} *to* 1070×10^{-6}in/in
e = 0.9 to 1.10
f = 20 to 130

Shrinkage at any time after age 7 days for moist cured concrete:

$$\epsilon_{shu} = K_s K_h K_H \frac{(t-7)}{35+(t-7)} 800 \times 10^{-6} \tag{4.19}$$

Shrinkage at any time after age 1-3 days for steam cured concrete:

$$\epsilon_{shu} = K_s K_h K_H \frac{(t-3)}{55+(t-3)} 730 \times 10^{-6} \tag{4.20}$$

To account for any variation in field conditions, correction factors are introduced and are shown graphically in Fig. 4.12.

Slump correction factor K_s:

$$K_s = 0.89 + 0.041S \tag{4.21}$$

where, S is the slump in inches.

Size correction factor K_h: use curve of Fig. 4.12b

Humidity correction factor K_H:

$$K_H = 1.4 - 0.01H 40 \leq H \leq 80 \tag{4.22}$$

$$K_H = 3.0 - 0.03H 80 \leq H \leq 100 \tag{4.23}$$

where, H is the ambient relative humidity in percent.

4.3.4 Creep

Creep can be defined as the increase in strain under sustained stress and, creep has in the past been referred to also as flow, plastic flow, plastic yield, plastic deformation, many of these terms arising from imperfect understanding of the nature of the phenomenon. A thorough understanding of the phenomenon of creep, leading to an ability to model it analytically is essential.

Several theories have been proposed to explain the mechanism of creep, but no theory has been capable of explaining all the major aspects of creep. These theories can be broadly classified as: mechanical defformation theory [46], plastic theories [47], viscous flow theories [48] and a theory based on

the seepage of gel water [49].

Several factors influence the creep of concrete. The major parameters have been identified as [50]: creep deformation is inversly proportional to the strength of concrete, the age of concrete at loading, the volume (maximum size, grading, shape) and modulus of elasticity of aggregate, the relative humidity, the ambient temperature, the thickness of the specimen, and the finess of cement. Finally, the creep deformation is directly proportional to the duration of the applied stress in an asymptotic fashion.

The quantitative determination of these factors is essentially a statistical problem as the experimental results are inherently random variables with coefficients of variation of the order of 15 to 20 percent at best [33]. However, solutions to date have been primarily deterministic in nature. Moreover, they only attempt to establish correlations between computed results and the behavior of actual structures. The correspondence between laboratory and field conditions are not yet well established.

Analytical Models

The different analytical models to represent creep can be divided into approximate methods, a differential formulation and an integral formulation. Approximate methods like the effective modulus (EMM) and rate of creep methods (RCM) were developed as simplified design methods. The differential formulation has been used, but numerical problems with implementation, have restricted its use. The integral formulation has been the most promising method and it is used in this investigation. The model, as described by Van Greunen [25], utilizes a set of state variables containing the stress history and takes into account under biaxial stress, age of the concrete, duration of loading, and temperature variations.

Creep under Biaxial Stress

The ratio of lateral creep strain to the creep strain in the direction of the applied stress is called the creep Poisson's ratio. Experimental studies have shown that the creep Poisson's ratio ranges from 0.16 to 0.25, which is similar to the elastic value.

Creep under High Stress Levels

It has been shown from experimental studies that creep is linearly proportional to stress up to $0.35f_c'$. Beyond this value the shape of the curves is as shown in Fig. 4.13. Experimentally it has also been established [51] that the relationship between creep recovery after removal of the loading and the stress level is linear as shown in Fig. 4.14.

Practical Models

Several practical models for predicting creep for a particular concrete and environmental conditions have been developed. The simplest one is the ACI Committee 209 model which has recommended the following expression:

$$C_t = K_s K_H K_h K_\tau \frac{(t-\tau)^{0.60}}{10+(t-\tau)^{0.60}} C_u \qquad (4.24)$$

where,

C_t = Creep coefficent
= Creep strain at time t / initial instantaneous strain
C_u = Ultimate creep coefficient
= 2.35 for standard conditions
K_s = 0.81 + 0.07s
K_H = 1.27 - 0.0067H, $H \geq 40$
K_h = 1.0 - 0.0167(SZ-6.0), $SZ > 6.0$
= 1.0, $SZ \leq 6.0$
K_τ = $1.25\tau^{-0.118}$ for moist cured concrete for 7 days
t = Observation time in days
τ = Age at loading in days

4.3.5 Reinforcing Steel

To model the constitutive relationship of the reinforcing steel a simple bi-linear model is used as shown in Fig. 4.15. In this model, steel can exhibit strain hardening with a Bauschinger effect or be taken to be perfectly elasto-plastic. Four parameters are needed to determine the stress-strain curve. These are (1) initial modulus of elasticity, E_S, (2) modulus of strain hardening portion, E_{Sh}, (3) yield stress, f_y, and (4) ultimate strain, ϵ_{us}. Failure is assumed to have taken place when the total strain in the reinforcing steel exceeds ϵ_{us}.

Assuming axis 1 is parallel to the longitudinal axis of the reinforcing bars and axis 2 is orthogonal to it, the incremental constitutive relationship can be written as:

$$\begin{Bmatrix} d\sigma_1 \\ d\sigma_2 \\ d\tau_{12} \end{Bmatrix} = \begin{bmatrix} E_{sc} & 0 & 0 \\ 0 & 0 & 0 \\ 0 & 0 & 0 \end{bmatrix} \begin{Bmatrix} d\epsilon_1 \\ d\epsilon_2 \\ d\gamma_{12} \end{Bmatrix} \tag{4.25}$$

where E_{sc} is the current modulus of elasticity of the steel.

4.4 Nonlinear Solution Techniques

All phenomena in solid mechanics are nonlinear, especially in reinforced concrete structures, and some problems require nonlinear analysis if realistic results are to be obtained. Structures may exhibit nonlinear behavior due to a nonlinear constitutive relationship (material nonlinearity) or a nonlinear strain-displacement relationship (geometric nonlinearity).

Depending on the sources of nonlinearities, we can divide nonlinear problems into three categories. The first category involves material nonlinearity problems in which the stresses are not linearly proportional to the strains, but in which only small displacements and small strains are considered. Many engineering problems fall under the first category, an example being elastic-plastic analysis of various structures. Although linear stress-strain equations are assumed to hold in the second category, problems involving geometric nonlinearity arise both from nonlinear stress-displacement relation and from finite changes in geometry. The problem of large deflections of plates lies in this category, where the geometry of the plate changes, so that membrane effects become significant. Finally, the third category is the combination of the first two categories. It involves nonlinear constitutive behavior as well as large strains and finite displacements.

In the case of reinforced concrete structures displacements are inherently small, geometric nonlinearities generally do not occur and attention can be restricted to material nonlinearities. These include: (1) cracking of the concrete; (2) nonlinear stress-strain for concrete, steel, bond and aggregate interlock; and (3) time dependent effects such as creep, shrinkage, temper-

ature and load history.

The solution of nonlinear problems by the finite element method is usually attempted by one of three basic techniques: incremental or stepwise procedures, iterative or Newton-Raphson methods, and step-iterative or mixed procedures. For simplification, only the nonlinear incremental equilibrium for a single element is considered

$$[k]\{\Delta\delta\} = \{\Delta F\} \tag{4.26}$$

Where the nonlinearity occurs in the stiffness matrix $[k]$, which is a function of nonlinear material properties $[D(\sigma)]$. The material parameters in $[k]$ are no longer constants, thus

$$[k] = [k\{\Delta\delta\}, \{\Delta F\}] \tag{4.27}$$

It is on the basis of this stress-strain or constitutive law that we determine the variable matrix $[D(\overline{\sigma})]$ for the nonlinear analysis.

Essentially, the incremental procedures approximates the nonlinear problem as a series of linear problems, that is, the nonlinearity is treated as piecewise linear. The iterative procedure consists of successive corrections to the solution until equilibrium under the total load is satisfied. The step-iteration procedures utilize a combination of both the incremental and iterative schemes.

These procedures are schematically shown in Figs. 4.16 to 4.18. Details of these methods may be found in any textbook on finite elements, for example of that of Desai and Abel [41].

4.5 Finite Element

A flat triangular shell finite element is selected. The element is formed by combining the 9 DOF Irons-Razzaque plate bending triangle [52] with the constant strain triangle (CST) as the membrane element to obtain a flat triangular element with 5 DOF at each node as it is shown in Fig. 4.19. Irons and Razzaque employed smoothed derivatives instead of the true derivatives of the shape function for the corresponding displacements element. The CST used is the one employed for plane stress analysis and it is used to represent the membrane or in-plane action of a slab. It should be noted that for plane stress systems, the element properties must be symmetric about the reference surface.

The element stiffness is given by Eq. 4.28 and it is generally evaluated by numerical integration.

$$[K] = \int_V [B]^T [D][B] dV = \begin{bmatrix} [K]_{mm} & [K]_{mb} \\ [K]_{bm} & [K]_{bb} \end{bmatrix} \tag{4.28}$$

where,

$[K]_{mm}$ = membrane stiffness matrix
$[K]_{bb}$ = bending stiffness matrix
$[K]_{mb}$ = coupling stiffness matrix ($[K]_{bm} = [K]_{mb}^T$)

The components of the element stiffness matrix are given below:

$$[K]_{mm} = \int_V [B]_m^T [C][B]_m dV = \int_A [B]_m^T \left[\int_h [C] dz\right] [B]_m dA = \int_A [B]_m^T [D]_{mm} [B]_m dA \tag{4.29}$$

$$[K]_{bb} = \int_V z^2 [B]_b^T [C][B]_b dV = \int_A [B]_b^T \left[\int_h z^2 [C] dz\right] [B]_b dA = \int_A [B]_b^T [D]_{bb} [B]_b dA \tag{4.30}$$

$$[K]_{bm} = \int_V -z[B]_b^T[C][B]_m dV = \int_A [B]_b^T \left[\int_h -z[C]dz\right][B]_m dA = \int_A [B]_b^T [D]_{bm}[B]_m dA \tag{4.31}$$

In the above equations, $[B]_m$ and $[B]_b$ represent the strain-displacement matrices and depend on the shape functions, whereas $[D]_{mm}$, $[D]_{bb}$ and $[D]_{bm}$ reflect the material constitutive relations.

To evaluate the material matrices, the reinforced concrete composite section is assumed to be made up of a system of concrete layers and "equivalent smeared" steel layers as shown in Fig. 4.20. The steel is converted to a uniform layer with an equivalent thickness given by:

$$t_s = \frac{A_S}{b} \tag{4.32}$$

where A_s is the bar area and b is the spacing of the bars.

Each layer is assumed to be in a state of plane stress and the material matrix for an element is obtained by summing the contribution of each layer.

4.6 General Solution Algorithm

To trace the nonlinear and time-dependent behavior of reinforced concrete structures, an incremental formulation of the finite element method, coupled with a step-by-step integration scheme through the time domain, is used. For each time step, an incremental load procedure combined with constant or tangent stiffness iterations in each load step is used to find the load displacement path.

During a time step the exterior loads are assumed to remain constant. The applied exterior loads are subdivided into a number of equal load steps as

shown in Fig. 4.21. The structure is then analyzed for each load step by an iterative approach and the increments calculated in the field variables (displacements, strains, stresses) are added to the previous totals to evaluate the current state in the structure. After all the load increments have been treated, the analysis for time-dependent effects from the current time to the next time is then performed. The time-dependent load vector may be subdivided into load steps and the same procdure as described previously is carried out at the beginning of the next step.

More aspects of the method of analysis along with the algorithm outlining the basic steps of the procedure are given in [25].

4.7 Solution Procedure for Time-Dependent Effects

A step-by-step integration scheme in the time domain is used to analyze the effects of time-dependent phenomenon on the behavior of reinforced concrete structures. An initial strain approach is adopted to determine the response of the structure.

The procedure as described in [25] is summarized here for a typical time step Δt_i:

1. The loads are applied at time t_i and remain constant for Δt_i. For these loads the current total values of the variables are found.
2. For the stress state of step 1, calculate the strain increments due to creep, shrinkage occuring in each concrete layer.

3. The equivalent nodal forces produced by the initial strain increment are determined. The element load vectors are then transformed to the global coordinates and the structural load vector assembled.

4. The structure is then analyzed using the general solution algorithm. The element stiffness matrices are formed using the concrete material properties at time t_{i+1}.

5. From the displacement increment, the local displacement increment for the element and the corresponding strain increment in a typical concrete layer, is computed.

6. The vector of stress increments in the concrete layer is calculated, for the first iteration only.

7. The current total values of all the field variables are then calculated, convergence checked and the solution completed for time step Δt_i.

At time t_{i+1} an equilibrium position for the structure, due to the applied load history including time-dependent phenomena up to time t_{i+1}, is therefore found.

4.8 Computer Program

To perform the method of analysis previously described, a computer program, NOPARC (NOnlinear analysis of Prestressed And Reinforced Concrete structures), was developed by Van Greunen et al.[25]. The program is able to trace the quasi-static response of reinforced and prestressed concrete slabs of arbitrary geometry and shear panels under instantaneous and sustained loads. Time-dependent phenomena such creep and shrinkage effects and temperature, can be simulated to trace the changes in the field

variables of such structures.

The program is coded in FORTRAN *IV* language, and was developed on the CDC 6400 computer at the University of California, Berkeley by Van Greunen in 1979, and then it was converted to CDC 7600 machine by E.C. Chan in 1983 and to IBM FORTRAN 77 by the author. Full details on the program can be found in [25].

The program is structured such that additional elements could be added easily. The equation solution is done by Gaussian elimination and the equation solver adopted to solve symmetric banded matrices by triangularization and then backsubstitution in two separate operations.

A flow chart of the logical structure of NOPARC is shown in Fig. 4.22 and an example of the input data for the program is presented in Appendix C.

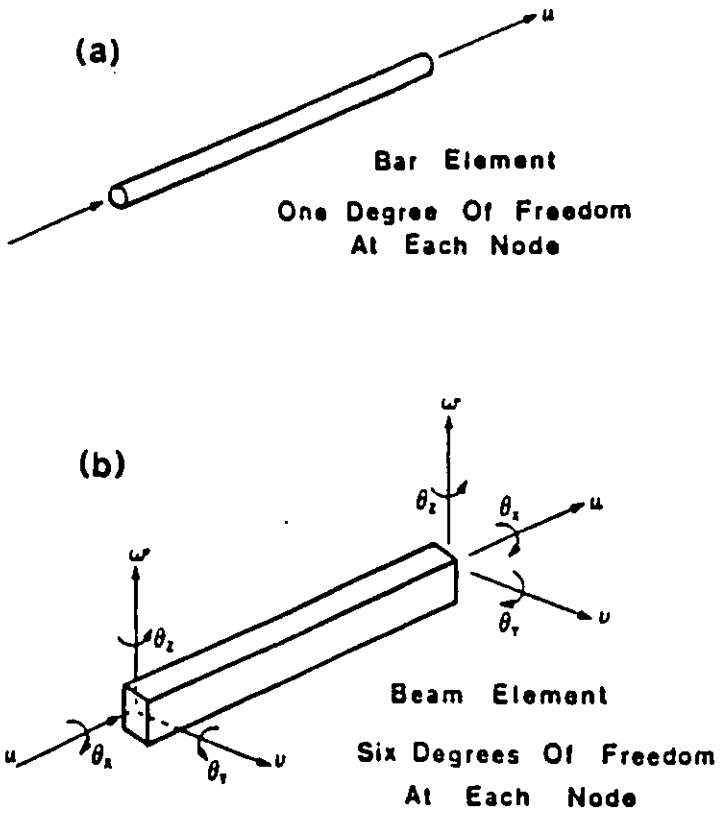

Figure 4.1: One-Dimensional Elements

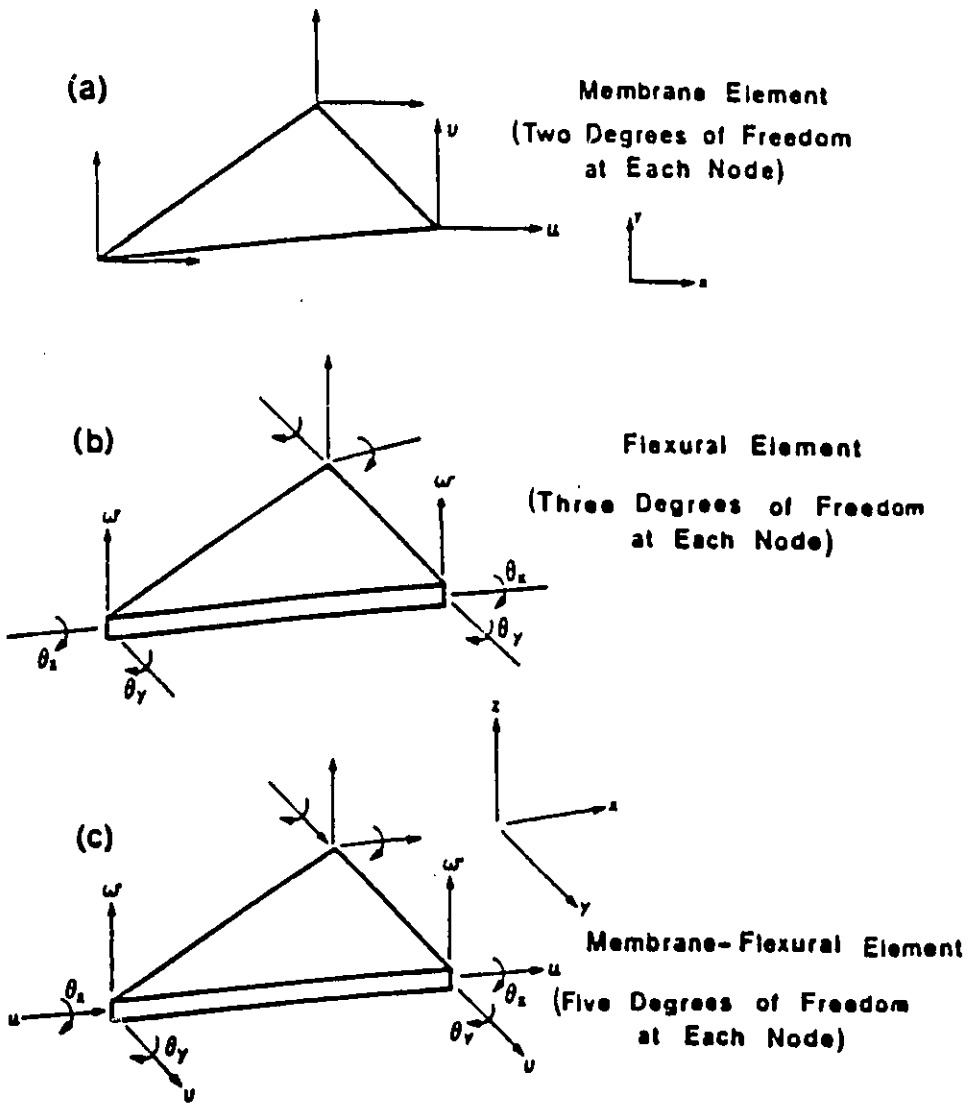

Figure 4.2: Two-Dimensional Elements

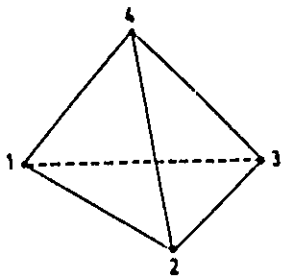

Four Noded
Tetrahedron

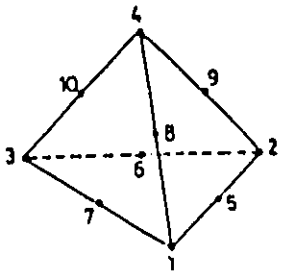

Ten Noded
Tetrahedron

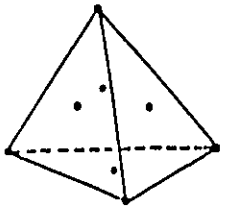

Eight Noded
Tetrahedron

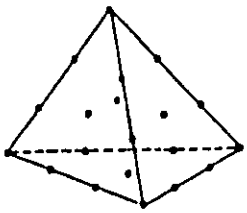

Twenty Noded
Tetrahedron

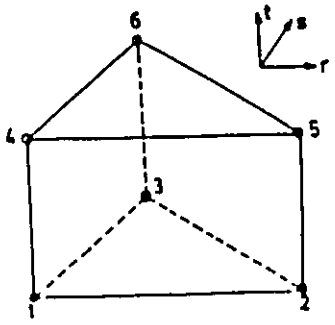

Six Noded Solid
Triangular Element

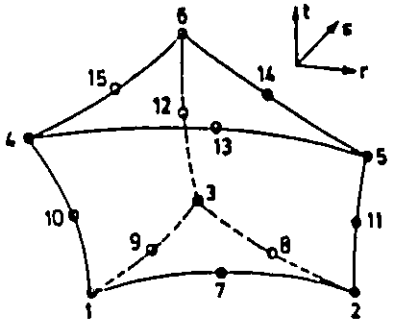

Fifteen Noded Solid
Triangular Element

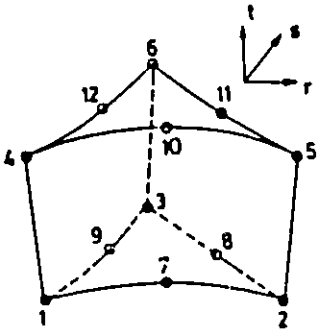

Twelve Noded Solid
Triangular Element

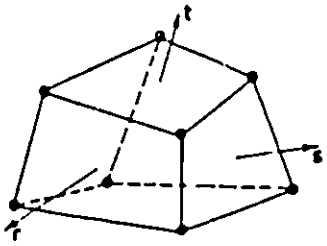

Eight Noded Hexahedral
Element

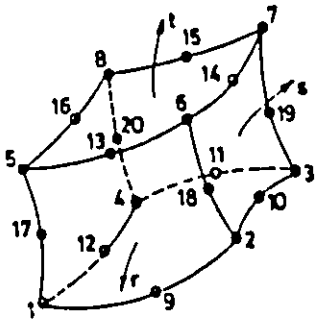

Twenty Noded Curved
Solid Element

Figure 4.3: Three-Dimensional Elements

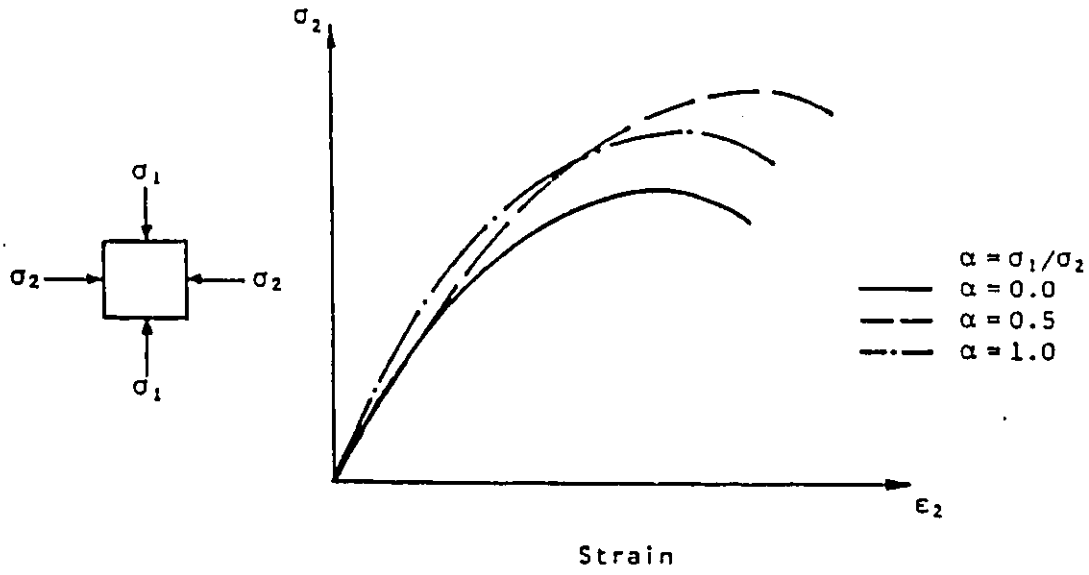

Figure 4.4: Stress-Strain Relationships of Concrete under Biaxial Compression

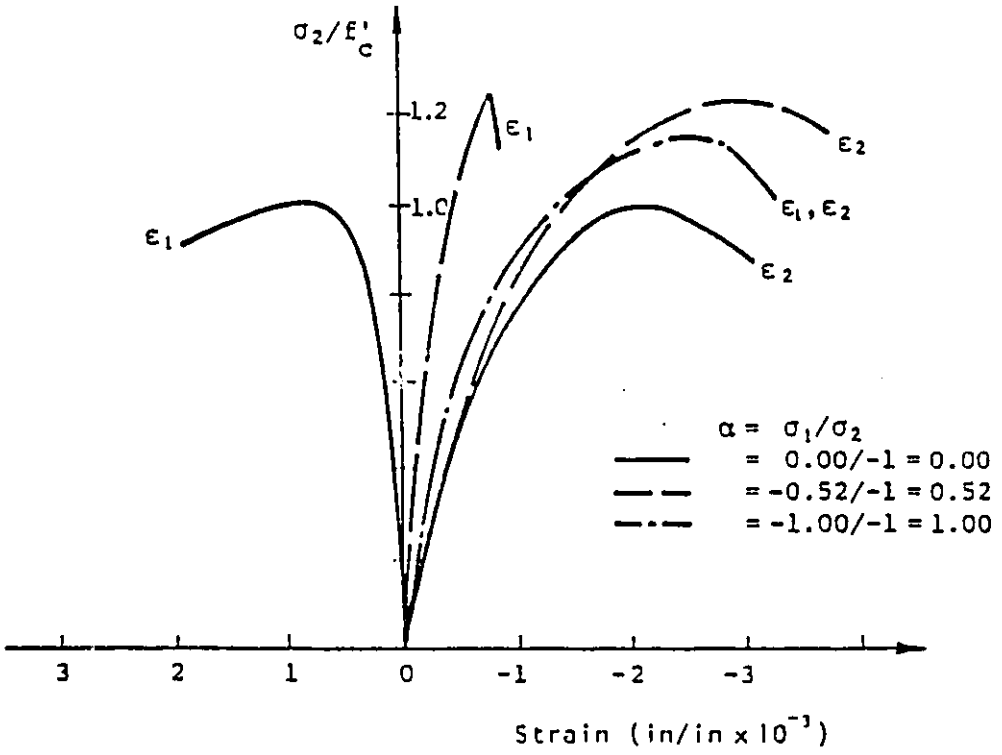

Figure 4.5: Experimental Stress-Strain Relationships Curves for Biaxial Compression

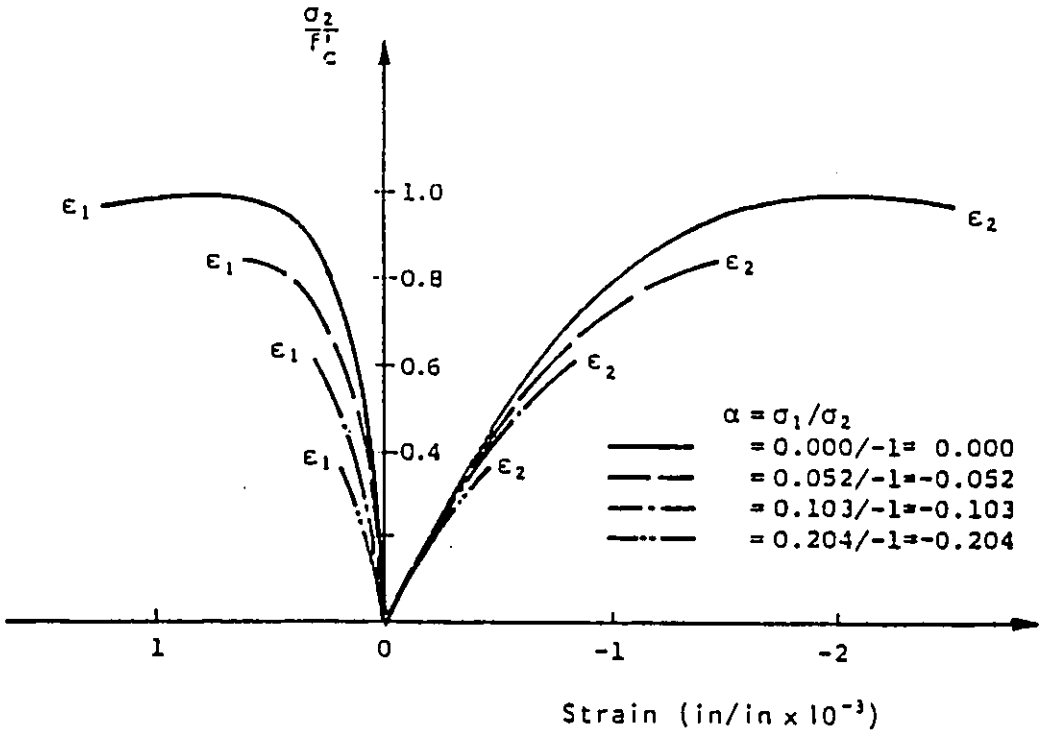

Figure 4.6: Experimental Stress-Strain Relationships Curves for Biaxial Tension-Compression

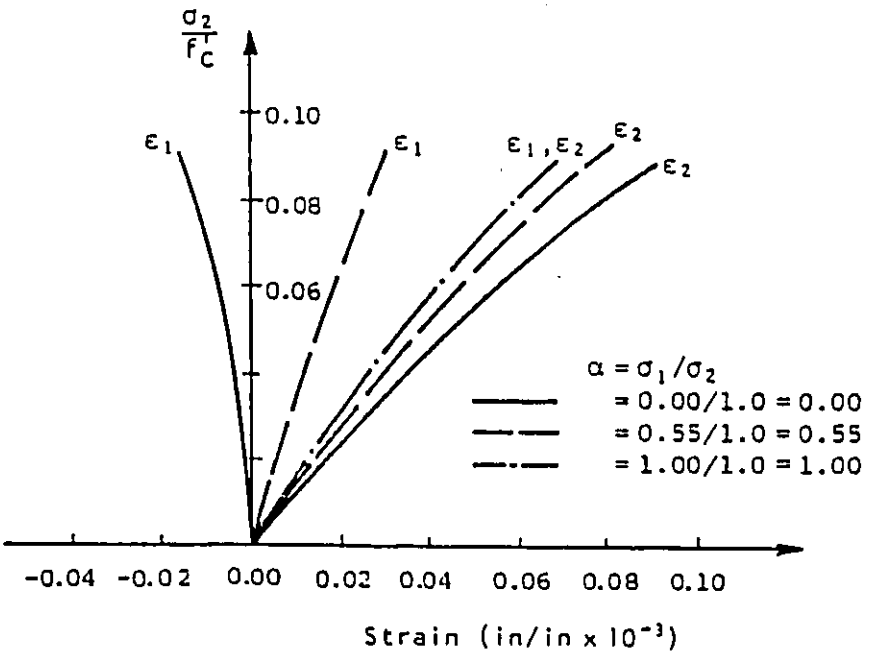

Figure 4.7: Experimental Stress-Strain Relationships Curves for Biaxial Tension

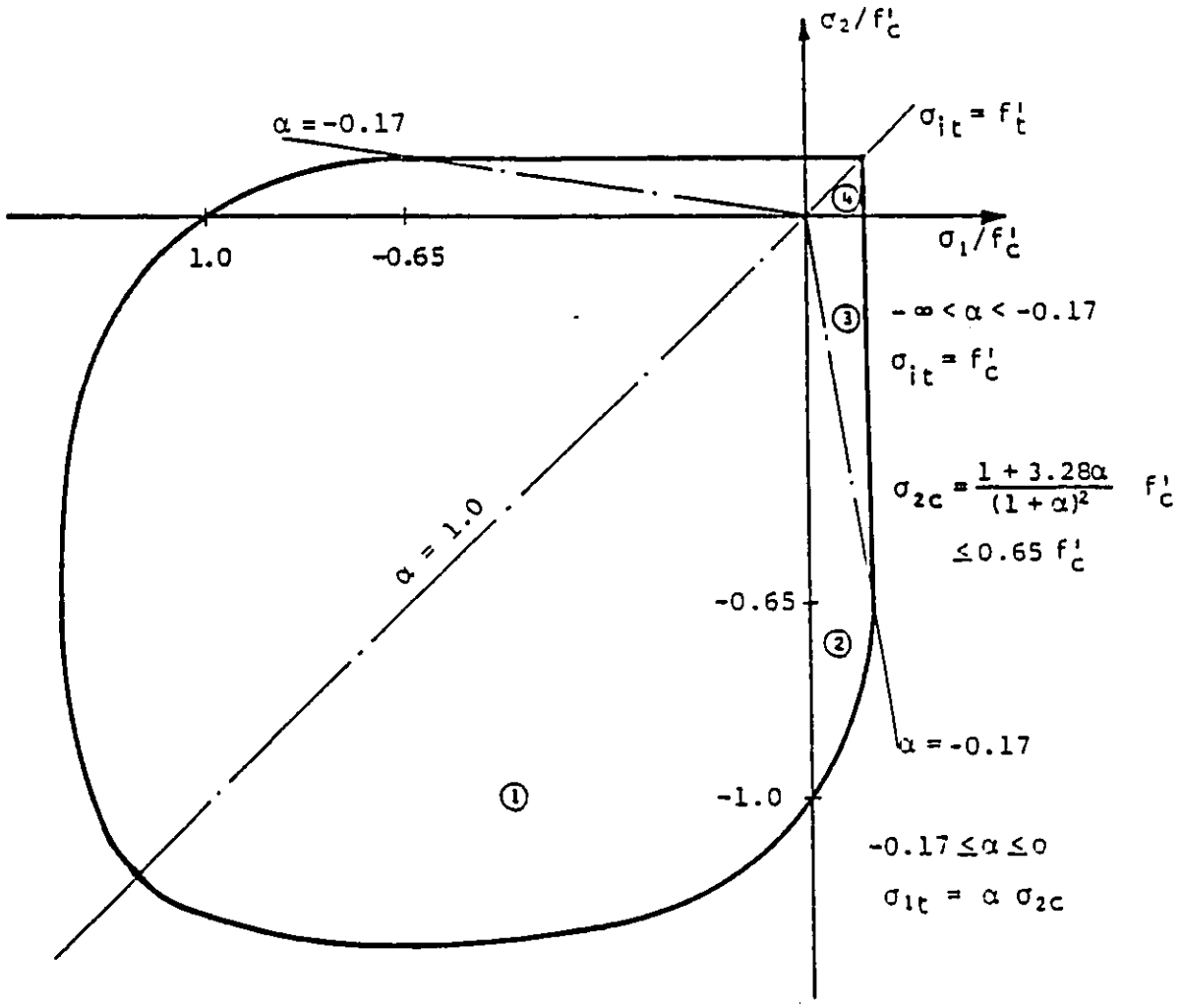

$$\sigma_{2c} = \frac{1 + 3.65\alpha}{(1+\alpha)^2} f'_c$$

$$\sigma_{1c} = \alpha\, \sigma_{2c}$$

$$\alpha = \sigma_1 / \sigma_2$$

Compression = -
Tension = +

Figure 4.8: Biaxial Strength Envelope

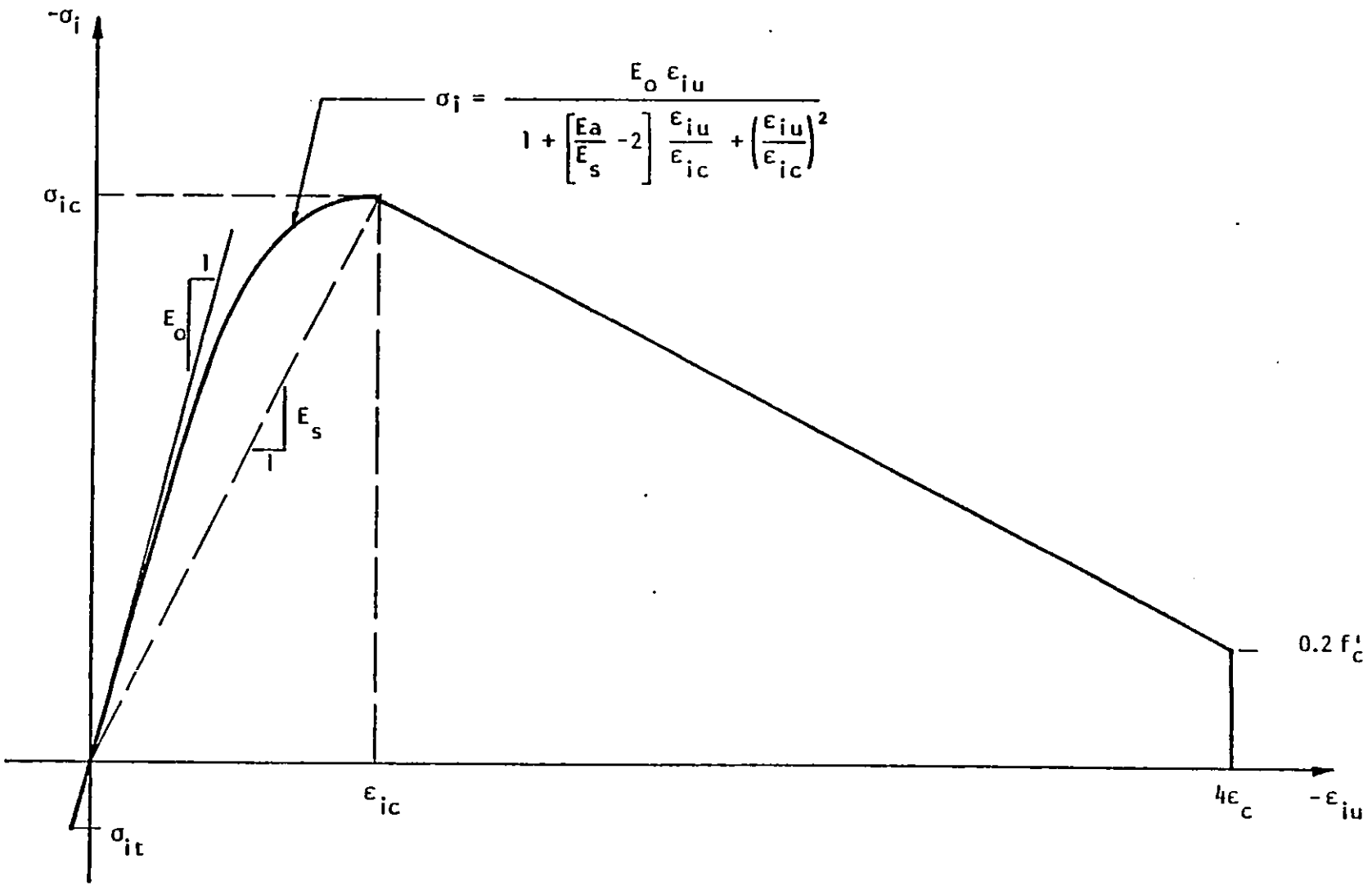

Figure 4.9: Uniaxial Stress-Strain Curve for Concrete

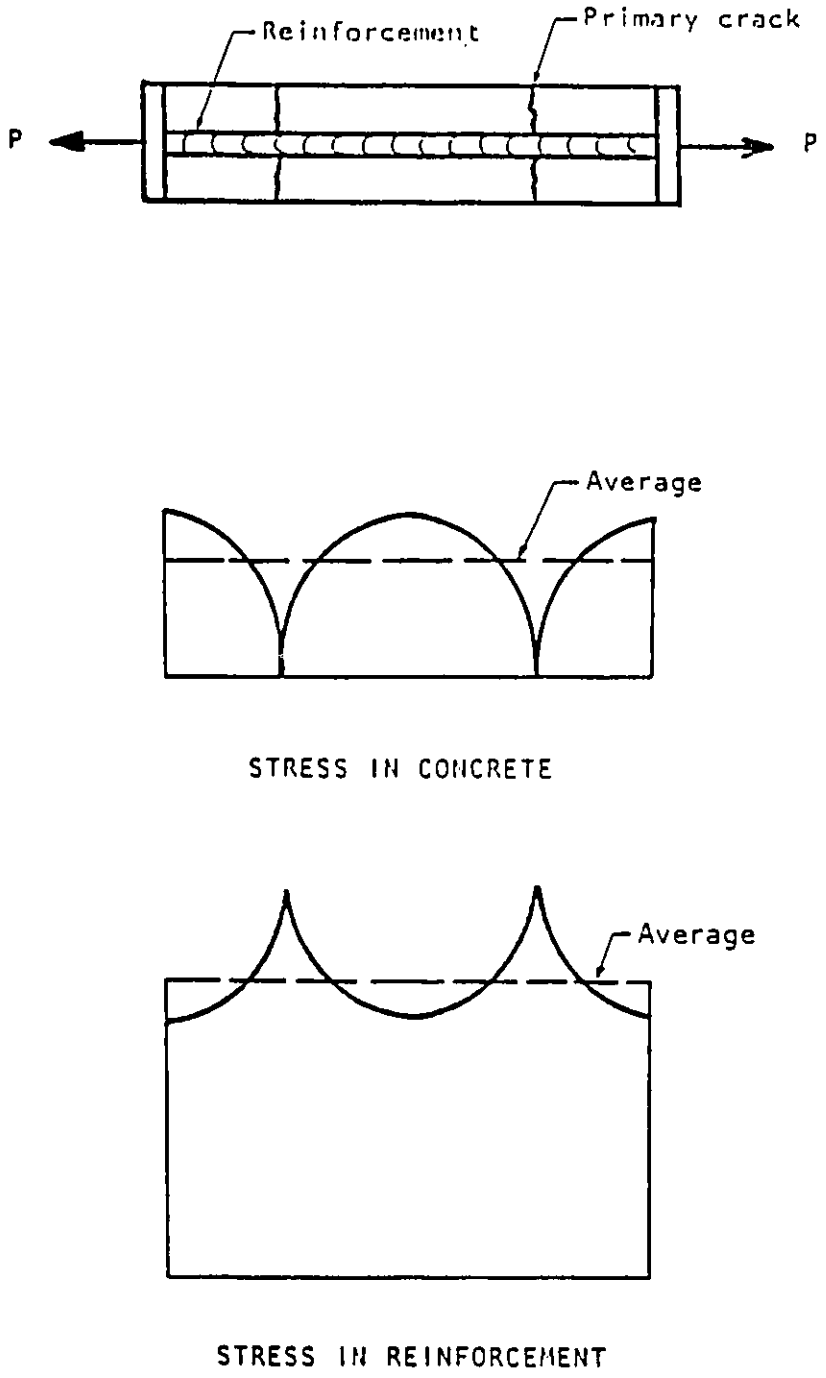

Figure 4.10: Stress Distribution in a Cracked Concrete Element

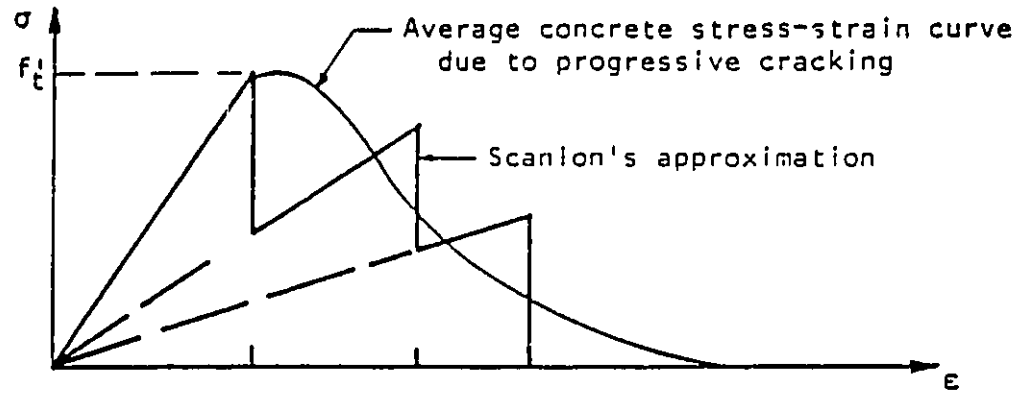

a. SCANLON'S STEPPED MODEL

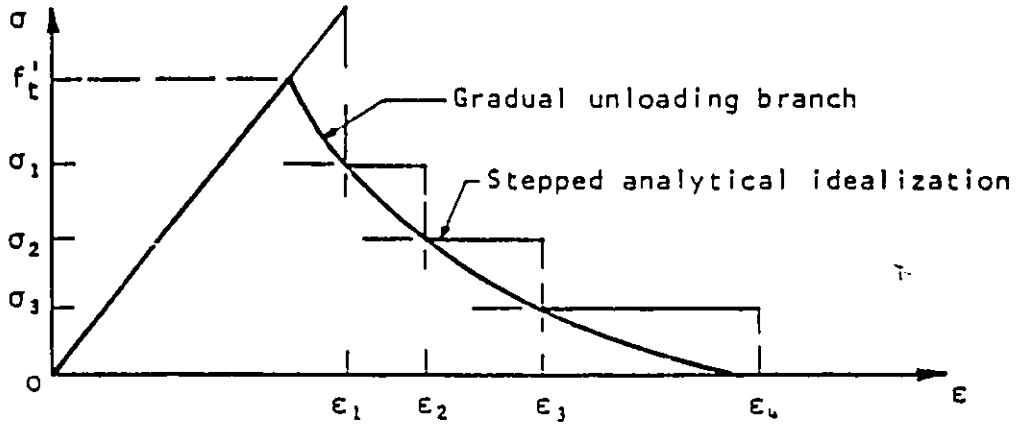

b. LIN'S GRADUALLY UNLOADING MODEL

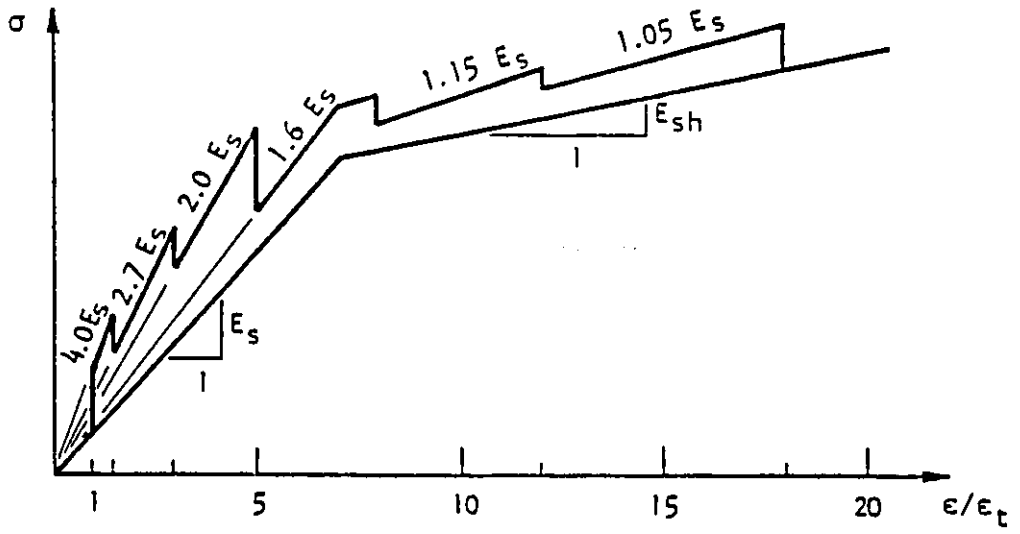

c. MODIFIED STRESS-STRAIN DIAGRAM FOR REINFORCING STEEL

Figure 4.11: Tension Stiffening Models

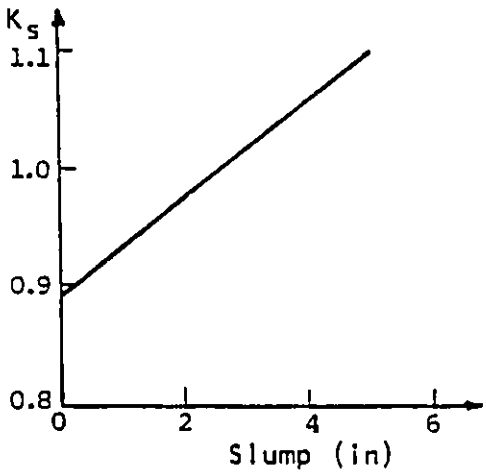

a. SLUMP CORRECTION

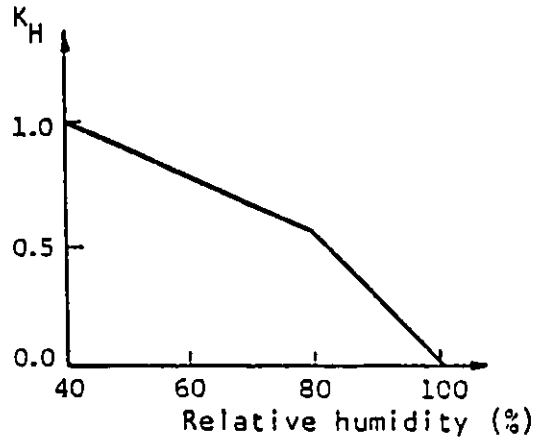

b. HUMIDITY CORRECTION

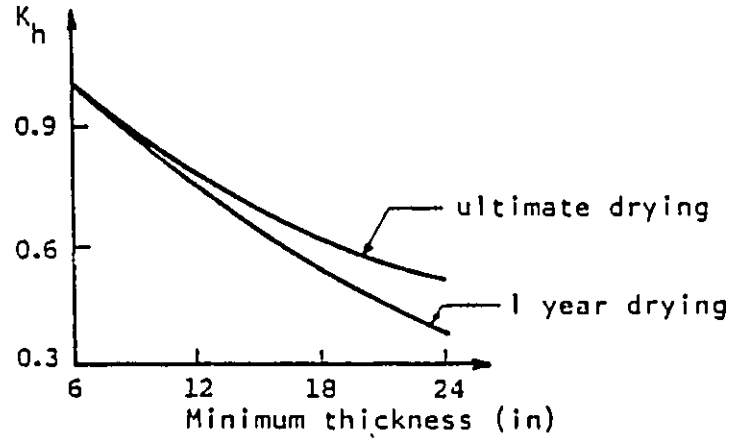

c. THICKNESS CORRECTION

Figure 4.12: Shrinkage Correction Factors

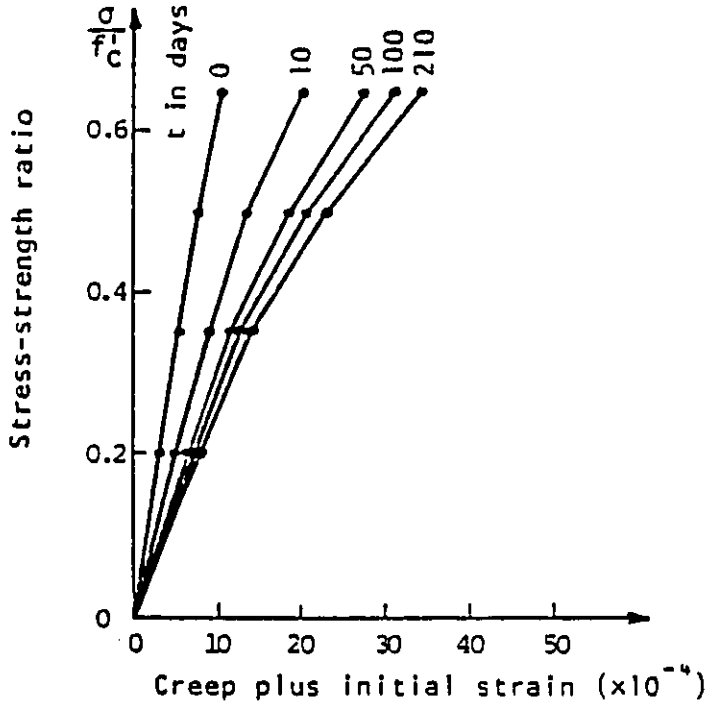

Figure 4.9: Creep under High Stress Levels

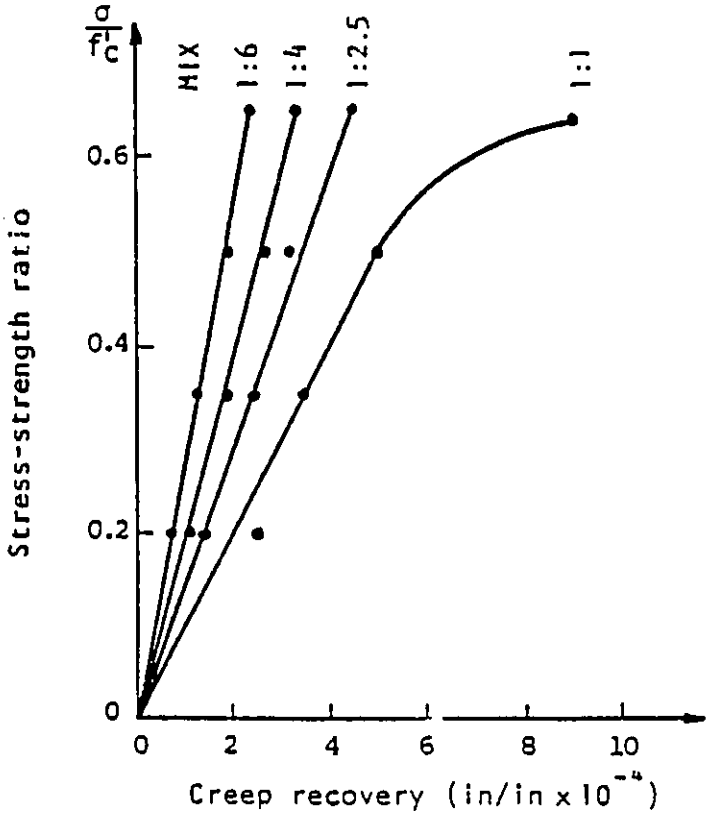

Figure 4.14: Stress Level vs Time-Dependent Recovery

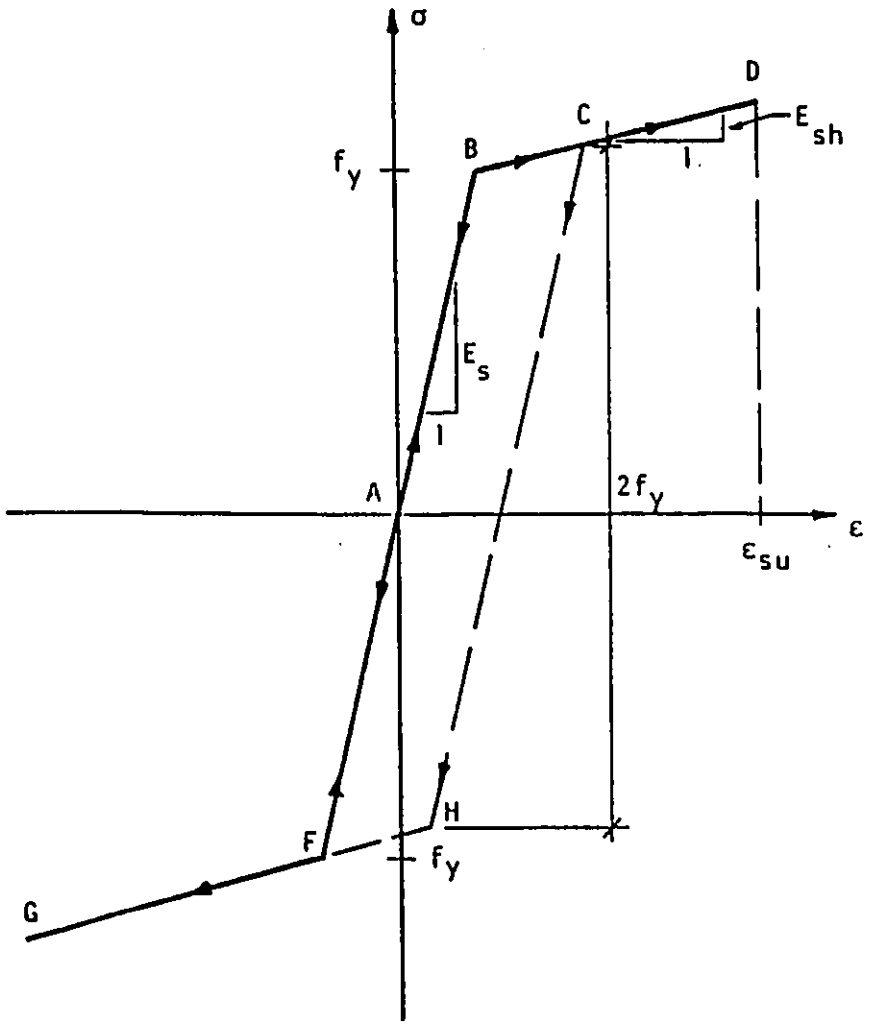

Figure 4.15: Stress-Strain Curve for Reinforcing Steel

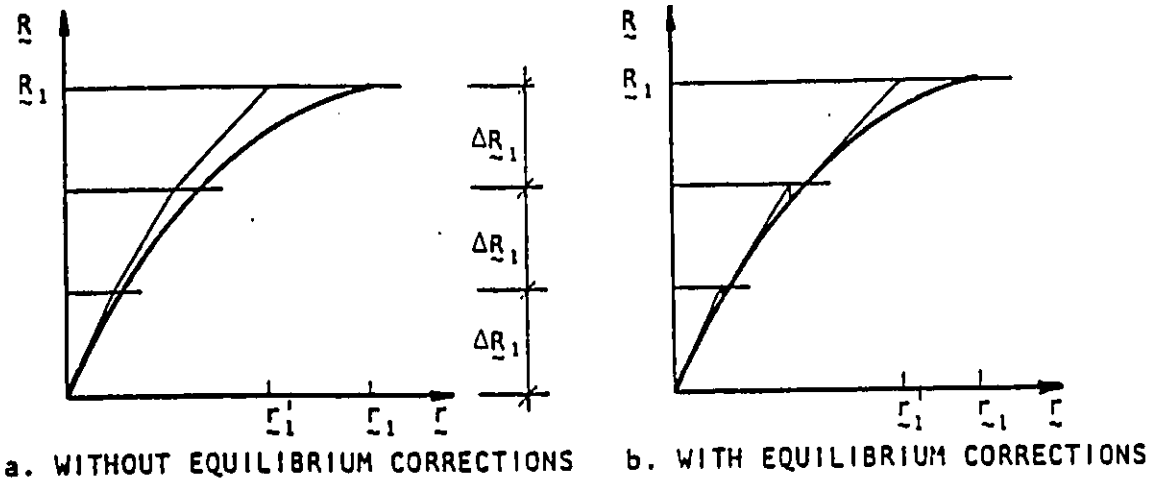

Figure 4.16: Incremental Load Method

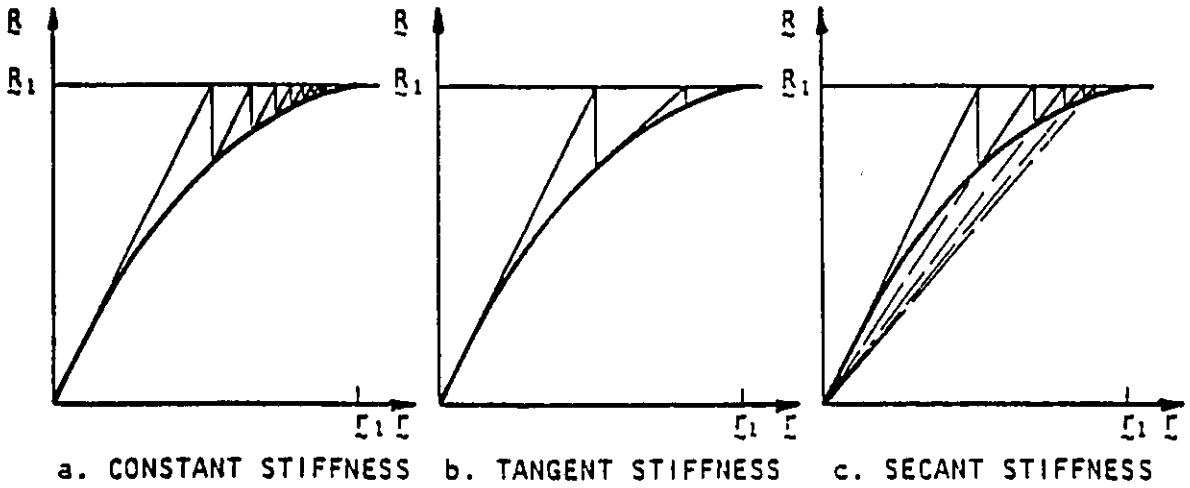

Figure 4.17: Iterative Method

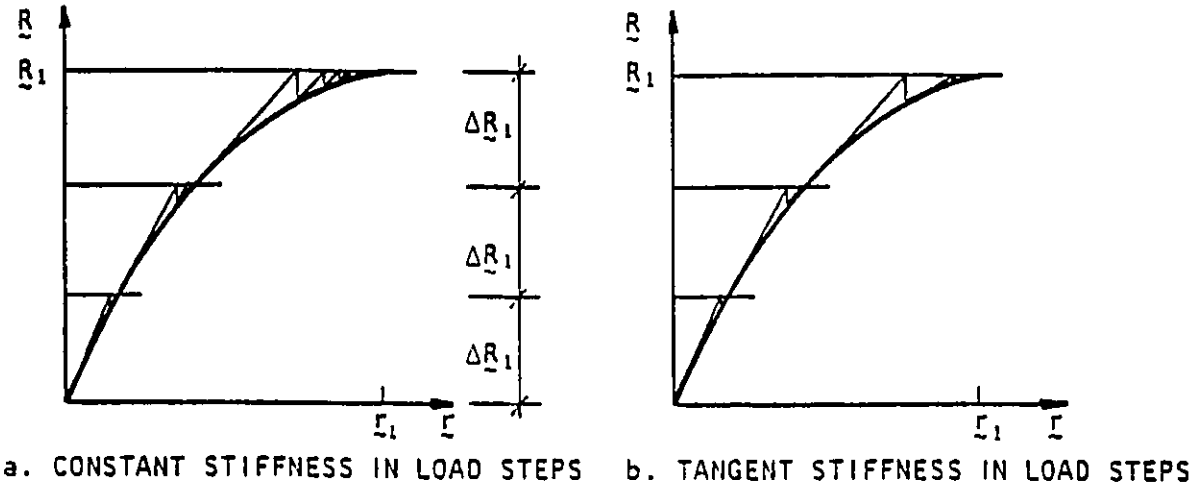

Figure 4.18: Combined Methods

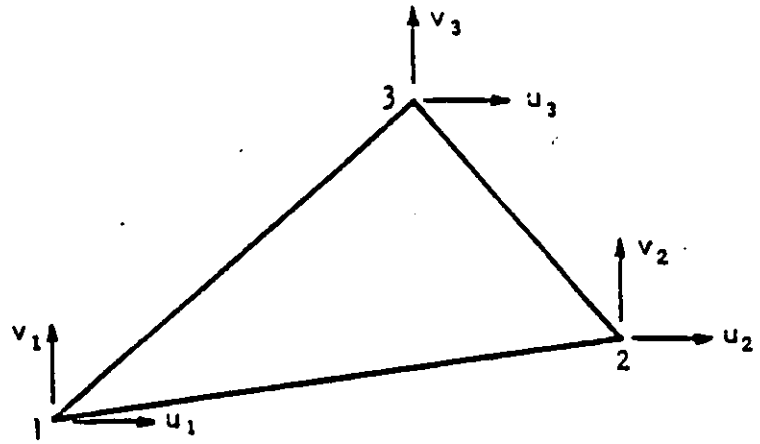

a. CONSTANT STRAIN TRIANGLE

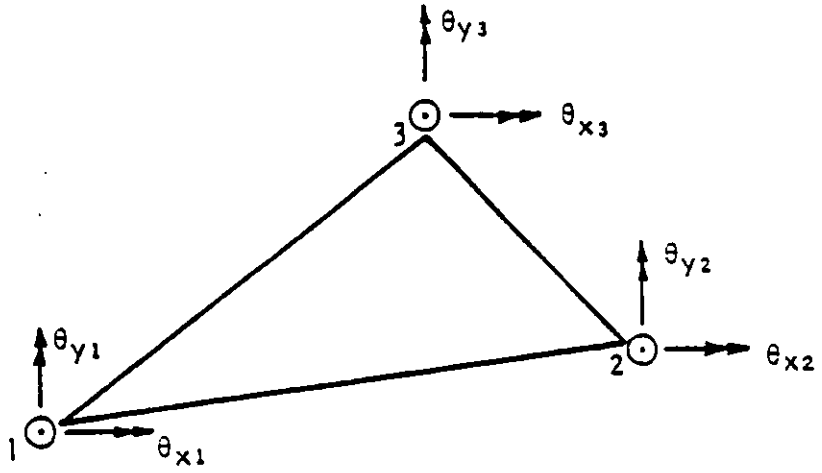

b. IRONS-RAZZAQUE PLATE BENDING TRIANGLE

Figure 4.19: Finite Element Used in this Study

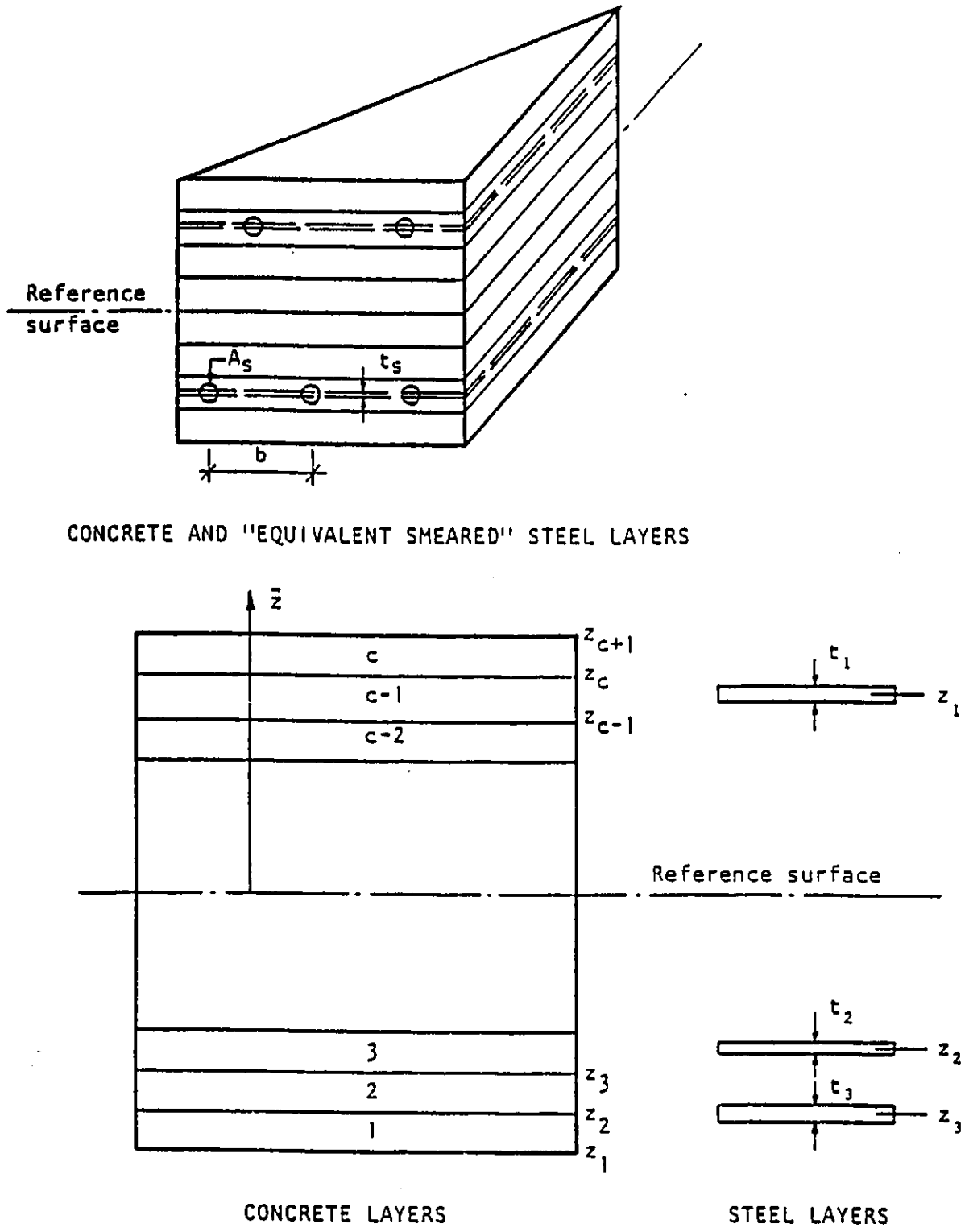

Figure 4.20: Layer System of a Triangular Element

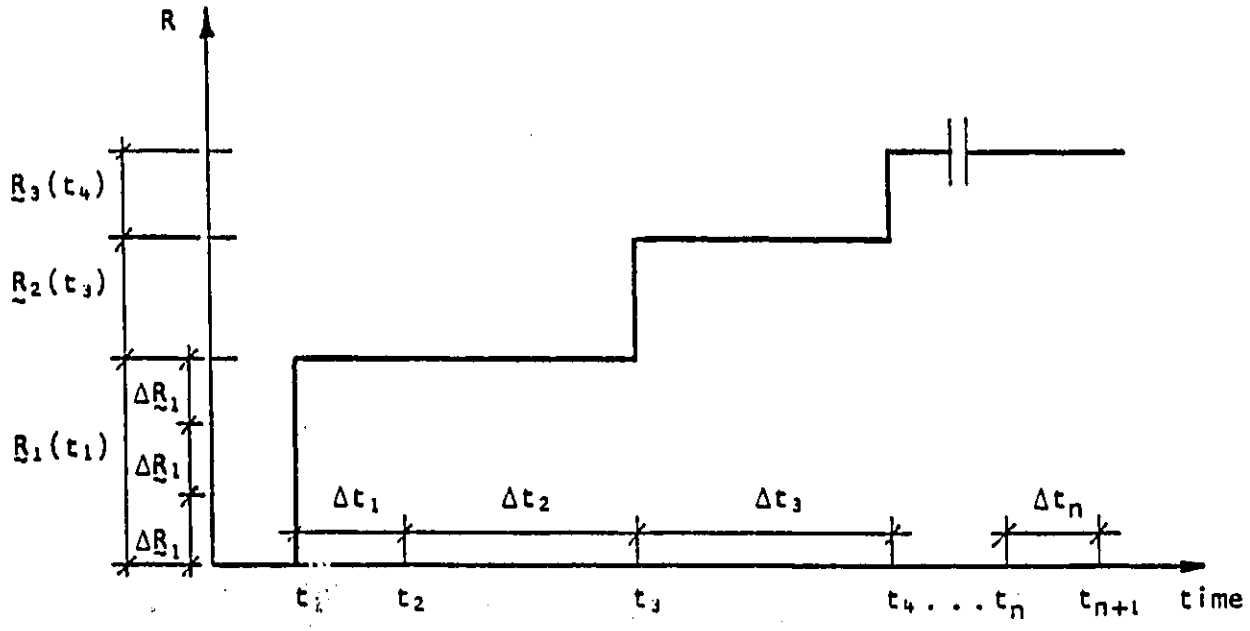

a. EXTERNAL LOAD HISTORY

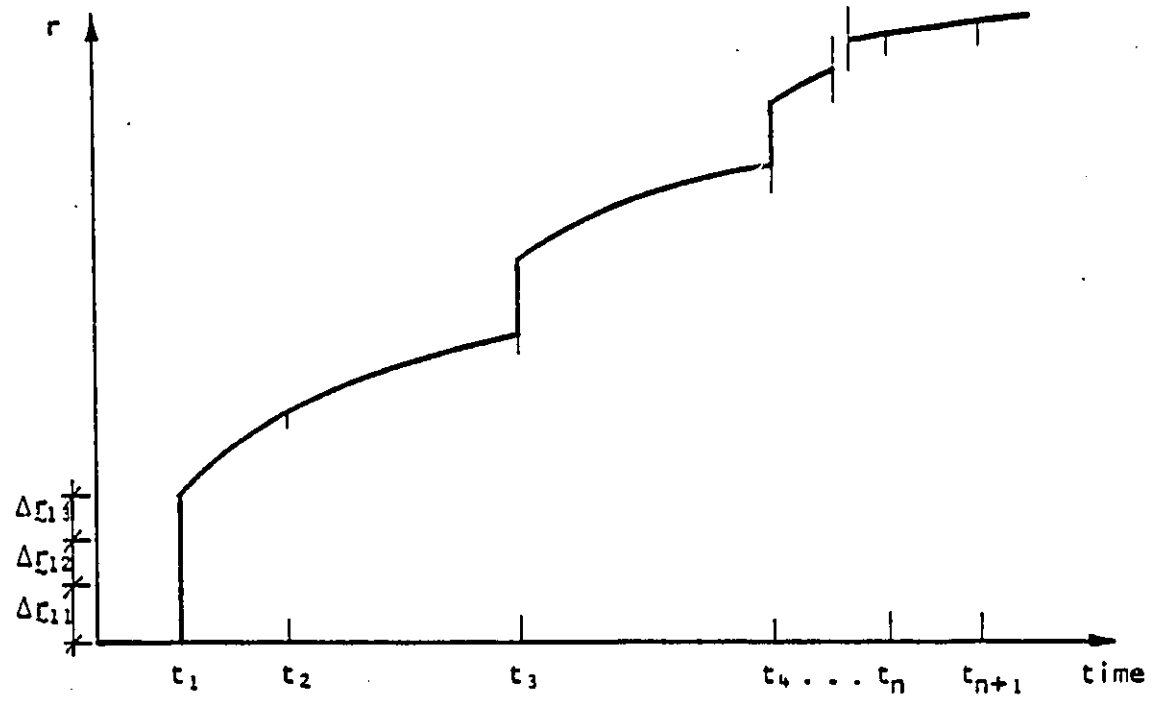

b. DISPLACEMENT HISTORY

Figure 4.21: Structural Response History Due to External Loads

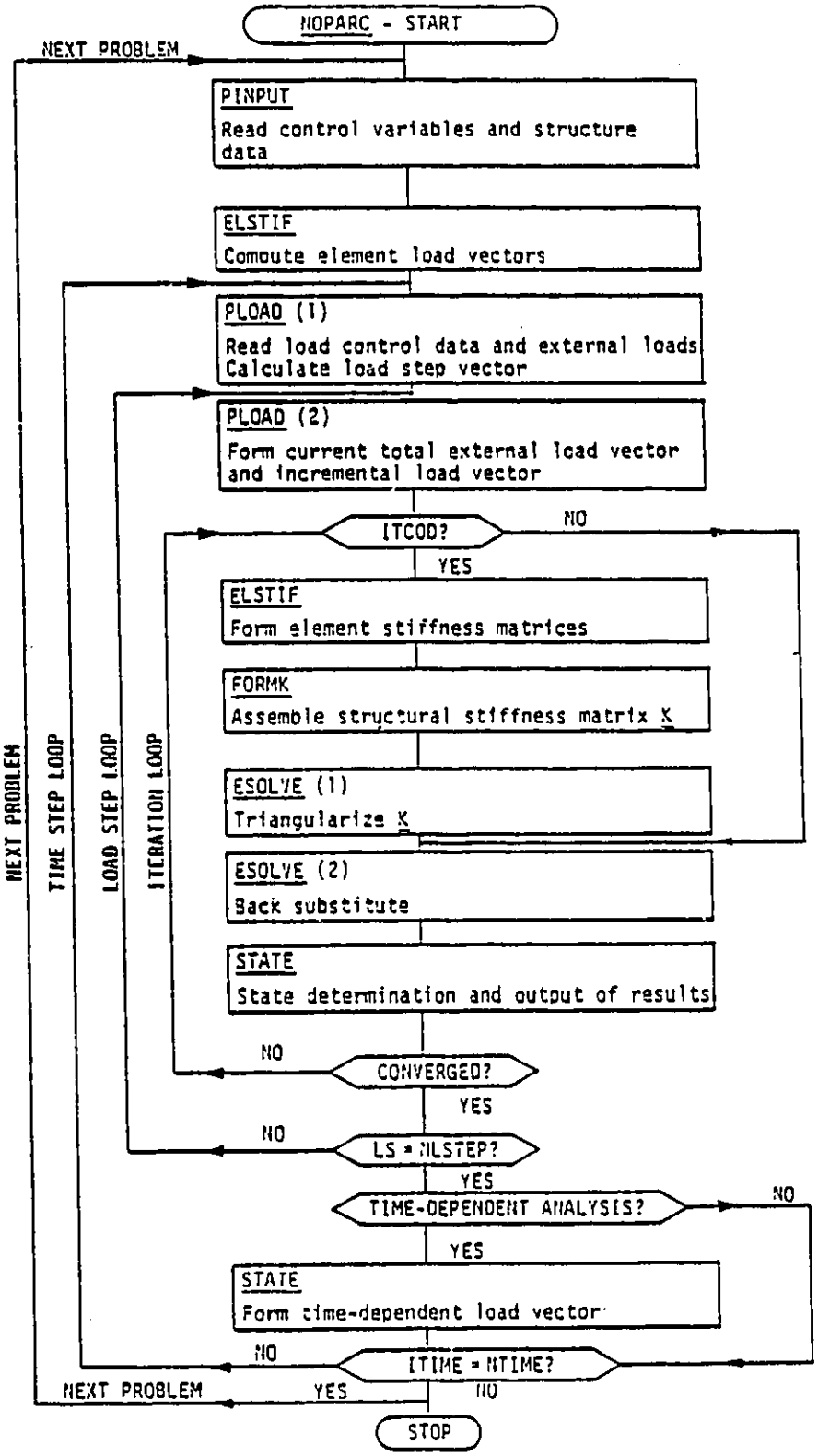

Figure 4.22: NOPARC Flow Chart

Chapter 5

DESCRIPTION OF THE PRESENT ANALYSIS

5.1 Validation of the Program

As a first step in this thesis, it was appropriate to check the validity of NOPARC program. The program was first converted from CDC FORTRAN Standard to IBM FORTRAN Standard and then run on the University of Ottawa AMDAHL 5860 computer.

A square corner-supported slab tested by McNeice [21] and analyzed by many investigators under concentrated load acting in the center of the slab, was analyzed. Initially, only the immediate (or short-time) deflection occuring on application of the load was considered. The slab analyzed is isotropically reinforced, 36 in. square by 1.75 in. thick and divided into 10 equal layers. Only one quarter of the slab is modeled by the finite element mesh as shown in Fig. 5.1. The material properties used for this analysis

and details of the slab are shown in Fig. 5.1. Note that only the 28-day compressive strength of concrete, the modulus of elasticity of concrete, and the modulus of elasticity of steel were given, while the remaining material properties were assumed.

In the first analysis, the concentrated midpanel load was applied in 4 load increments of 1 kip each. The various tension stiffening models mentioned in Section 4.3 were incorporated in the analysis to check which model fits best. With regard to the tensile strength of the concrete represented by the modulus of rupture, the analysis was carried out using both the full value of the modulus of rupture taken equal to 1/10 the compressive strength at 28 days i.e 550 psi and a reduced value of 275 psi.

The results for the short-time analysis were compared with those obtained from the experiment as shown in Fig. 5.2 and Fig. 5.3. From the load-deflection curves for node 12 it can be observed that the tension stiffening model based on unloading in the concrete results in the behavior of the slab being too stiff after the initial cracking. The tension stiffening employing an increased steel modulus shows a very good agreement with the experiment curve. The model using the assumption that there is no tension stiffening at all produces a greater increase in deflection than the previous tension stiffening models. The concrete is assumed to carry no stress normal to a crack but an additional stress, representing the total internal tensile force carried by the concrete between cracks, will be carried at the steel level in the direction of the bars. This is probably a more accurate representation of the actual orientation of stress in the cracked region of a slab, than the concept of considering an average tensile stress in the concrete [58]. Consequently, the model for tension stiffening effect using an increased steel modulus was used throughout the present analysis. Also, from Figs. 5.2 and 5.3 it can be noticed that deflections increase significantly as the modulus of rupture is reduced by 50 percent or to a lower value. The effect of

varying the tensile strength of concrete is therefore of paramount importance in estimating deflections of reinforced concrete slabs.

The time-dependent analysis consisted of analyzing the slab due to the effects of shrinkage, creep and load history. Prediction of creep and shrinkage effects were based on ACI Committee 209 recommendations. A simple load history as shown in Fig. 5.4. was adopted. The deflection-time plot for the analyzed slab is also shown in Fig. 5.4. A good agreement was obtained between the finite element results and the hand calculation results as shown in Appendix A and Table A1. The ratio of computed one-year deflection to the immediate deflection at 28 days was found to be 2.5.

5.2 Present Analysis

5.2.1 General Remarks

The analytical determination of the deflection of two-way reinforced concrete slab systems is complicated by the three-dimensional nature of the problem; the effect of the flexural and torsional rigidities of supporting slab elements; the stiffening effect of columns; slab aspect ratio and continuity of the panels; cracking of the concrete; and the time-dependent concrete deformation. Consequently, the accurate assessment of flat slabs deflections is dependent on an understanding of the different factors involved. For most slab systems, the main contributing factors to problematic deflections can be grouped into the following categories:

1. material properties
2. slab geometry

3. loads

4. construction procedures

Building contractors involved in concrete construction tend to remove formwork and proceed to the next stage of construction as quickly as is safely possible. Therefore, it is appropriate to assess the structural adequacy of young concrete structures. Rules of concrete design standards are commonly used when dealing with the load resistance of a young concrete stucture. However, code provisions are primarily based on tests of relatively mature concrete elements. In ACI 318-83, the tensile strength of concrete is expressed in terms of the square root of the compressive strength. However, recent researches [53,54] have shown that a square root relationship between tensile strength and compressive strength is not the most appropriate relationship for young concrete. These researches tend to support a power law larger than the North American codes values. For comparison, the ACI and CEB relationships are given, together with relationships published by Carino and Lew [54] and Gardner et al.[55]

$$
\begin{aligned}
f_t' &= 0.62\,(f_c')^{0.50} && \text{ACI} \\
f_t' &= 0.30\,(f_c')^{0.67} && \text{CEB} \\
f_t' &= 0.24\,(f_c')^{0.71} && \text{Carino and Lew} \\
f_t' &= 0.46\,(f_c')^{0.60} && \text{Gardner et al.}
\end{aligned}
$$

In the above expressions, f_t' and f_c' are expressed in MPA.

In a recent paper by Dilger et al.[56], a close examination of methods for prediction for shrinkage was presented. It reveals enormous discrepancies among results predicted with these models and great differences between

predicted values and experimental findings in many cases. The paper investigated the more popular shrinkage prediction models (ACI 209-82, CEB-FIP 78 etc.). From comparisons made of their influencing parameters, time development function and with some long-term results, Dilger et al. concluded the following with respect to ACI 82 model:

1. Neglecting the effect of the amount of water used in the concrete makes ACI 82 inaccurate model.
2. ACI 82 model does not work for swelling prediction for concrete under water or in saturated air, and may overestimate shrinkage for small members.
3. ACI 82 model assumes a constant value for f in Eq. 4.18 (Section 4.3.3) which results in a constant time development of shrinkage for any size of the member and any relative humidity (RH) of the air.
4. ACI 82 model fails in predicting a swelling of concrete in RH of 100 percent.
5. The shrinkage modification factor for curing time in the ACI 82 model disagrees with the experimental observations.

Alternatively, and based on a set of experimental investigations on the creep and shrinkage of concrete Brayant et al.[57] developed the following time development function for the prediction of shrinkage strains

$$(\epsilon_{sh})_t = \frac{(t/T_d^2)^\alpha}{\overline{f} + (t/T_d^2)^\alpha} (\epsilon_{sh})_u \tag{5.1}$$

where,

$\overline{f}$ $= f/T_d^{2\alpha}$

t = days of drying

T_d = equivalent thickness

α = 1.0024

Eq. 5.1 can be rewritten as:

$$(\epsilon_{sh})_t = \frac{t^\alpha}{f + t^\alpha} (\epsilon_{sh})_u \tag{5.2}$$

In the above expression f is a function of the shape and the size of the member:

$$f = 2.24 (T_d)^{2.0028} \tag{5.3}$$

where T_d is expressed in $days/in^2$.

Based on the above observations the whole analysis presented here was carried out using the relationships given by Gardner et al. and Bryant et al. for the tensile strength of the concrete and for the prediction of shrinkage deformations respectively. Prediction of creep deformations were based on the expressions proposed by ACI 209 Committee as outlined in Section 4.3.4.

5.2.2 Slab Details

Analyses were conducted for a 3-bay flat plate system in X and Y directions. Due to symmetry, only one quarter of the slab system was considered in the analysis as shown in Fig. 5.5. Ten flat plates of different thicknesses, spans, and live load to dead load ratios were designed using the Direct Design Method of the ACI Building Code [4]. Loads, other than self weight,

used for the slab design included a superimposed dead load of 15.5 psf (0.75 KPa). The design strength was taken as 3000 psi (20 MPa) and a steel yield stress of 60,000 psi (400 MPa) was used. Slab details and material properties are shown in Table 5.1 and Table 5.2 respectively.

For all designs, required steel areas were not matched with available reinforcing bar sizes. Instead, the computed area of steel per unit width was specified as input for the computer analysis. Calculated effective steel depths assumed 0.8 in. (20 mm) clear cover to all bars, with #15 bars used in both the column strip and the middle strip. Fig. 5.6 shows the reinforcement plan used for a typical panel. Each quarter of an interior panel is divided into four quadrants, separated by the middle and column strip boundaries. Reinforcement areas for each quadrant of the designed slabs are given in Table 5.3. No attempt has been made to design all the exterior and interior panels for flexure. Only, an interior panel was designed and the computed areas of steel adopted for all panel types of the slab.

One mesh layout was used throughout this study for all slabs. The layout has the general configuration of the mesh shown in Fig. 5.7 with the dimensions adjusted to suit the column strip and the middle strip as well for each slab.

Three construction load histories labeled L1, L2, and L3 were selected as shown in Fig. 5.8. The first loading history consisted of a load of 1.35 DL applied at 7 days and held constant up to 1000 days. In the second case a load of 1.43 DL was applied at 14 days and maintained constant thereafter. In loading history L3, a load of 1.60 DL is applied at 28 days and kept constant thereafter. In this DL denotes the self-weight (dead load) of the slab. Ultimate long-time deflections were assumed to occur 1000 days after casting.

It is worth noting that, for the present investigation we are assuming a constant value of the effective modulus of rupture over the entire slab. However greater restraint stresses would be expected to occur in the vicinity of the columns and around the boundaries compared with those at midpanel [59]. Therefore, it may be desirable to consider the realistic distribution of the modulus of rupture values across the slab in accordance with the expected degree of restraint. Such consideration is not included in this study.

In total, 20 runs were carried out using the computer program NOPARC. The computer simulation experiments were designated test series S1 to S10. Test series S1 to S5 were analyzed under the loading histories L1, L2, and L3 while test series S6 to S10 were only analyzed under loading history L1, and for a typical loading history the analysis was performed by taking into account the effects of creep and shrinkage together.

Table 5.1: Slab Details

Slab designation	Spans		Column width (in)	Clear spans		Slab Thickness (in)	$\frac{L}{D}$
	l_1 (in)	l_2 (in)		l_{1n} (in)	l_{2n} (in)		
S1	236	236	26	210	210	6	1.0
S2	330	330	26	304	304	10	1.0
S3	400	400	26	374	374	13.2	1.0
S4	276	184	26	250	158	6	1.0
S5	296	148	26	270	122	6	1.0
S6	236	157	26	210	131	6	1.0
S7	236	118	26	210	92	6	1.0
S8	236	236	26	210	210	8	0.5
S9	236	236	26	210	210	8	1.0
S10	236	236	26	210	210	8	2.0

Table 5.2: Material Properties

Concrete	28-day Compressive strength	$f_c'(28)$	=	3000 psi
	Tensile strength	f_t'	=	$1.25\,(f_c')^{0.6}$ psi
	Modulus of elasticity	$E_0(t)$	=	$33.0\,W^{1.5}\sqrt{f_c'}$ psi
	Poisson's ratio	ν	=	0.15
	Unit weight (normal weight)	W	=	144 pcf
Steel	Yield strength	f_y	=	60000 psi
	Modulus of elasticity	E_s	=	$29\,(10^6)$ psi
	Modulus of strain hardening	E_{sh}	=	0.0
	Ultimate strain	ϵ_{su}	=	0.1 in/in

Table 5.3: Reinforcement Details

Slab	Quadrant	Reinforcement areas (in^2/in)			
		Top X-Direction	Top Y-Direction	Bottom X-Direction	Bottom Y-Direction
1	1	0.0400	0.0400	0.0160	0.0160
	2	0.0110	0.0120	0.0160	0.0110
	3	0.0120	0.0110	0.0110	0.0160
	4	-	-	0.0110	0.0110
2	1	0.0700	0.0700	0.0300	0.0300
	2	0.0200	0.0236	0.0300	0.0200
	3	0.0236	0.0200	0.0200	0.0300
	4	-	-	0.0200	0.0200
3	1	0.1004	0.1004	0.0386	0.0386
	2	0.0264	0.0299	0.0386	0.0264
	3	0.0299	0.0264	0.0264	0.0386
	4	-	-	0.0264	0.0264
4	1	0.0550	0.0378	0.0236	0.0162
	2	0.0179	0.0120	0.0157	0.0162
	3	0.0120	0.0120	0.0236	0.0120
	4	-	-	0.0157	0.0120
5	1	0.0427	0.0305	0.0183	0.0129
	2	0.0139	0.0120	0.0122	0.0129
	3	0.0120	0.0120	0.0183	0.0120
	4	-	-	0.0122	0.0120

Table 5.3: Reinforcement Details (Cont'd)

Slab	Quadrant	Reinforcement areas (in^2/in)			
		Top X-Direction	Top Y-Direction	Bottom X-Direction	Bottom Y-Direction
6	1	0.0280	0.0250	0.0090	0.0090
	2	0.0150	0.0090	0.0090	0.0090
	3	0.0090	0.0090	0.0140	0.0090
	4	-	-	0.0090	0.0090
7	1	0.0380	0.0250	0.0090	0.0090
	2	0.0200	0.0090	0.0090	0.0090
	3	0.0130	0.0090	0.0130	0.0090
	4	-	-	0.0090	0.0090
8	1	0.0260	0.0260	0.0100	0.0100
	2	0.0100	0.0100	0.0100	0.0140
	3	0.0100	0.0100	0.0140	0.0100
	4	-	-	0.0100	0.0100
9	1	0.0360	0.0360	0.0100	0.0100
	2	0.0100	0.0100	0.0100	0.0200
	3	0.0100	0.0100	0.0200	0.0100
	4	-	-	0.0120	0.0120
10	1	0.0560	0.0560	0.0100	0.0100
	2	0.0100	0.0100	0.0100	0.0300
	3	0.0100	0.0100	0.0300	0.0100
	4	-	-	0.0180	0.0180

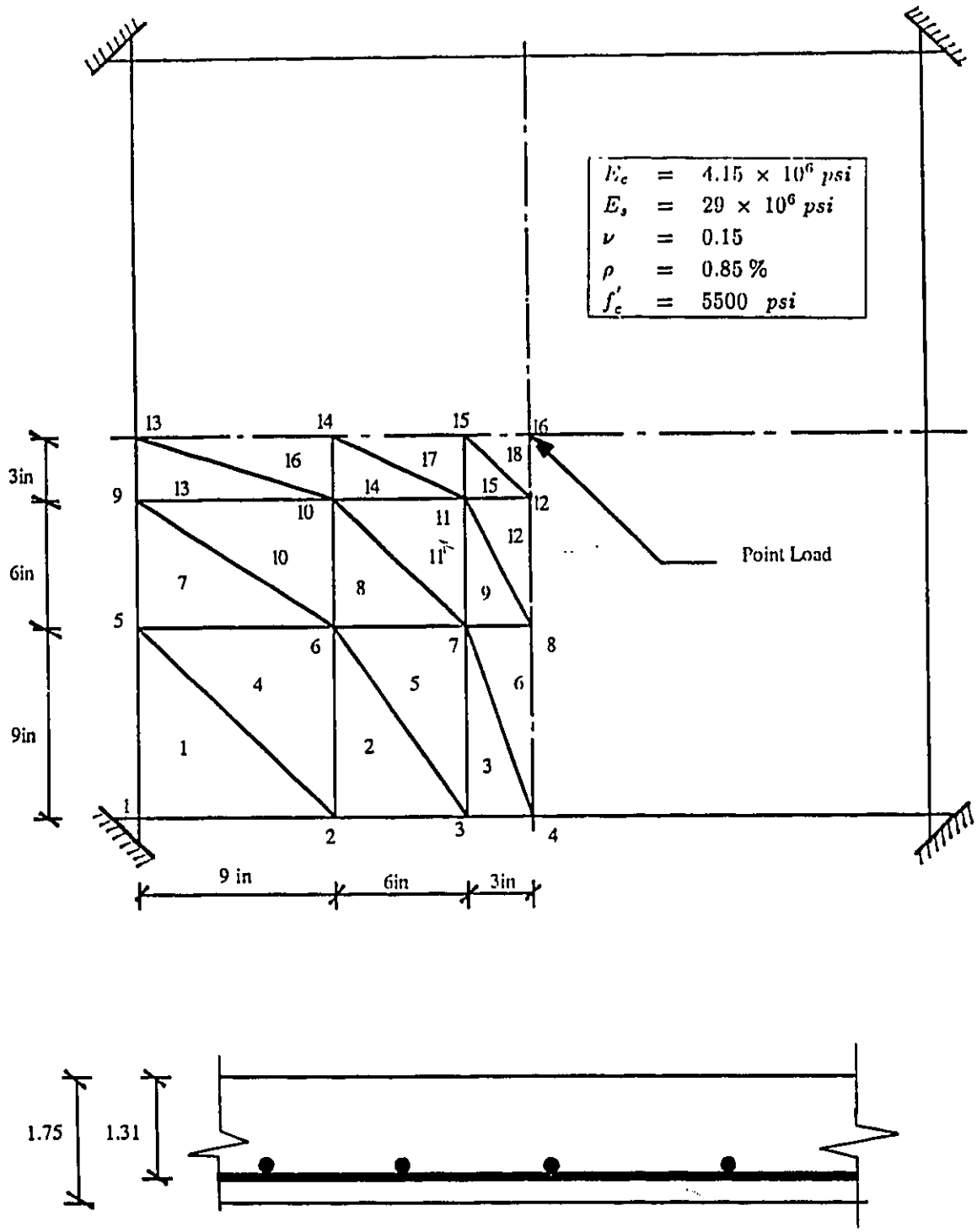

Figure 5.1: McNeice Slab: Details and Material Properties

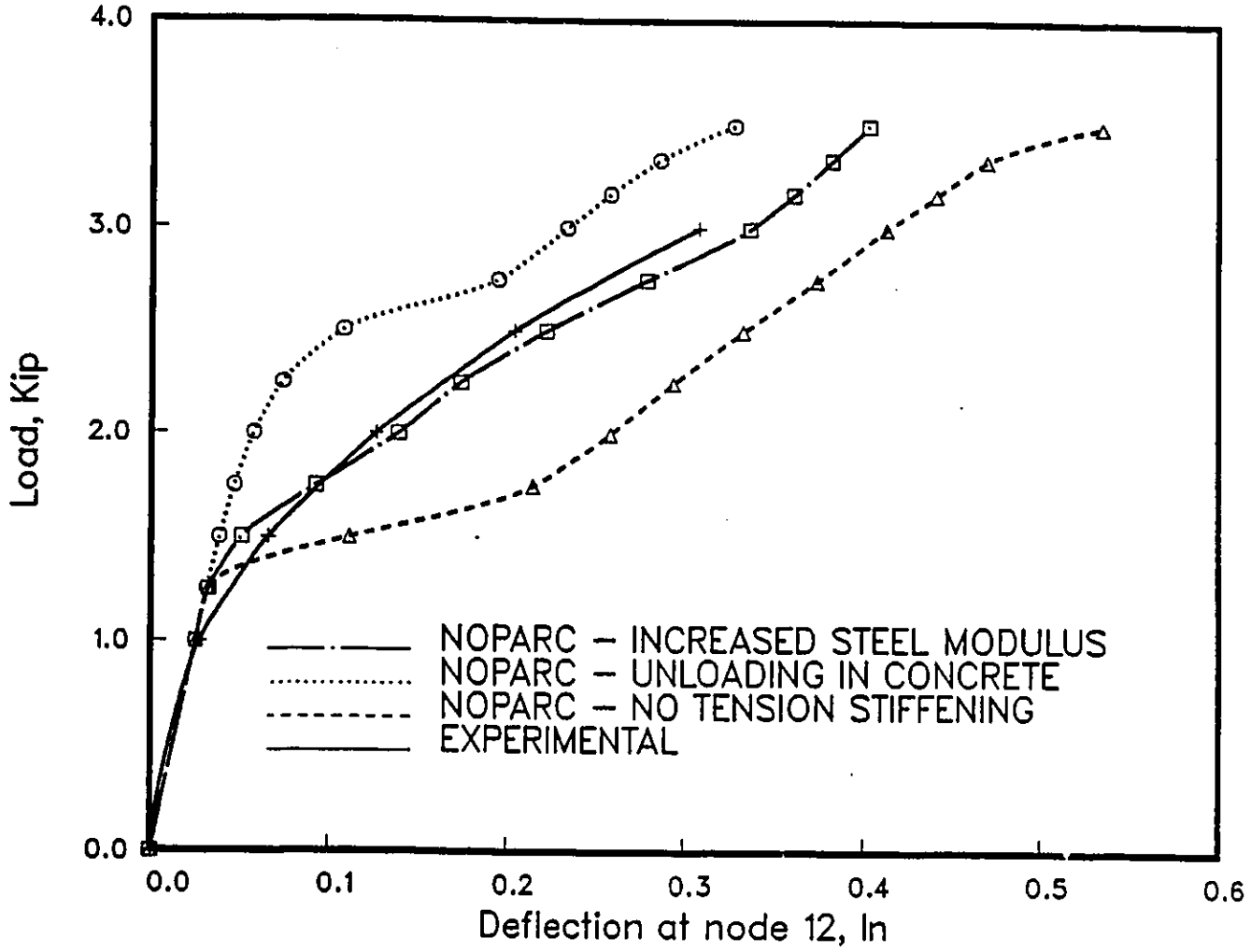

Figure 5.2: McNeice Slab: Load-Deflection Plot ($f_r = 550$ psi)

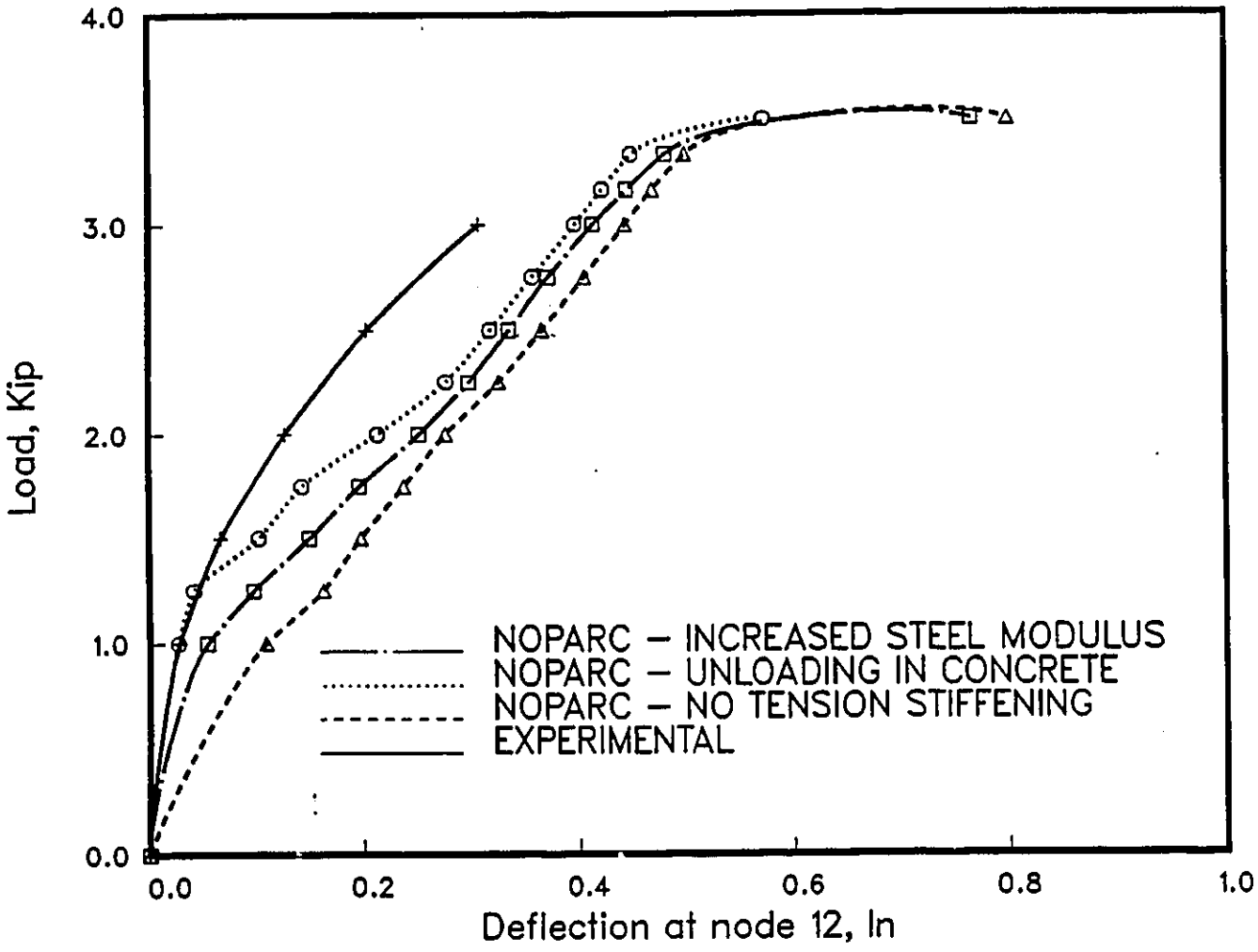

Figure 5.3: McNeice Slab: Load-Deflection Plot ($f_r = 225$ psi)

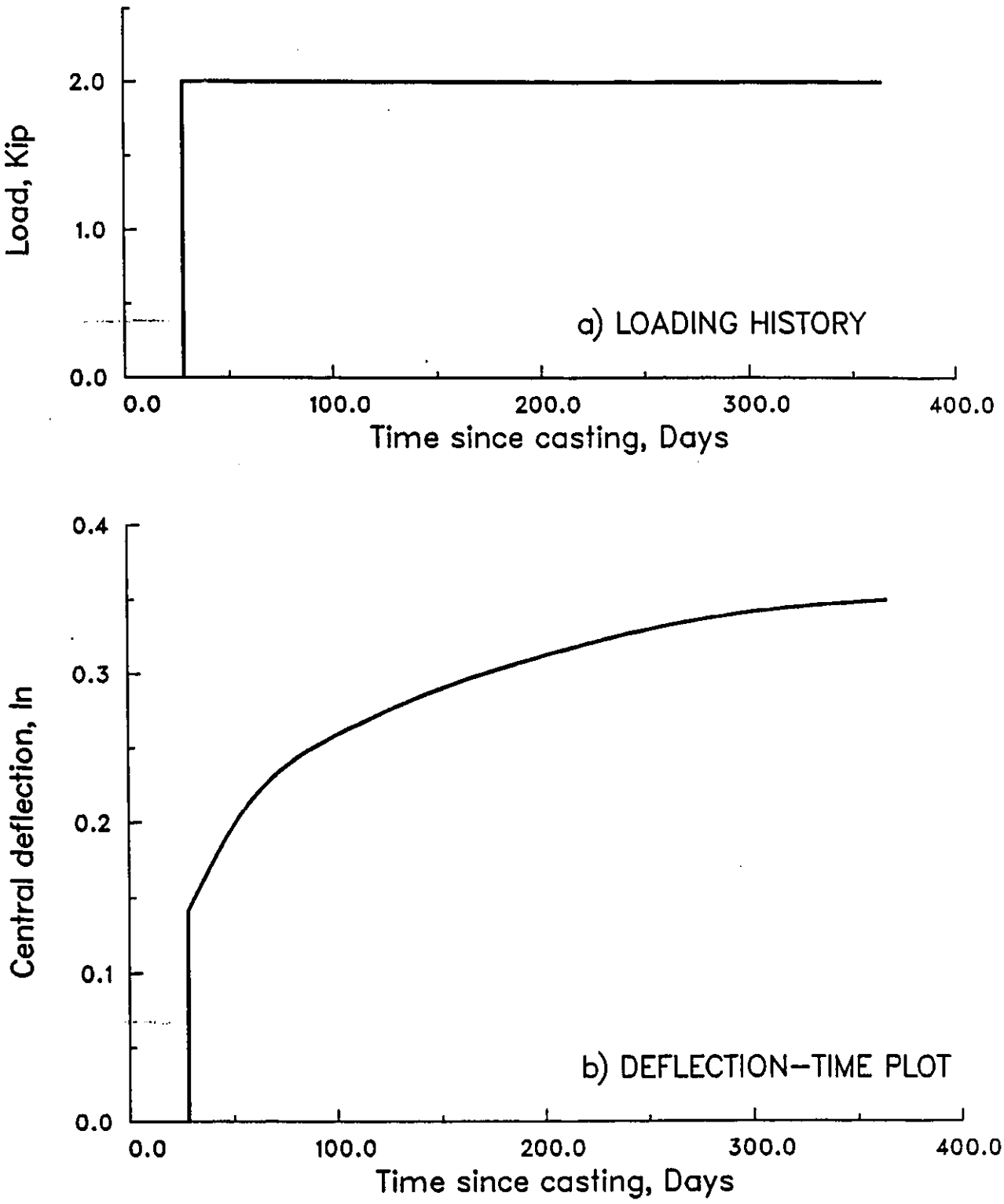

Figure 5.4: McNeice Slab: Loading History and Deflection-Time Plot

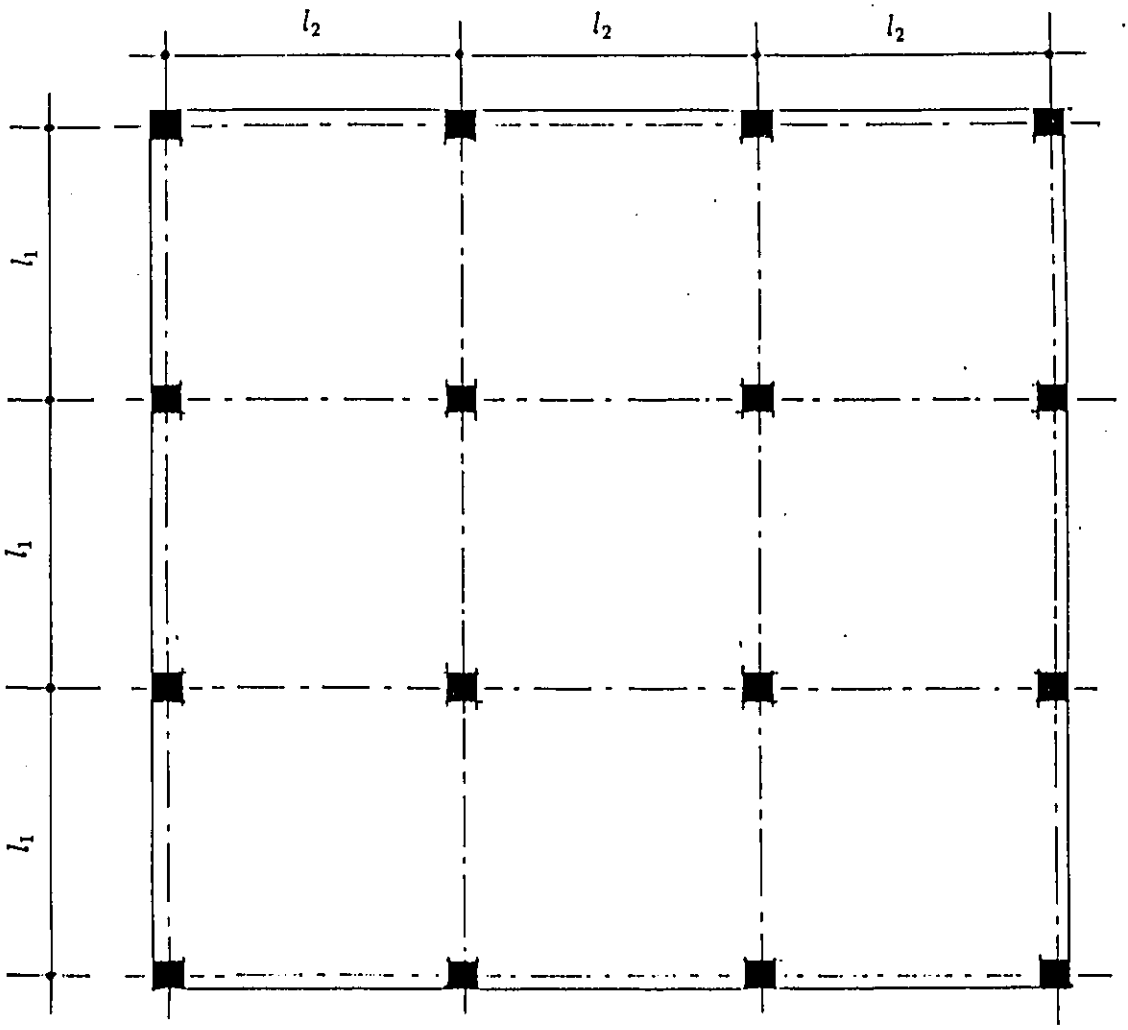

Plan View

All columns 26 *in* × 26 *in*

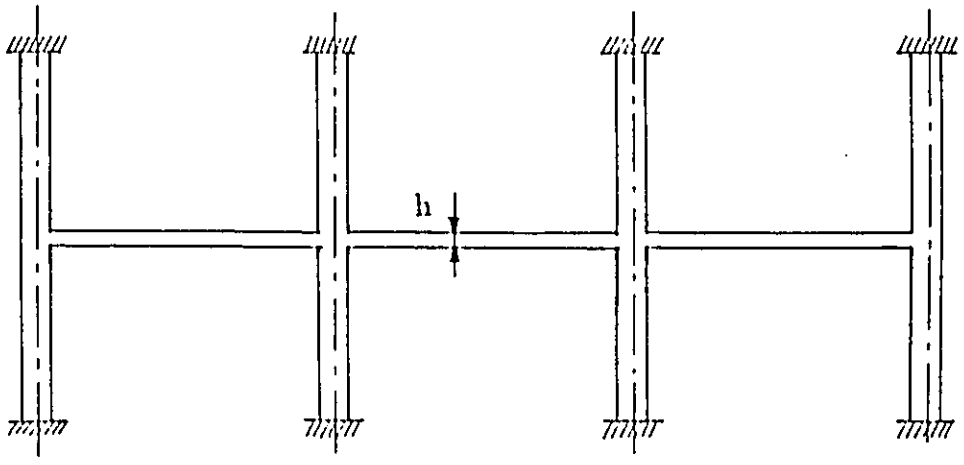

Elevation

Figure 5.5: Slab Details

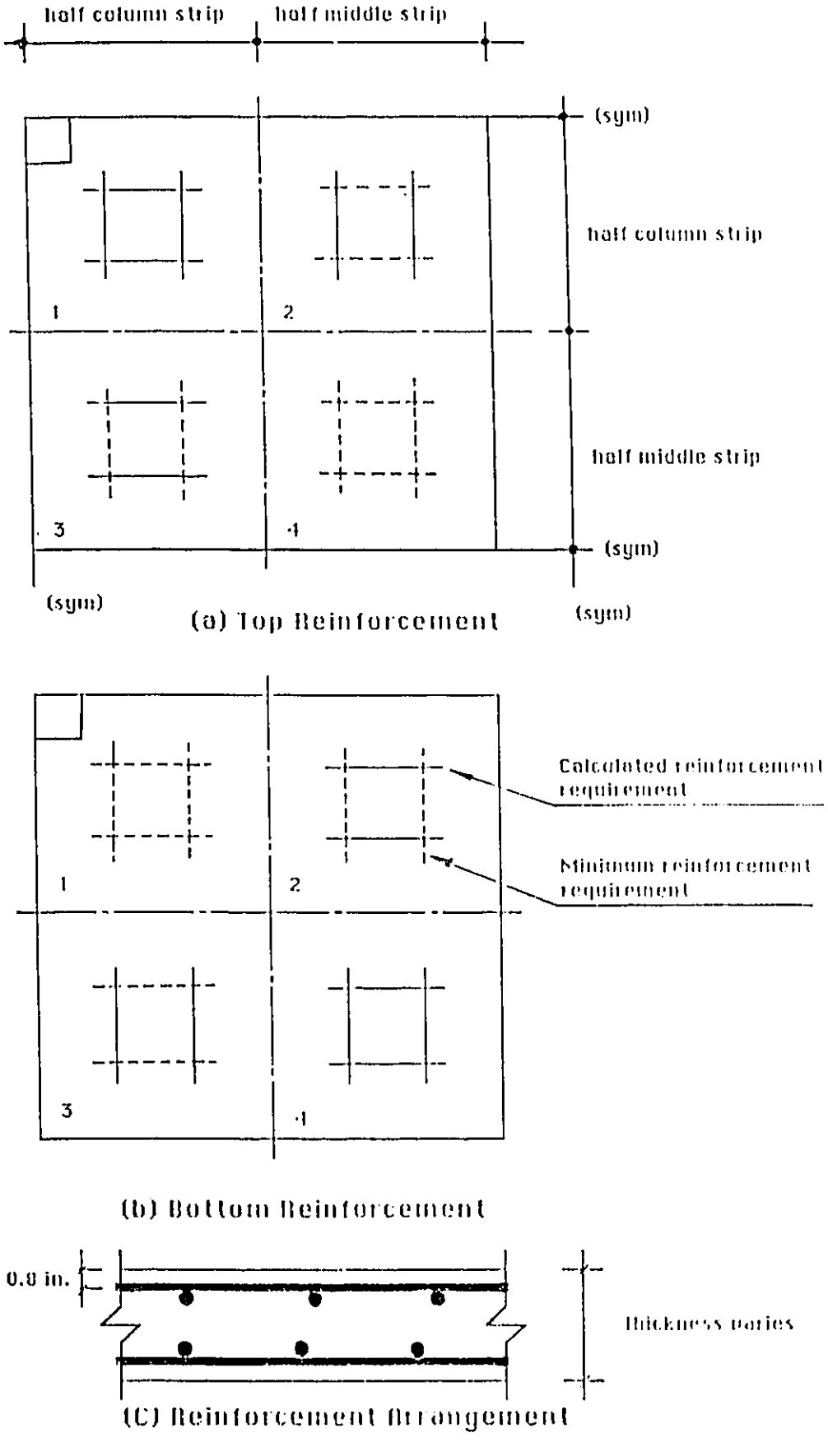

Figure 5.6: Reinforcing Steel Details

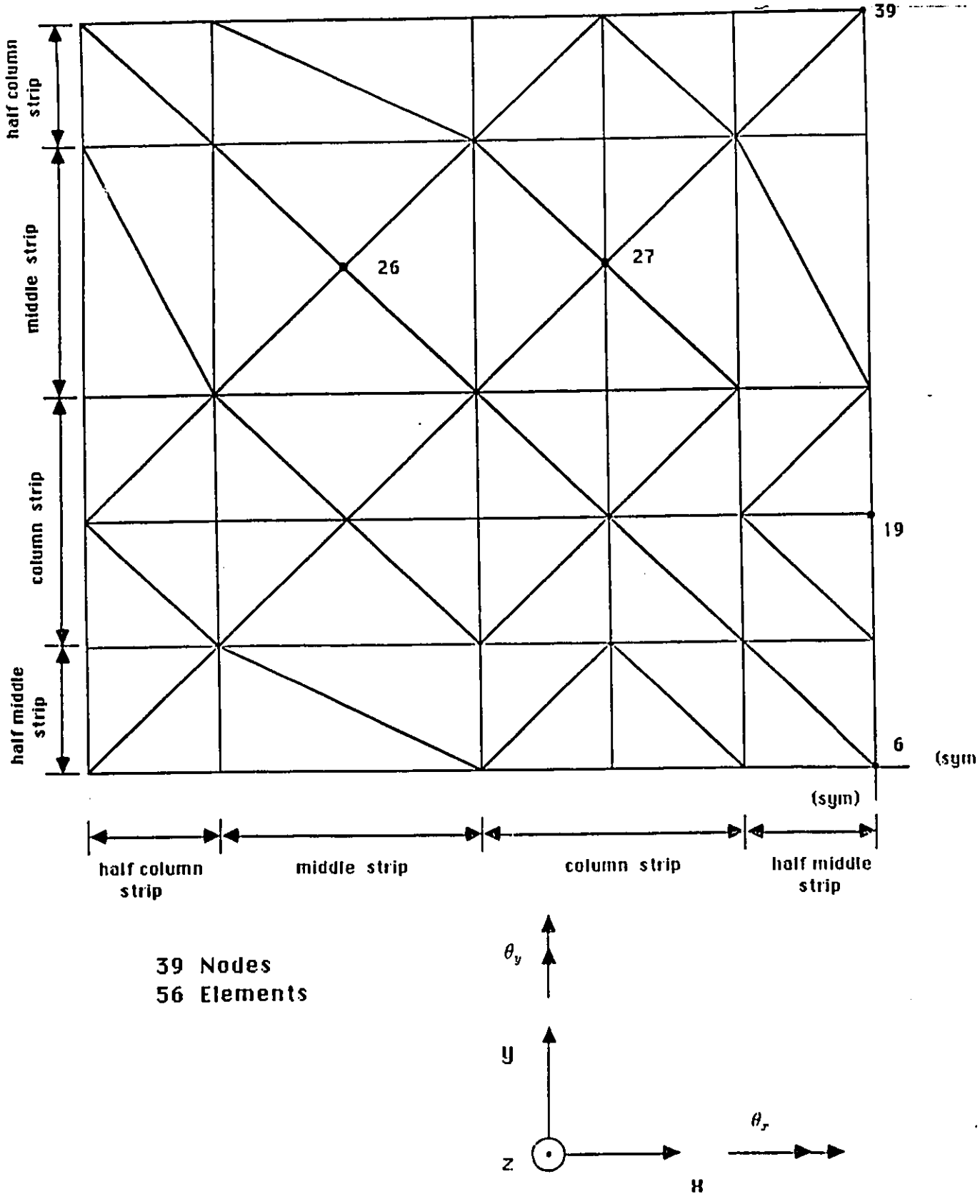

Figure 5.7: Finite Element Grid

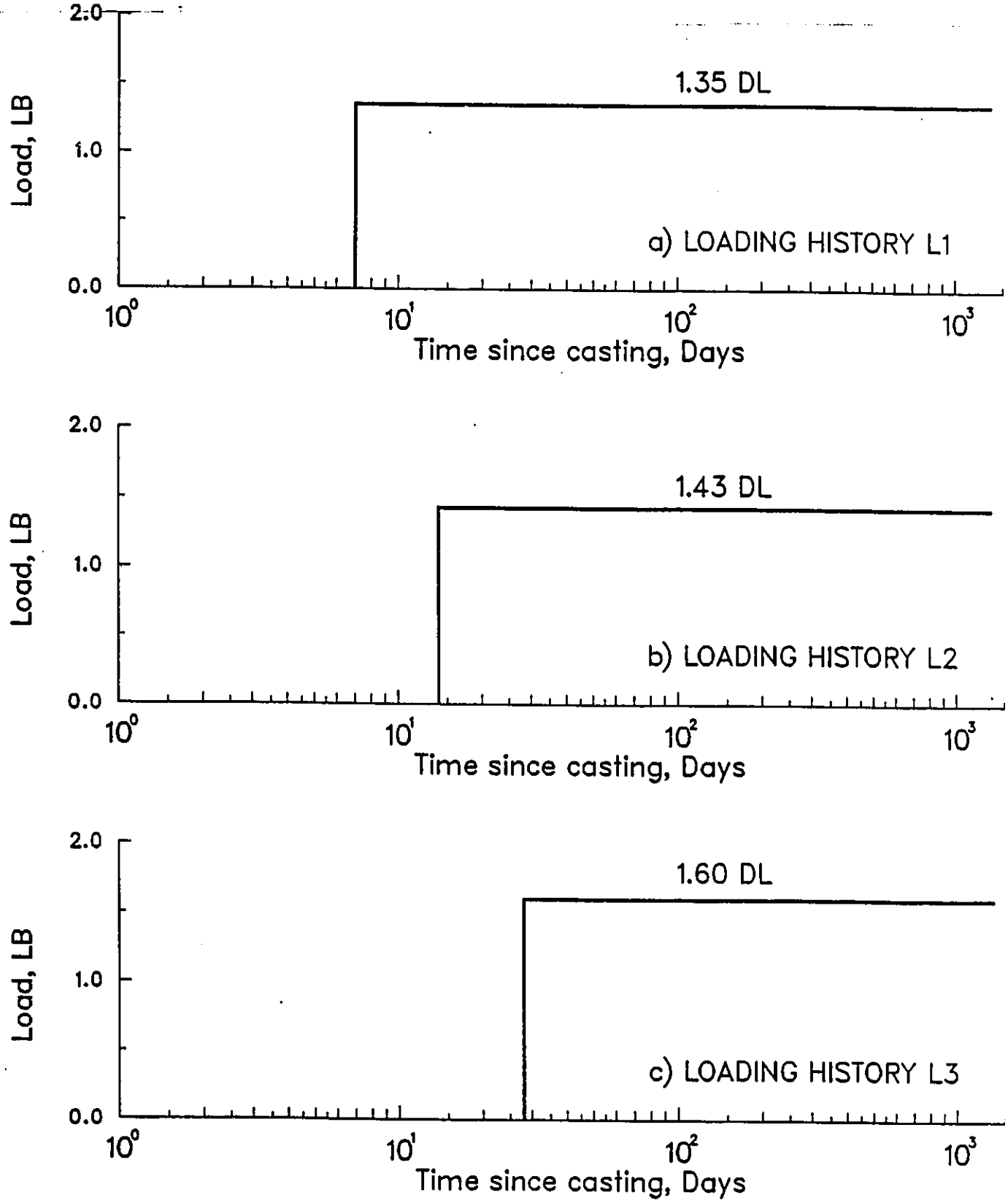

Figure 5.8: Loading Histories for the Analyzed slabs

Chapter 6

PRESENTATION AND DISCUSSION OF RESULTS

6.1 General

It has been generally recognized by many investigators, including Gilbert [60] and Scanlon [28] that the main factors affecting slab behaviour can be broadly categorized into those associated with:

- Material properties
- Slab geometry (including quantity and location of reinforcement and the boundary conditions)
- Environment (in particular, average relative humidity)
- load history and construction procedures

In calculating two-way slab deflections, several additional factors need to be considered and must all be modelled adequately namely; the three dimensional nature of the slab, the influence of cracking and tension stiffening and the development of biaxial creep and shrinkage strains.

In addition, the final deflection of a slab depends on the extent of initial cracking which, in turn, depends on the construction procedures, the amount of early shrinkage, the degree of curing and so on [61]. In recent field measurements of the deflection of many supposed identical panels [39, 62] a large variability was reported. Deflections of identical panels after one year differed by over 100 percent in some cases.

6.2 Deflection Criteria

Calculated deflections will be compared with the present code deflection limits as well as a limit on total deflections. The present code provisions require calculated slab deflections to be less than $l/360$ for live loads as well as $l/240$ or $l/480$ for incremental deflections. Although ACI 318-83 and CSA A23.3-M84 codes contain no specified limit on total deflections, other codes, including the British [63] and Australian [64] codes, do include limits on calculated total deflections. For this study, a limit of $l/240$ on total deflections recommended by ACI Subcommittee 435 [65] for outdoor decks as well as a limit of $l/200$ recommended by Thompson and Scanlon[7] will be considered. The span length l defined only in the ACI and CSA codes for beams will be taken as the clear span length of the diagonal between opposite column corners when considering midpanel deflections.

6.3 Results and Discussion

The calculated midpanel deflections for interior panels versus time curves under the different loading cases (L1, L2, and L3) are shown in Fig. 6.1 through Fig. 6.5, and a summary of the midpanel deflections of the interior and exterior panels of the test series is given in Tables 6.1 and 6.2 along with the long-term to short-term deflection ratio. Calculated deflections in exterior panels of equal span lengths were found to be considerably larger (some 80 %) than the appropriate interior panels. In the following discussion only the midpanel deflections for interior panels will be considered.

Close examination of the long-term deflections of Tables 6.1 and 6.2 indicates an interaction between creep, shrinkage, the age at first loading, and the sustained load and these effects can not be considered separately and summed. Under load history L2, slab S1 is largely uncracked, may have only localized cracking over the supports resulting in low immediate deflection but a large time-dependent effect. However, under load history L3 extensive cracking occurs throughout the slab, but the long-term deflection is only slightly greater than for the similar slab under load history L2. It is equally interesting to note that the long-term to short-term deflection ratio in case L2 is slightly higher than the value obtained under load history L3. In the case of load history L1, the slab S1 suffers the biggest long-term deflection for this series of slabs, and the highest ratio of the long-term to short-term deflection is obtained. This is primarly because the slab was loaded at an early age resulting in large creep effects and shrinkage deflections. Similar results were obtained in Test Series S2 through Test Series S5.

The effect of varying the ratio of long span to short span (panel aspect ratio β) on the deflection versus time curves is illustrated in Fig. 6.6. The aspect ratio, β, affects the long-term deflection in the same manner it af-

fects the short-term deflection, however the highest long-term to short-term deflection ratio occurs when β is equal to 1.5 (Test Series S6). A similar result was obtained by Gilbert [60].

Fig. 6.7 demonstrates the sensitivity of the calculated midpanel slab deflections using different live load to dead load ratios (L/D) with attendant different steel ratios. It appears that the effect of varying L/D has a marked influence on the magnitude of the long-term deflections. Slabs designed using high live load/dead load ratios resulted in low long-term deflections and vice versa. In general, due to the amount of the reinforcing steel needed by the higher live load to dead load ratio slabs, the calculated long-term deflection is reduced.

Fig. 6.8 shows the variation of the ultimate midpanel deflections with span-to-depth (l/h) ratio for Test Series S1 and S9. As can be seen; for the narrow range of slab thicknesses considered, the ultimate deflections varied significantly. It would appear that the influence of cracking on slab stiffness increases with larger l/h ratios.

Table 6.3 compares calculated slab deflections at midpanel for an inner and outer panel with the code permissible deflections specified in CSA3 -A23.3 M84. Also calculated deflections are compared with the selected limits on net total deflections. The table indicates the following:

- In all cases simulated in this thesis, computed live load deflections are well within the permissible limit of $l/360$.
- The selected incremental deflection limit proved to be critical in the case of a rectangular panel having its aspect ratio $\beta = 1.5$, and in the case of a square panel when the live load to dead load ratio L/D is equal to 0.5.

- Calculated total deflections met the deflection limit of $l/200$, while the code specified limit of $l/240$ for some of the simulated cases proved to be difficult to satisfy. For Test Series S6 ($\beta = 1.5$) and Test Series S8 ($L/D = 0.5$), neither the code limit of $l/240$ nor the recommended $l/200$ limit is satisfied.

- Both calculated total deflections and calculated incremental deflections in exterior panels for the whole test series of slabs investigated in this study do not meet the code specified permissible deflections. The boundary conditions particularly the discontinuity at the edge of the panel resulted in excessive exterior panel deflections. It is concluded therefore that the thickness of an exterior corner panel needs to be increased to control deflections by satisfying code limits.

Using the computer simulation deflections and assuming that the deflection is inversely proportional to h^3; the thicknesses required to satisfy the code-specified permissible deflections are calculated. Table 6.4 summarises the calculated thicknesses. Comparing the required thicknesses determined to satisfy $l/240$ limit on total deflection in Table 6.4 and the thicknesses given by CSA A23.3 M-84 (Eq. 9.9 in the present code) reveals that this equation is inconsistent of insuring a thickness that would satisfy the less restrictive criterion on permitted total deflections. Scanlon [7] arrived to the same conclusion and suggested a limit of $l/200$. In addition, Table 6.4 indicates that an increase of the thickness by at least 15 percent in panels with discontinous edges would be more appropriate than the current recommendation of 10 percent. The principal reason for this is that many factors affecting the true magnitude of the long-term deflections have been ignored such as the loads resulting from the construction method which have a greater influence on slab deflections than service live loads.

As a first approach to tackle this problem, the following equation is pro-

posed which take into account the age of concrete at the time of loading, the construction loads, and slab design live load/dead load.

$$h > \frac{l_n\,[\,(\epsilon_{sh})_t + f_y \times K_1 \times K_2 \times C_t\,]}{36,000 + 5000\beta(1+\beta_s)} \tag{6.1}$$

where,

l_n	= clear span length
$(\epsilon_{sh})_t$	= shrinkage strain after t days of drying
K_1	= construction load factor expressed in term of dead load
K_2	= factor to account for the age of concrete at the time of loading
C_t	= creep coefficient after t days of loading
β	= ratio of long to short clear spans
β_s	= ratio of length of continuous edges to total perimeter of a slab panel

K_1 and K_2 are given by the following equations:

$$K_1 = \frac{construction\ load}{1.25D + 1.5L} \tag{6.2}$$

$$K_2 = \frac{E_c(28)}{E_c(t)} = \sqrt{\frac{4.2 + 0.85t}{t}} \tag{6.3}$$

Eq. 6.1 was derived using the $l/200$ criterion. At ultimate this equation can be rewritten as

$$h > \frac{l_n\,[\,800 + f_y \times K_1 \times K_2 \times K_3 \times C_u\,]}{36,000 + 5000\beta(1+\beta_s)} \tag{6.4}$$

where K_3 is factor given by:

$$K_3 = 1.25\,t^{-0.118}\,(1 - \frac{t^{0.6}}{10 + t^{0.6}}) \tag{6.5}$$

Comparing the maximum span to thickness ratio given by the proposed equation with the maximum span to thickness ratio determined using the thickness given by the computer simulation in Table 6.5 indicates that the prediction formulae gives comparable results only for loading history L1. The origin of this discrepancy can be attributed to the term K_3 in Eq. 6.4. To remedy to this Eq. 6.4 is modified resulting in the following equation:

$$h > \frac{l_n\,[\,800 + f_y \times K_1 \times K_2 \times K_3\,]}{36,000 + 10,000\beta} \tag{6.6}$$

where K_1, K_2, and K_3 are terms reflecting the construction load effect, the age of the slab at first loading, and the creep effect and are given respectively by the following equations:

$$K_1 = \frac{construction\ load}{1 + 1.2(L/D)} \tag{6.7}$$

$$K_2 = \frac{E_c(28)}{E_c(t)} = \sqrt{\frac{4.2 + 0.85t}{t}} \tag{6.8}$$

$$K_3 = 1 + 1.25\,t^{-0.118}\,(\frac{\tau^{0.6}}{10 + \tau^{0.6}} - \frac{t^{0.6}}{10 + t^{0.6}})C_u \tag{6.9}$$

where,

τ = age at which the analysis is required

t = age of the concrete at loading

Table 6.5 summarizes the maximum span/thickness ratios given by the present formulae described above. The comparison shown in this table indicates that Eq. 6.6 gives satisfactory agreement with the maximum span/thickness ratio predicted by the computer simulation and can be used to specify minimum thickness of flat plates.

Table 6.6 compares the Span/thickness ratios calculated from Eq. 6.6 with the ACI 318–CSA A23.3 ratios and Scanlon's suggestion [7]. The table shows clearly the influence of construction schedule on limiting span/thickness ratio while satisfying the $l/200$ limiting deflection requirement. Note that the construction loads used, which relate to shore reshore system, are examples only and can be changed.

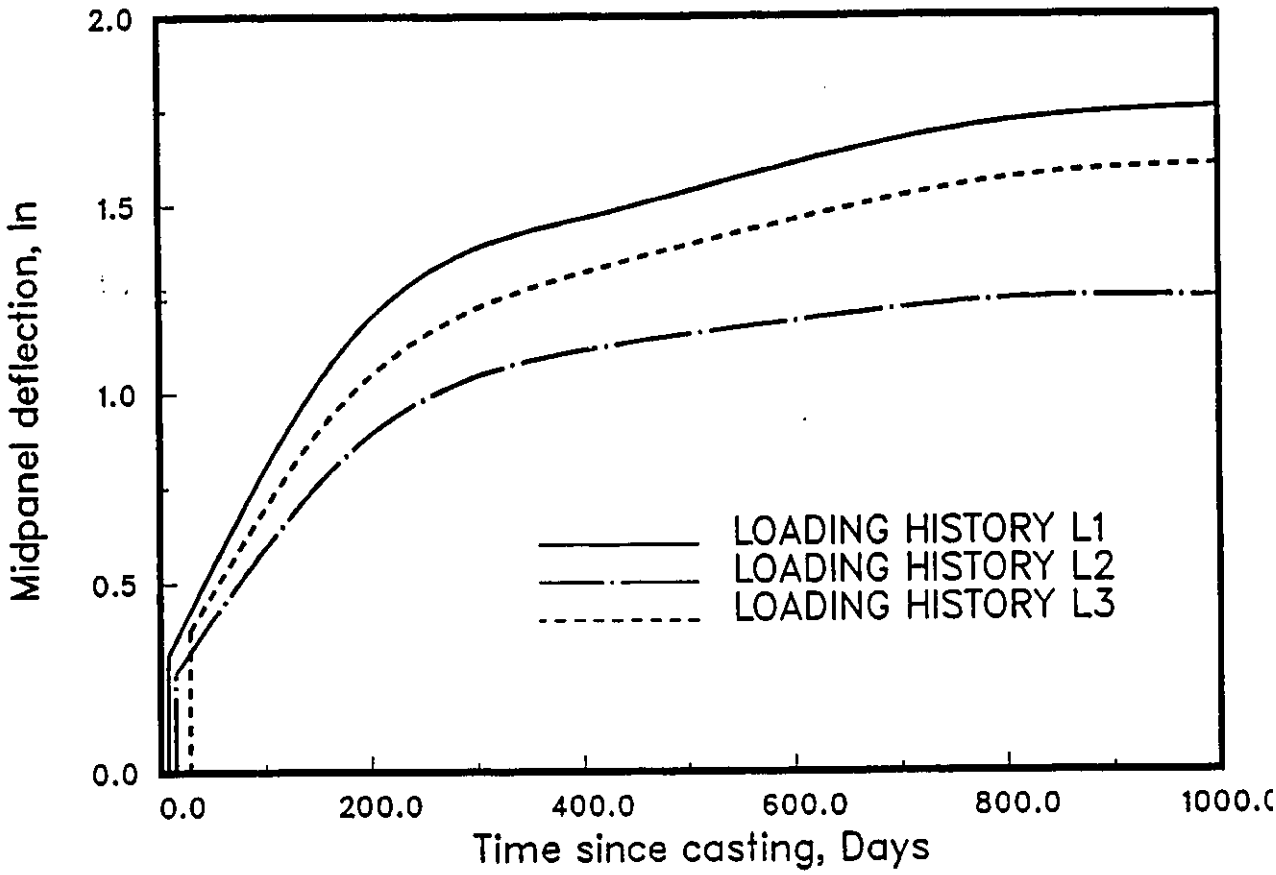

Figure 6.1: Test Series S1: Calculated Long-term Deflections

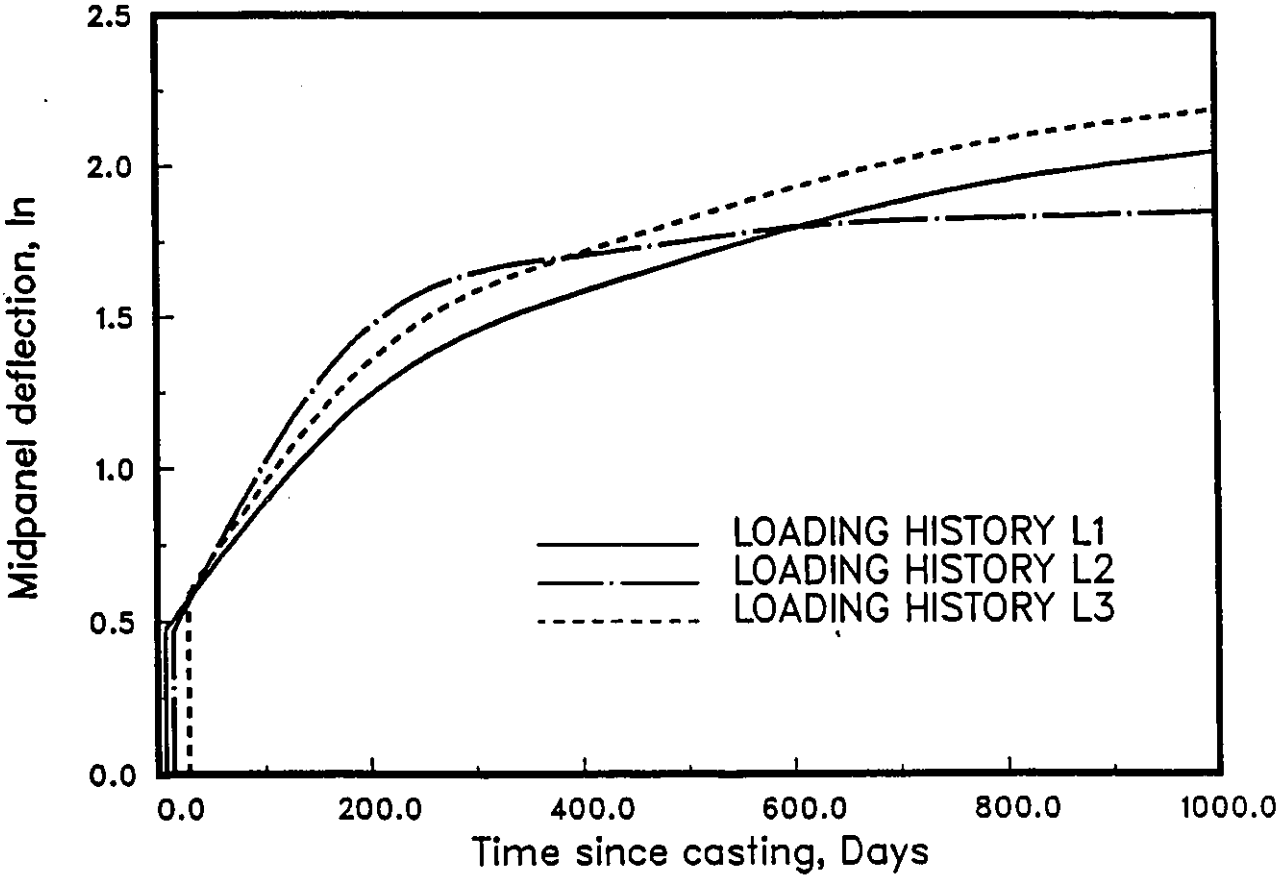

Figure 6.2: Test Series S2: Calculated Long-term Deflections

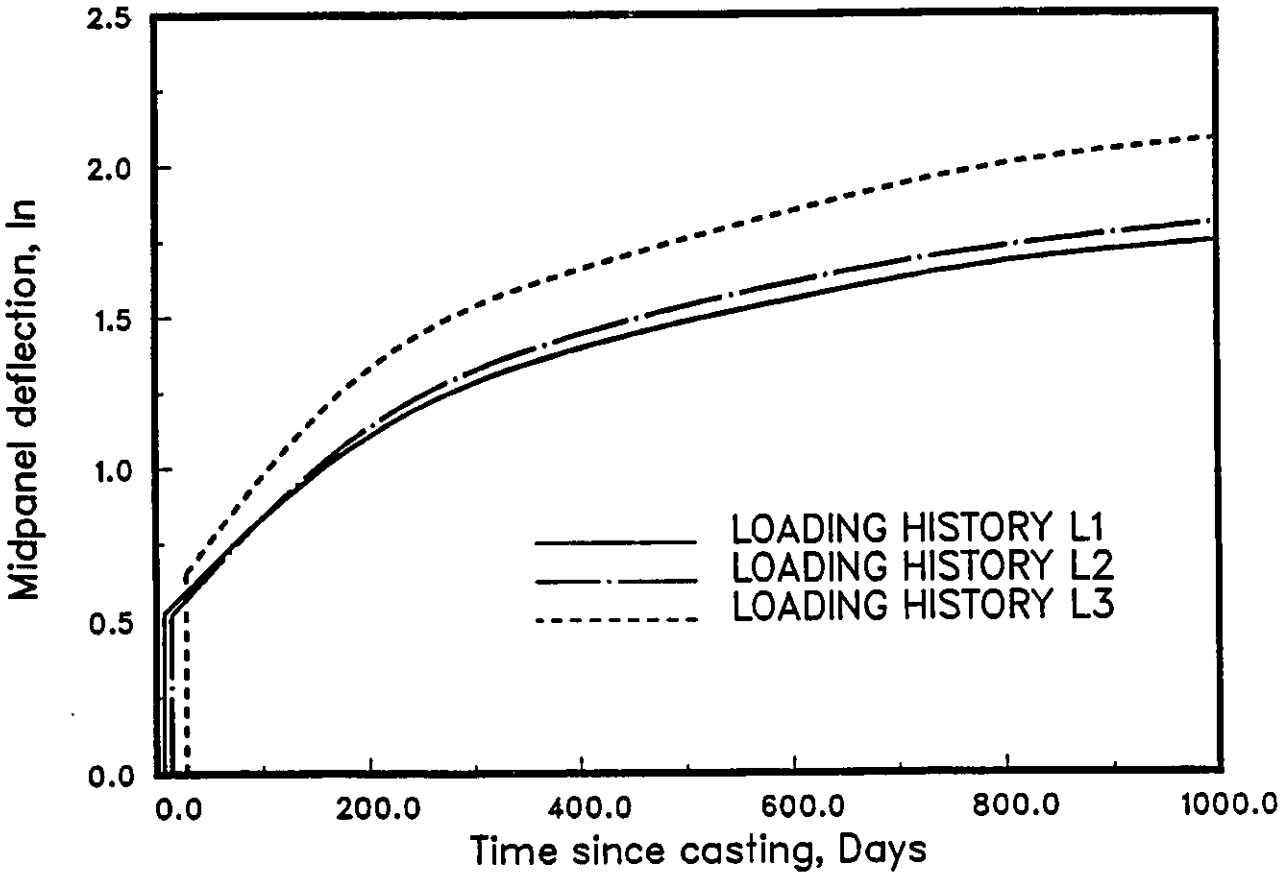

Figure 6.3: Test Series S3: Calculated Long-term Deflections

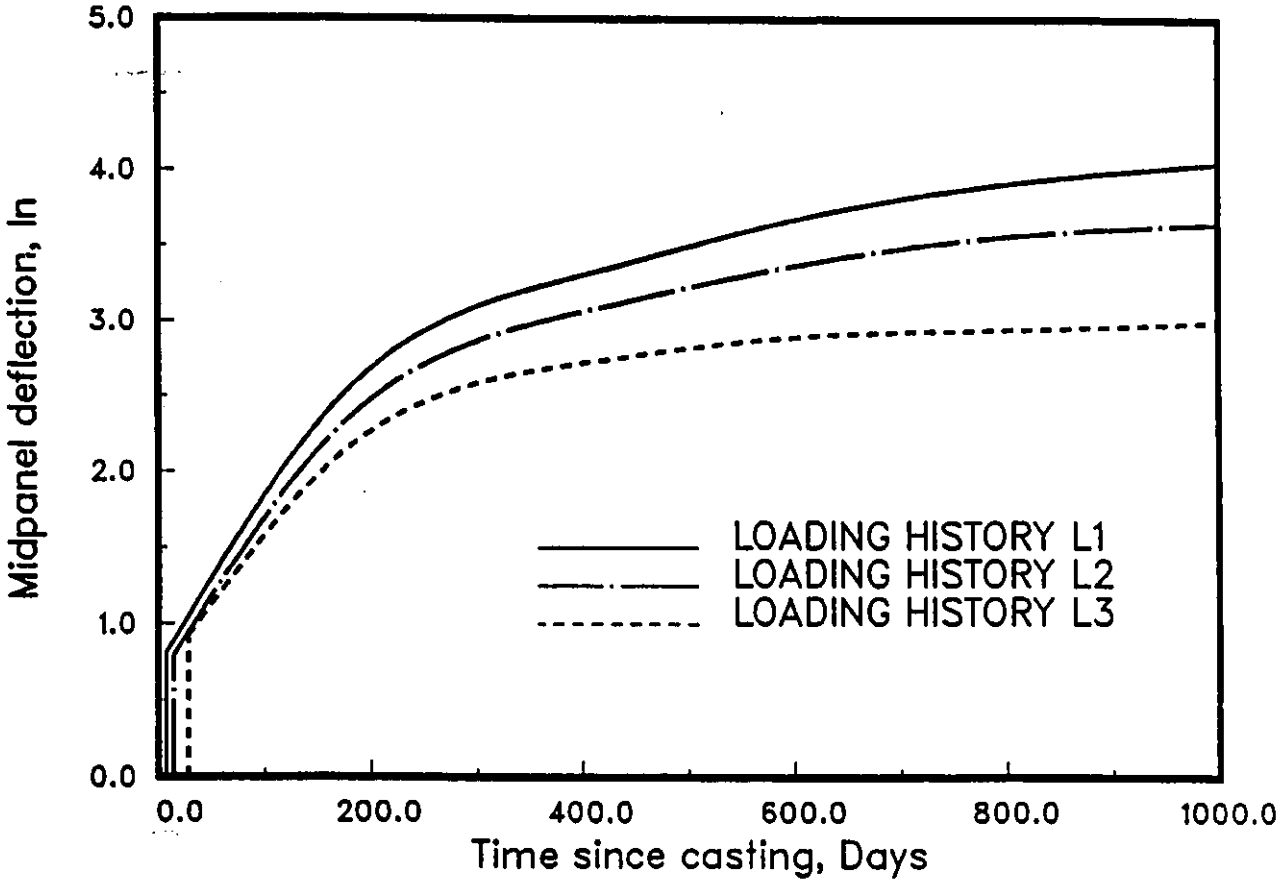

Figure 6.4: Test Series S4: Calculated Long-term Deflections

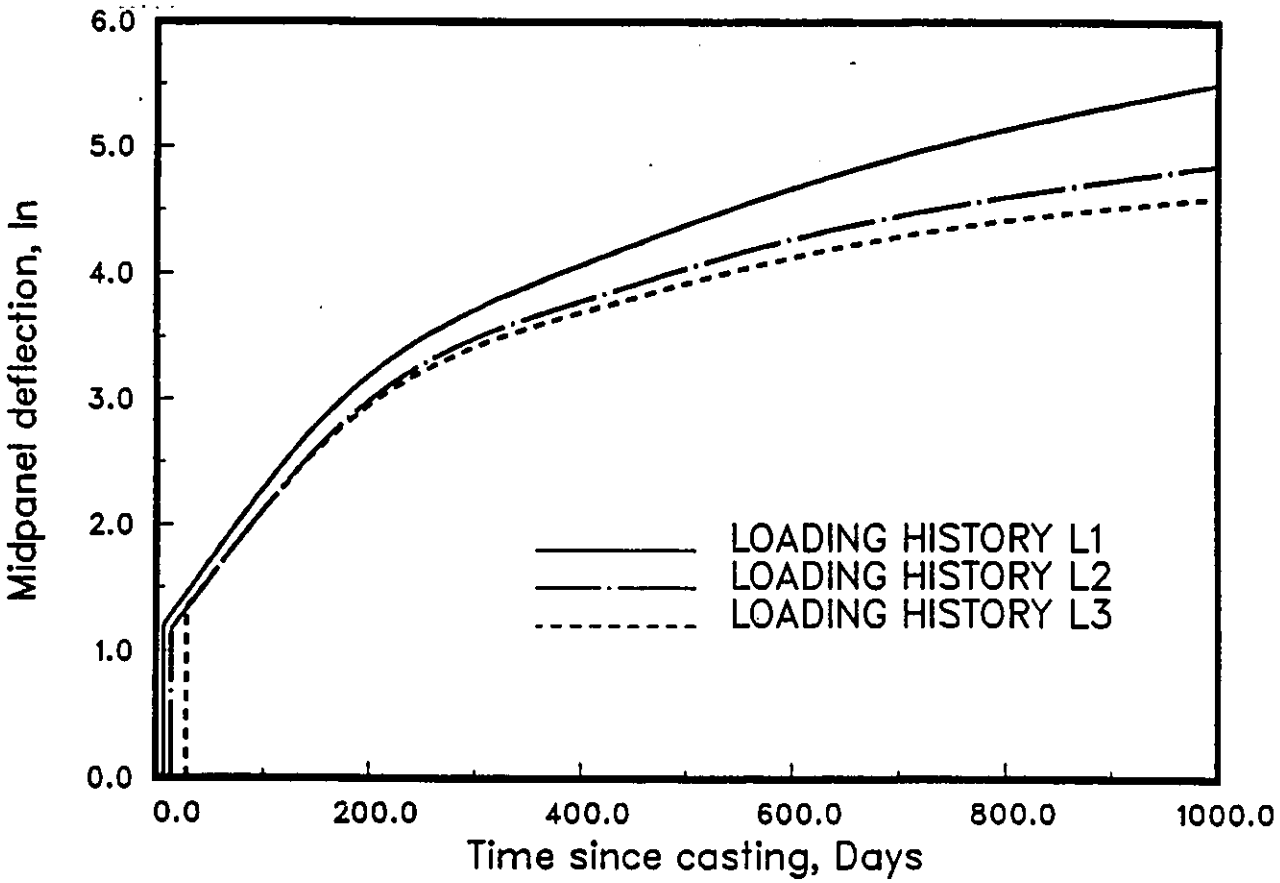

Figure 6.5: Test Series S5: Calculated Long-term Deflections

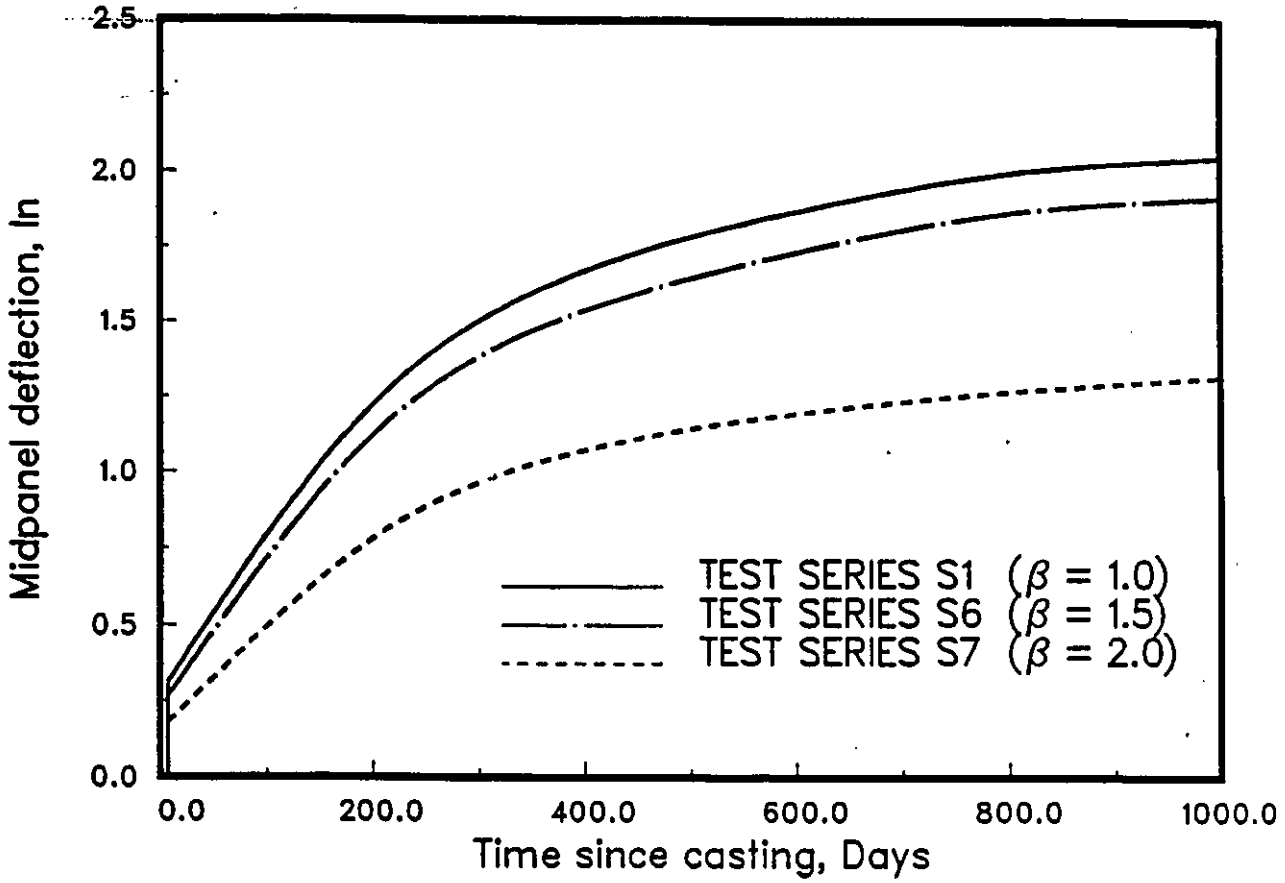

Figure 6.6: Effect of Panel Aspect Ratio on Calculated Long-term Deflections

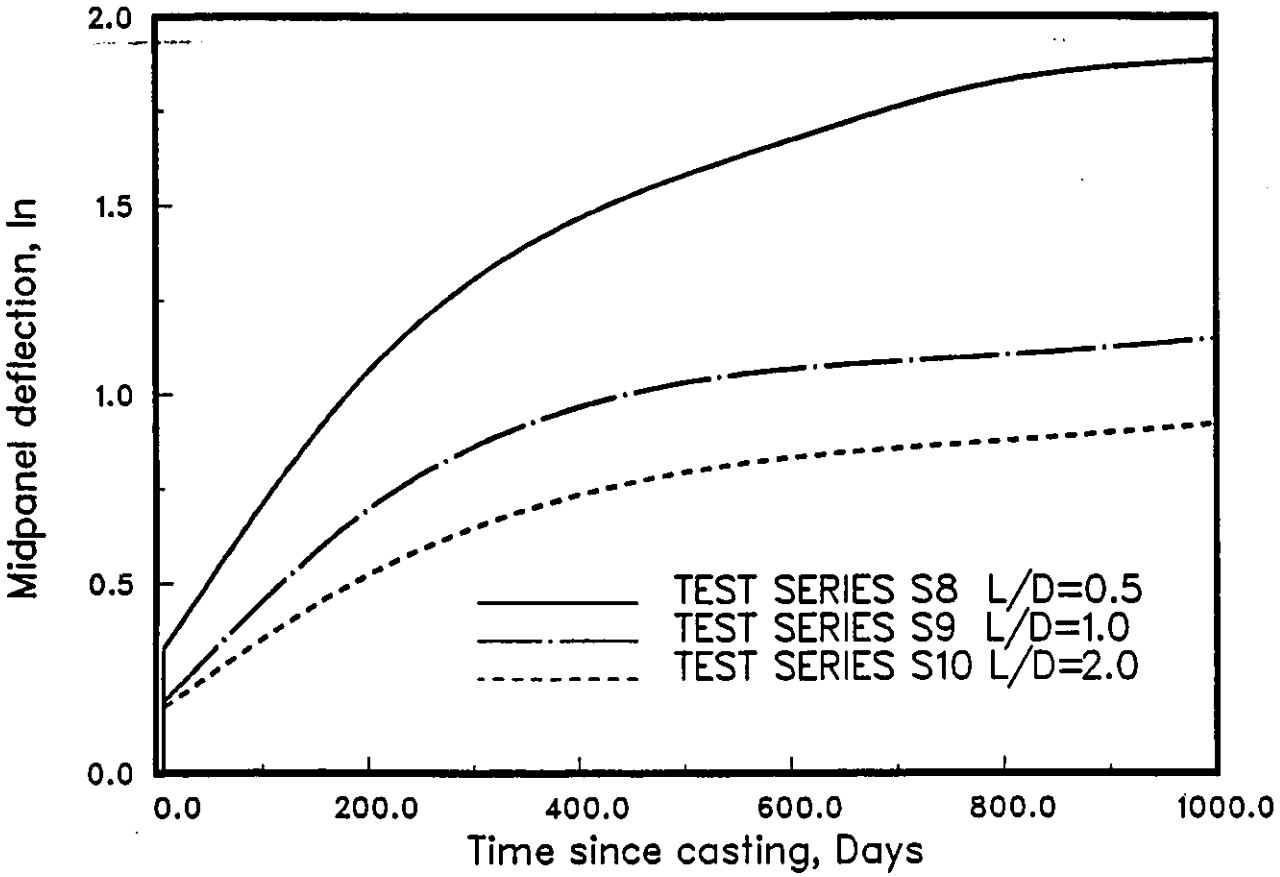

Figure 6.7: Effect of Live Load/Dead Load Ratio on Calculated Long-term Deflections

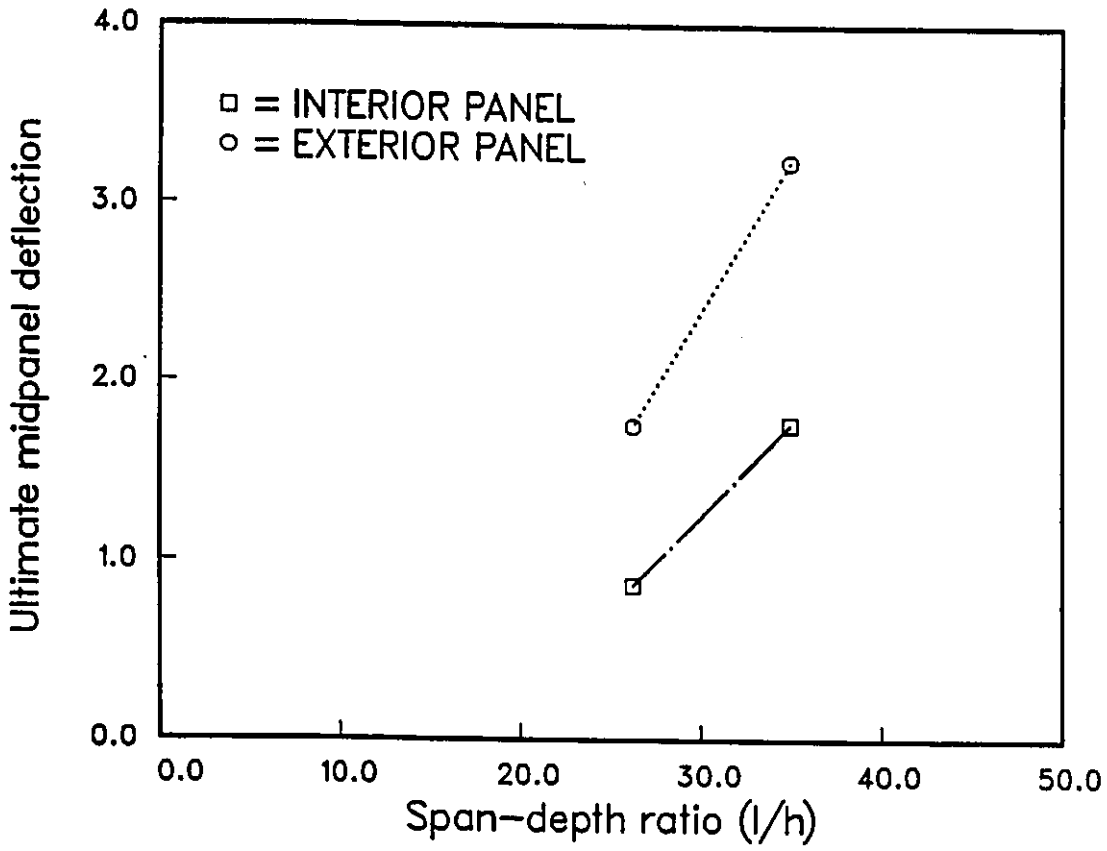

Figure 6.8: Variation of Calculated Long-term Deflections and Span-to-Depth (l/h) Ratio

Table 6.1: Deflection at Node 6

Slab	Loading history	Immediate deflection (in)	1000-day deflection (in)	Total long-term deflection (in)	Incremental deflection 180-1000 days (in)	Long-term to short-term deflection ratio
S1	L1	0.30436	1.7569	1.4525	0.6084	4.77
	L2	0.25870	1.2242	0.9655	0.3617	3.73
	L3	0.37122	1.6077	1.2365	0.6034	3.33
S2	L1	0.46668	2.0495	1.5826	0.8574	3.38
	L2	0.46464	1.8033	1.3386	0.9993	2.88
	L3	0.58334	2.1890	1.6056	0.9389	2.75
S3	L1	0.51561	1.7473	1.2317	0.6787	2.38
	L2	0.50923	1.8084	1.2991	0.7145	2.55
	L3	0.64716	2.0846	1.4374	0.8029	2.55
S4	L1	0.79452	4.0492	3.2547	1.4702	4.09
	L2	0.78431	3.6498	2.8655	1.2656	3.65
	L3	0.91207	2.8383	1.9262	0.6477	2.11
S5	L1	1.1915	5.5014	4.3099	2.4319	3.60
	L2	1.1519	4.8575	3.7056	1.9845	3.20
	L3	1.3302	4.6002	3.2700	1.7537	2.46
S6	L1	0.26083	1.6476	1.3867	0.6020	5.31
S7	L1	0.17283	0.9941	0.8213	0.2677	4.75
S8	L1	0.32223	1.7975	1.4753	0.7948	4.58
S9	L1	0.17992	0.8613	0.6814	0.2002	3.78
S10	L1	0.16660	0.7962	0.6296	0.3034	3.77

Table 6.2: Deflection at Node 26

Slab	Loading history	Immediate deflection (in)	1000-day deflection (in)	Total long-term deflection (in)	Incremental deflection 180-1000 days (in)	Long-term to short-term deflection ratio
S1	L1	0.66044	3.2372	2.5767	1.1153	3.90
	L2	0.57900	2.5799	2.0009	0.8282	3.45
	L3	0.81282	2.7786	1.9658	1.0033	2.42
S2	L1	1.0229	3.3300	2.3071	2.0302	2.25
	L2	1.0027	2.9743	1.9716	1.5193	1.96
	L3	1.2075	3.4388	2.2313	1.3731	1.85
S3	L1	1.2891	3.0912	1.8021	1.1425	1.40
	L2	1.2974	3.1278	1.8304	1.1389	1.41
	L3	1.5676	3.4960	1.9284	1.1814	1.23
S4	L1	0.81382	3.3271	2.5133	1.1258	3.08
	L2	0.78125	2.9454	2.1641	0.9564	2.77
	L3	1.00160	2.7796	1.7780	0.6382	1.77
S5	L1	1.3764	6.5927	5.2163	3.3741	3.79
	L2	1.3034	5.7554	4.4520	2.7324	3.41
	L3	1.5594	6.5286	4.9692	3.2596	3.19
S6	L1	0.45908	2.4484	1.9893	0.9090	4.33
S7	L1	0.26855	1.6030	1.3344	0.4637	4.97
S8	L1	0.62808	2.7785	2.1504	1.1935	3.42
S9	L1	0.38198	1.7452	1.3632	0.3938	3.57
S10	L1	0.25076	1.2316	0.9808	0.5063	3.91

Table 6.3: Computed Slab Deflections and Code Permissible Deflections

Slab	Clear span (in)	Loading history	Computed Deflections (in)						Code Permissible Deflections			
			Inner panel			Outer panel						
			Δ_{tot}	Δ_{inc}	Δ_L	Δ_{tot}	Δ_{inc}	Δ_L	$l/200$	$l/240$	$l/480$	$l/360$
S1	210	L1	1.7569	0.6084	0.3044	3.2372	1.1153	0.6704	1.48	1.23	0.62	0.82
		L2	1.2242	0.3617	0.2587	2.5799	0.8282	0.5790				
		L3	1.6077	0.6034	0.3712	2.7786	1.0033	0.8128				
S2	304	L1	2.0495	0.8574	0.4667	3.3300	2.0302	1.0229	2.15	1.79	0.89	1.19
		L2	1.8033	0.9993	0.4646	2.9743	1.5193	1.0027				
		L3	2.1890	0.9389	0.5833	3.4388	1.3731	1.2075				
S3	374	L1	1.7473	0.6787	0.5156	3.0912	1.1425	1.2891	2.64	2.20	1.10	1.47
		L2	1.8084	0.7145	0.5092	3.1278	1.1389	1.2974				
		L3	2.0846	0.8029	0.6471	3.4960	1.1814	1.5676				
S4	250	L1	4.0492	1.4702	0.7945	3.3271	1.1258	0.8138	1.47	1.23	0.61	0.82
		L2	3.6498	1.2656	0.7843	2.9454	0.9564	0.7812				
		L3	2.8383	0.6477	0.9121	2.7796	0.6382	1.0016				
S5	270	L1	5.5014	2.4319	1.1915	6.5927	3.3741	1.3764	1.48	1.23	0.61	0.82
		L2	4.8575	1.9845	1.1519	5.7554	2.7324	1.3034				
		L3	4.6002	1.7537	1.3302	6.5286	3.2596	1.5594				
S6	210	L1	1.6476	0.6020	0.2608	2.4484	0.9090	0.4591	1.24	1.03	0.51	0.68
S7	210	L1	0.9941	0.2677	0.1728	1.6030	0.4637	0.2685	1.14	0.95	0.47	0.63
S8	210	L1	1.7975	0.7948	0.3222	2.7785	1.1935	0.6281	1.48	1.23	0.62	0.82
S9	210	L1	0.8613	0.2002	0.1799	1.7452	0.3938	0.3819	1.48	1.23	0.62	0.82
S10	210	L1	0.7962	0.3034	0.1666	1.2316	0.5063	0.2507	1.48	1.23	0.62	0.82

Table 6.4: Required Thickness at 1000 Days

Slab	Clear span (in)	Actual thickness (in)	Thickness (in) (CSA A23.3 M84)		Loading history	Required thickness (in) to satisfy code limits					
						$l/200$		$l/240$		$l/480$	
			Inner Panel	Outer Panel		Inner Panel	Outer Panel	Inner Panel	Outer Panel	Inner Panel	Outer Panel
S1	210	6.0	6.27	6.90	L1	6.34	7.78	6.74	8.26	5.96	7.30
					L2	5.62	7.21	5.97	7.66	5.01	6.61
					L3	6.16	7.40	6.54	7.85	5.95	7.05
S2	304	10.0	9.07	9.98	L1	9.84	11.57	10.46	12.29	9.85	13.13
					L2	9.43	11.14	10.02	11.84	10.37	11.92
					L3	10.06	11.70	10.69	12.43	10.16	11.53
S3	374	13.2	12.28	13.51	L1	11.50	13.90	12.21	14.77	11.23	13.36
					L2	11.63	13.96	12.35	14.83	11.42	13.34
					L3	12.20	14.48	12.95	15.40	11.87	13.51
S4	250	6.0	9.03	9.93	L1	8.39	7.86	8.92	8.35	8.01	7.33
					L2	8.10	7.55	8.61	8.02	7.62	6.94
					L3	7.45	7.40	7.92	7.86	6.10	6.07
S5	270	6.0	10.73	11.80	L1	9.29	9.87	9.87	10.48	9.47	10.57
					L2	8.91	9.43	9.47	10.02	8.85	9.85
					L3	8.75	9.83	9.30	10.45	8.50	10.45
S6	210	6.0	6.27	6.90	L1	6.60	7.53	7.01	8.00	6.31	7.25
S7	210	6.0	6.27	6.90	L1	5.72	6.70	6.08	7.13	4.94	5.94
S8	210	8.0	6.27	6.90	L1	8.52	9.85	9.06	10.47	8.69	9.96
S9	210	8.0	6.27	6.90	L1	6.67	8.44	7.08	8.97	5.49	6.88
S10	210	8.0	6.27	6.90	L1	6.50	7.51	6.90	7.98	6.30	7.48

Table 6.5: Maximum Span/Thickness Ratio Comparison

Slab	Clear span (in)	Loading history	Maximum span/thickness ratio		
			Eq. 6.1	Eq. 6.6	Computer
S1	210	L1	33.2	29.8	33.1
		L2	40.6	32.5	37.4
		L3	52.5	33.8	34.1
S2	304	L1	33.2	29.8	30.9
		L2	40.6	32.5	32.2
		L3	52.5	33.8	30.2
S3	374	L1	33.2	29.8	32.5
		L2	40.6	32.5	32.2
		L3	52.5	33.8	30.7
S4	250	L1	44.1	33.0	29.8
		L2	53.8	35.9	30.9
		L3	69.6	37.5	33.5
S5	270	L1	52.1	36.3	29.1
		L2	63.7	39.5	30.3
		L3	83.6	41.2	30.8
S6	210	L1	44.1	33.0	31.8
S7	210	L1	52.3	36.3	36.7
S8	210	L1	29.4	25.3	24.7
S9	210	L1	33.2	29.8	31.5
S10	210	L1	37.8	35.9	32.3

Table 6.6: Span/thickness Ratio Comparison (Interior Panels)

Casting cycle (days)	Number of reshores	Const. load	L/D ratios			ACI-CSA	Scanlon
			0.5	1.0	2.0		
3	1 + 4	1.30	19.3	23.5	29.7	33.75	30.0
7	1 + 3	1.35	23.5	28.1	34.2	33.75	30.0
14	1 + 2	1.43	26.1	30.6	36.7	33.75	30.0
28	1 + 1	1.60	27.3	31.9	37.8	33.75	30.0

Chapter 7

CONCLUSIONS AND RECOMMENDATIONS

7.1 General

Both CSA A23.3-M84 and ACI 318-83 allow two methods for controlling deflections of slabs. Slab deflections need not be checked if the slab thicknesses are larger than those specified in the code. If thinner slabs are used the deflections must be calculated explicitly, and the results compared with deflection code-specified limits established considering the consequence of excessive flexibility.

The specified minimum thicknesses are established primarily from past experience with slab systems designed using these minimum thicknesses. No extensive systematic studies to date have been reported to investigate the validity of the minimum thickness equations except the one reported by Thompson and Scanlon [7].

Chapter 9 of both Codes contains a Table (Table 9.1 in CSA A23.3-M84) for beams and one-way slabs, with depths expressed as a simple fraction of the span. For two-way construction analogous expressions are included. These are complicated by the need to consider such factors as the aspect ratio of the slab panels, the boundary conditions on all sides of the panels, and the flexural stiffness of the supporting beams. For cases where deflection is calculated explicitly, Chapter 9 of both Codes contain a Table (Table 9.2 in CSA A2 .3 M-84) of maximum permissible deflections.

7.2 Conclusions

Based on the results of the computer simulations the following conclusions are presented:

1. The tensile strength of concrete plays an important role in the service load behaviour of concrete slabs. Slab deflections increase as the modulus of rupture, concrete tensile strength, is reduced.

2. There exists a complex interaction between creep, shrinkage, and cracking in reinforced concrete slabs behaviour and the separate factors can not be considered separately and their effects simply summed.

3. Creep and shrinkage effects are of paramount importance for predicting the long-term behaviour of reinforced concrete slabs.

4. Construction loading, applied to a concrete slab at early age can alter drastically the subsequent deflections. Calculated deflections that do not take into account construction loading are likely to be significantly less than actual deflections.

5. Total deflections are many times as great as the immediate deflections. Deflection multipliers recommended by current Building Codes are generally unsuitable for predicting long-term deflections.

6. Corner panel deflections are found to be approximately twice the interior panel deflections. Present ACI 318 - CSA A23.3 Code requirement of increasing the minimum thickness by 10 percent in the panel with discontinous edge is too small and should be increased to 15 percent.

7. All slabs studied met the deflection limit of $l/360$ for live load deflections.

8. For the slabs studied the total deflection criterion (limit of $l/240$) was a more restrictive limitation than an incremental deflection of $l/480$.

9. The 28-day design of the slab does influence the percentage of reinforcement; slabs designed for large L/D ratios are less susceptible to deflection problems.

10. The current ACI Building Code and Canadian Standards provisions for minimum thickness of slabs are too simplistic and should include appropriate correction factors to reflect the age of concrete at the time of loading, the construction rate, and slab design live load/ dead load ratio.

11. Revised minimum slab thickness requirement is proposed.

7.3 Recommendations

The following recommendations for revisions to CSA A23.3 are presented for consideration.

1. Equation 9.8 included in Clause 9.5.3.2 of the current Code should be revised to the following equation.

$$h > \frac{l_n\,[\,800 + f_y \times K_1 \times K_2 \times K_3\,]}{36,000 + 10,000\beta}$$

K_1, K_2, and K_3 are given by:

$$K_1 = \frac{construction\ load}{1 + 1.2(L/D)}$$

$$K_2 = \frac{E_c(28)}{E_c(t)} = \sqrt{\frac{4.2 + 0.85t}{t}}$$

$$K_3 = 1 + 1.25\,t^{-0.118}\,(\frac{\tau^{0.6}}{10 + \tau^{0.6}} - \frac{t^{0.6}}{10 + t^{0.6}})C_u$$

At infinity ($\tau = \infty$), the term K_3 becomes:

$$K_3 = 1 + 1.25\,t^{-0.118}\,(1 - \frac{t^{0.6}}{10 + t^{0.6}})C_u$$

where,

τ = age at which the analysis is required

t = age of the concrete at loading

2. The minimum thickness required by the proposed equation (Eq. 6.6) should be increased by at least 15 percent in panels with discontinuous edges.

Bibliography

[1] Grundy, P., and Kabaila, A., *Construction Loads on Slabs with Shored Formwork in Multistory Buildings,* ACI Journal, Proceedings V. 60, No. 12, Dec. 1963, pp. 1729-1738.

[2] Agarwal, R.K., and Gardner, N.J., *Form and Shore Requirements for Multistory Flat Slab Type Building,* ACI Journal, Proceedings V. 71, No. 11, Nov. 1974, pp. 559-569.

[3] *Design of Concrete Structures for Buildings,* CSA-A23.3 M84, Canadian Standards Association, Rexdale, Dec. 1984, 281 pp.

[4] ACI Committee 318, *Building Code Requirements for Reinforced Concrete (ACI 318-83),* American Concrete Institute, Detroit, 1983, 111 pp.

[5] Gilbert, R.I., *Deflection Control of Slabs Using Allowable Span to Depth Ratios,* ACI Journal, Proceedings V. 82, No. 1, Jan. - Feb. 1985, pp. 559-569.

[6] Rangan, B.V., and McMullen, A.E., *A Rational Approach to the Control of Slab Deflections,* ACI Journal, Proceedings V. 75, No. 6, June 1978, pp. 256-262.

[7] Thompson, D.P., and Scanlon A., *Minimum Thickness Requirements for Control of Two-Way Slab Deflections,* ACI Structural Journal, Proceedings V. 85, No. 1, Jan. - Feb. 1988, pp. 12-22.

[8] Mayer, H., and Rush, H., *Building Damage Caused by Deflection of Reinforced Concrete Building Components,* Technical Translation 1412 by J.H. Rainer, National Research Council, Ottawa, Canada.

[9] Carino, N.J., Woodward, K.A., Leyendecker, E.V., and Fattal, S.G., *A Review of the Skyline Plaza Collapse,* Concrete International, American Concrete Institute, July 1983, pp. 35-42.

[10] Taylor, P.J., *Effects of Formwork Stripping Time of Deflection of Flat Slabs and Plates,* Australian Civil Engineering and Construction, Feb. 1967, pp.31-35.

[11] Marosszeky, M., *Construction Loads Imposed in Multistory Structures,* The Institution of Engineers, Civil Engineering Transactions, V. CE14, No. 1, April 1972, pp. 91-93.

[12] Gardner, N.J., *Control of Construction Loads on Multifloor Buildings,* Canadian Journal of Civil Engineering, V. 6, 1979, pp. 253-259.

[13] Chan, C.M., *Scheduled Reshoring for Flat Plate Slabs,* M. Eng. Thesis, Department of Civil Engineering, University of Ottawa, Canada, 1984.

[14] Sbarounis, J.A., *Multistory Flat Plate Buildings - Construction Loads and Immediate Deflections,* Concrete International, V. 6, No. 2, Feb. 1984, pp. 70-77.

[15] Timoshenko, S., and Woinowsky-Kreiger, S., *Theory of Plates and Shells,* McGraw-Hill Book Co., New York, 1959, 580 p.

[16] Vanderbilt, M.D., Sozen, M.A.,and Seiss, C.P., *Deflections of Multiple-Panel Reinforced Concrete Floor Slabs,* Proceedings ASCE Structural Division, V. 91, No. ST4, August 1965, pp. 77-101.

[17] Nilson, A.H., and Walters, D.B.Jr., *Deflection of Two-Way Floor Systems by the Equivalent Frame Method,* ACI Journal, Proceedings V. 72, No. 5, May 1975, pp.210-218.

[18] Kripanarayanan, K.M., and Branson, D.E., *Short-Time Deflections of Flat Plates, Flat Slabs, and Two-Way Slabs* , ACI Journal, Proceedings V. 73, No. 12, Dec. 1976, pp. 686-690.

[19] Rangan, B.V., *Prediction of Long-Term Deflections of Flat Plates and Slabs,* ACI Journal, Proceedings V. 73, No. 4, April. 1976, pp. 686-690.

[20] Scanlon, A., and Murray, D.W., *Practical Calculation of Two-Way Slab Deflections,* Concrete International: Design and Construction, V. 4, No. 11, Nov. 1982, pp. 43-50.

[21] Jofriet, J.C., and McNeice, G.M., *Finite Element Analysis of Reinforced Concrete Slabs,* Proceedings, ASCE, V. 97, ST3, March 1971, pp. 785-806.

[22] Scanlon, A., *Time-Dependent Deflections of Reinforced Concrete Slabs,* PhD Thesis, Department of Civil Engineering, University of Alberta, Edmonton, Alberta, Canada, 1971.

[23] Scanlon, A., and Murray, D.W., *Time-Dependent Reinforced Concrete Slab Deflections,* Proceedings, ASCE, V. 100, ST9, Sept. 1974, pp. 1911-1924.

[24] Hand, F.R., Pecknold, D.A., and Schnobrich, W.C., *NonLinear Layered Analysis of RC Plates and Shells,* Proceedings, ASCE, V. 99, ST7, July 1973, pp. 1491-1505.

[25] Van Greunen, J., *Time-Dependent Analysis of Reinforced and Prestressed Concrete Salbs and Panels,* PhD Dissertation, Division of Structural Engineering and Structural Mechanics, University of California, Berkeley, UC-SESM Report No. 79-3, October 1979.

[26] Fu, H.C., and Gardner, N.J., *Effect of Construction Loads on the Long-Term Behaviour of Slab Structures,* Concrete at Early Ages, SP-95, American Concrete Institute, Detroit, 1986, pp. 173-200

[27] Sbarounis, J.A., *Multistory Flat Plate Building - Effect of Construction Loads on Long-Term Deflections,* Concrete International: Design and Construction, V. 6, No. 4, April 1984, pp. 62-70.

[28] Graham, C.J., and Scanlon, A., *Long-Time Multipliers for Estimating Two-Way slab Deflections,* ACI Journal, Proceedings V. 83, No. 6, Nov. - Dec. 1986, pp. 899-908.

[29] Branson, D.E, and Christianson, M.L., *Concrete Properties Related to Design Strength and Elastic Properties - Creep and Shrinkage,* Designing for Effects of Creep, Shrinkage, and Temperature in Concrete Structures, SP-27, American Concrete Institute, Detroit, 1971, pp. 257-277

[30] Branson, D.E., *Design Procedures for Computing Deflection,* ACI Journal, Proceedings V. 65, No. 9, Sept. 1968, pp. 730-742.

[31] Taylor, P.J., *Long-Term Deflection Calculation Methods for Flat Plates,* Constructional Review, Technical Supplement, Sydney, V. 43, No. 2, May 1970, pp. 68-74.

[32] ACI Committee 435, *Deflections of Reinforced Concrete Flexural Members,* ACI Journal, Proceedings V. 63, No. 6, June 1966, pp. 637-674.

[33] ACI Committee 209, *Prediction of Creep, Shrinkage, and Temperature Effects in Concrete Structures,* SP-27, American Concrete Institute, Detroit, 1971, pp. 51-93.

[34] ACI Committee 435, *Observed Deflections of Reinforced Concrete Slab Systems, and Causes of Large Deflections,* Deflections of Concrete

Structures, SP-86, American Concrete Institute, Detroit, 1984, pp. 15-61.

[35] Blakey, F.A., *Deformations of an Experimental Lightweight Flat Plate Structure,* Civil Engineering Transactions, The Institution of Engineers, Australia, V. CE3, No. 1, March 1961, pp. 18-24.

[36] Blakey, F.A., *Australian Experiments with Flat Plates,* ACI Journal, Proceedings V. 60, No. 4, April 1963, pp. 515-525.

[37] Branson, D.E., *Deformation of Concrete Structures,* McGraw-Hill Book Company, New York, 1977, 546 pp.

[38] Jenkins, B.R., *Tests on Flat Plate Floor,* Civil Engineering Transactions, The Institution of Engineers, Australia, V. CE16, No. 2, 1974, pp. 164-167.

[39] Sbarounis, J.A., *Multistory Flat Plate Building - Measured and Computed One-Year Deflections,* Concrete International: Design and Construction, V. 6, No. 8, August 1984, pp. 31-34.

[40] Zienkiewicz, O.C., *The Finite Element Method,* Third Edition, McGraw-Hill, London, 1977.

[41] Desai, C.S., and Adel, J.F., *Introduction to The Finite Element Method,* Van Nostrand Reinhold, N.Y., 1972.

[42] Kupfer, H., Hilsdorf, H.K., and Rush, H., *Behaviour of Concrete under Biaxial Stresses,* ACI Journal, Proceedings V. 6, No. 8, August 1969, pp. 656-666.

[43] Darwin, D., and Pecknold, D., *Cyclic Biaxial Loading of Reinforced Concrete,* SRS No. 409, University of Illinois at Urbana-Champaign, Illinois, July 1974.

[44] Saenz, L.G., *Equation for the Stress-Strain Curve of Concrete,* ACI Journal, Proceedings V. 61, No. 9, Sept. 1964, pp. 1227-1935.

[45] Lin, C.S., *Nonlinear Analysis of Reinforced Concrete Slabs and Shells,* Ph.D. Dissertation, Department of Civil Engineering, University of California, Berkeley, UC-SESM Report No. 73-7, April 1973.

[46] Freyssinet, E., *The Deformation of Concrete,* Concrete Research, No. 8, 1951.

[47] Vogt, F., *On the Flow and Extensibility of Concrete,* Norges Tekniske Hoiskole, Norway, 1935.

[48] Thomas, F.G., *Creep of Concrete under Load,* International Association of Testing Materials, London, April 1937.

[49] Lyman, C.G., *Growth and Movement in Portland Cement Concrete,* Oxford University Press, London, 1934.

[50] Bresler, B. (Ed.), *Reinforced Concrete Engineering,* V. I, Wiley, New York, 1974.

[51] Roll, F., *Long-Time Creep Recovery of Highly Stressed Concrete Cylinders,* Symposium on Creep of Concrete, ACI Special Publication SP-9, March 1964.

[52] Razzaque, A., *Program for Triangular Bending Elements with Derivatives Smoothing,* Int. J. Num. Meth. Engrg., V. 6, 1973, pp. 333-343.

[53] Gardner, N.J., and Poon, S.M., *Time and Temperature Effects on Tensile, Bond, and Compressive Strength,* ACI Journal, Proceedings V. 73, No. 7, July 1976, pp. 405-409.

[54] Carino, N.J., and Lew, H.S., *Re-examination of the Relation between Splitting Tensile and Compressive Strength of Normal Weight Con-*

crete, ACI Journal, Proceedings V. 59, No. 3, May - June 1982, pp. 214-219.

[55] Gardner, N.J., Sau, P.L., and Cheung, M.S., *Strength Development and Durability of Concretes Cast and Cured at 0 C,* ACI Materials Journal, Nov. - Dec. 1988, pp. 529-536.

[56] Wang, C.Q., and Dilger, W.H., *Shrinkage Prediction for Practical Designs,* Proceedings, 1989 CSCE/CPCA Structural Concrete Conference, March 1989, Montréal, Québec.

[57] Bryant, A.H., and Vadhanavikkit, C., *Creep, Shrinkage, Size, and Age at Loading Effects,* ACI Materials Journal, Mar. - Apr. 1987, pp. 117-123.

[58] Gilbert, R.I., and Warner, R.F., *Tension Stiffening in Reinforced Concrete Slabs,* ASCE, V. 104, Dec. 1978, pp. 1885-1900.

[59] Graham, C.J., and Scanlon, A., *Deflection of Reinforced Concrete Slabs under Construction Loading,* Structural Engineering Report No. 117, University of Alberta, Edmonton, Aug. 1984, 201 pp.

[60] Gilbert, R.I., *Computer Experiments with Reinforced Concrete Slabs,* UNICIV Report No. R-195, School of Civil Engineering, University of New South Wales, Sydney, March 1980, 64 pp.

[61] Gilbert, R.I., *Time Effects in Concrete Structures,* Elsevier Science Publishers B.V., Amsterdam, 1988, 317 pp.

[62] Jokinen, E.P., and Scanlon, A., *Field Measured Two-way Salb Deflections,* Canadian Journal of Civil Engineering, V. 14, No. 6, December 1987, pp. 807-819.

[63] *The Structural Use of Concrete, (BS 8110),* British Standards Institute, London, 1985, Part 1 and 2.

[64] *Draft for Australian Standard for Concrete Structures, (AS 1480),* Standards Association of Australia, Sydney, Australia, 1985.

[65] ACI Committee 435, *Allowable Deflections,* ACI Journal, Proceedings V. 65, No. 6, June 1986, pp. 433-444.

Appendix A

McNEICE SLAB: LONG-TIME DEFLECTIONS COMPUTATION

This appendix presents the hand computation of the long-time deflections at the midpanel of McNeice slab. The notations and the formula given here are those used in the computer program.

Slab data		
l	=	36 in
h	=	1.75 in
p	=	0.85 %
K_W	=	1/8
C_u	=	2.35
ϵ_{shu}	=	800 $\times$ 10^{-6} in/in
$(f_c')_\tau$	=	6388 psi

Age at loading τ: 28 days
Age at which the analysis is required t: 365 days

Correction Factors				
Creep				
	CF_{FC}	= $\sqrt{4000/(f_c')_\tau}$	=	0.79
	CF_{SL}	= $0.81 + 0.07\,Slump$	=	1.0
	CF_{SZ}	= $1.0 - 0.0167\,(SZ - 6.0)$	=	1.0
		if SZ $\leq$ 6.0 in, $CF_{SZ} = 1.0$		
	CF_{RH}	= $1.27 - 0.0067\,RH$	=	1.0
		if RH $\leq$ 40 %, $CF_{RH} = 1.0$		
Shrinkage				
	CF_{SL}	= $0.9 + 0.04\,Slump$	=	1.0
	CF_{RH}	= $1.40 - 0.010\,RH$	=	1.0
		if RH $\leq$ 40 %, $CF_{RH} = 1.0$		
	CF_{SZ}	= $1.0 - (SZ - 6)/30$	=	1.0
		if SZ $\leq$ 6.0 in, $CF_{SZ} = 1.0$		

The following expressions are used in the calculation

1. Deflection due shrinkage

$$\Delta_{sh} = K_W \, \phi_{sh} \, (L\sqrt{2})^2 \tag{A.1}$$

2. Shrinkage curvature

$$\phi_{sh} = 0.7\frac{\epsilon_{sh}}{h} \, p^{1/3} \tag{A.2}$$

3. Shrinkage strain

$$\epsilon_{sh} = CF_{sh}[(\frac{t-7}{35+(t-7)} - \frac{\tau-7}{35+(\tau-7)})]\epsilon_{shu} \tag{A.3}$$

4. Deflection due creep

$$\Delta_{cp} = k_r C_t \Delta_i \tag{A.4}$$

5. Compression steel factor

$$k_r = 0.85 - 0.45\frac{A_S^{'}}{A_S} \tag{A.5}$$

6. Creep coefficient

$$C_t = CF_c\frac{(t-\tau)^{0.6}}{10+(t-\tau)^{0.6}}C_u \tag{A.6}$$

7. Total final deflection

$$\Delta_t = \Delta_i + \Delta_{sh} + \Delta_{cp} \tag{A.7}$$

Hand Computation Results

Shrinkage correction factor	CF_{sh}	=	1.0
Shrinkage strain	ϵ_{sh}	=	$428.8 \times (10^{-6})\ in/in$
Shrinkage curvature	ϕ_{sh}	=	$162.5 \times (10^{-6})\ in^{-1}$
Deflection due to shrinkage	Δ_{sh}	=	$0.05265\ in$
Creep correction factor	CF_c	=	0.79
Creep coefficient	C_t	=	1.423
Compression steel factor	k_r	=	0.85
Deflection due to creep	Δ_{cp}	=	$0.16942\ in$
Total final deflection	Δ_t	=	$0.36214\ in$

Table A.1: Comparison of Long-term Deflections for McNeice Slab

Case	Midpanel deflections (in)	
	Computer results	Hand calculation
Immediate	0.14007	0.14007[1*]
Immediate and shrinkage	0.22126	0.19272
Immediate and creep	0.29248	0.30949
Total long-term	0.34432	0.36214

[1*] The immediate deflection is taken equal to that given by the computer prediction

Appendix B

SUMMARY OF SLAB DEFLECTIONS

Table B.1: Slab Deflections: Test Series S1

Node number	Age (days)	Deflection (in)		
		L1	L2	L3
6	7	0.30436	-	-
	14	-	0.25870	-
	28	-	-	0.37122
	180	1.14850	0.85450	1.00430
	1000	1.75690	1.22420	1.60770
26	7	0.66044	-	-
	14	-	0.57900	-
	28	-	-	0.81282
	180	2.12190	1.75170	1.77530
	1000	3.23720	2.57990	2.77860
19	7	0.26106	-	-
	14	-	0.23261	-
	28	-	-	0.30783
	180	0.85907	0.67581	0.72643
	1000	1.31590	0.98570	1.15480
27	7	0.37914	-	-
	14	-	0.33174	-
	28	-	-	0.45854
	180	1.14930	0.95472	0.97616
	1000	1.76800	1.41040	1.53240
39	7	0.18836	-	-
	14	-	0.16666	-
	28	-	-	0.21870
	180	0.70564	0.54387	0.56423
	1000	1.10180	0.82291	0.91254

Table B.2: Slab Deflections: Test Series S2

Node number	Age (days)	Deflection (in)		
		L1	L2	L3
6	7	0.46686	-	-
	14	-	0.46464	-
	28	-	-	0.58334
	180	1.19210	0.80393	1.25010
	1000	2.04950	1.80330	2.18900
26	7	1.02290	-	-
	14	-	1.00270	-
	28	-	-	1.20750
	180	1.29980	1.45500	2.06570
	1000	3.33000	2.97430	3.43880
19	7	0.36912	-	-
	14	-	0.36134	-
	28	-	-	0.43641
	180	0.49743	0.56005	0.86612
	1000	1.37820	1.21760	1.50810
27	7	0.61175	-	-
	14	-	0.58781	-
	28	-	-	0.70520
	180	0.73944	0.82658	1.18320
	1000	1.88200	1.66690	1.97770
39	7	0.22217	-	-
	14	-	0.20838	-
	28	-	-	0.24520
	180	0.32637	0.36626	0.50814
	1000	0.96253	0.83019	0.92935

Table B.3: Slab Deflections: Test Series S3

Node number	Age (days)	Deflection (in)		
		L1	L2	L3
6	7	0.51561	-	-
	14	-	0.50923	-
	28	-	-	0.64716
	180	1.06860	1.09390	1.28170
	1000	1.74730	1.80840	2.08460
26	7	1.28910	-	-
	14	-	1.29740	-
	28	-	-	1.56760
	180	1.94870	1.98870	2.31460
	1000	3.09120	3.12780	3.49600
19	7	0.41776	-	-
	14	-	0.40614	-
	28	-	-	0.50962
	180	0.73750	0.74996	0.90056
	1000	1.19290	1.21580	1.43190
27	7	0.76736	-	-
	14	-	0.76648	-
	28	-	-	0.91345
	180	1.11210	1.14280	1.32590
	1000	1.74370	1.78110	1.96840
39	7	0.25742	-	-
	14	-	0.25116	-
	28	-	-	0.29015
	180	0.49275	0.48014	0.53520
	1000	0.85321	0.83370	0.88429

Table B.4: Slab Deflections: Test Series S4

Node number	Age (days)	Deflection (in)		
		L1	L2	L3
6	7	0.79452	-	-
	14	-	0.78431	-
	28	-	-	0.91207
	180	2.57900	2.38420	2.19060
	1000	4.04920	3.64980	2.83830
26	7	0.81382	-	-
	14	-	0.78125	-
	28	-	-	1.00160
	180	2.20130	1.98900	2.14140
	1000	3.32710	2.94540	2.77960
19	7	0.78525	-	-
	14	-	0.77580	-
	28	-	-	0.91091
	180	2.46920	2.29830	2.13900
	1000	3.84580	3.49920	2.75830
27	7	0.14979	-	-
	14	-	0.14905	-
	28	-	-	0.20002
	180	0.51139	0.46580	0.49145
	1000	0.80088	0.72490	0.65185
39	7	0.62599	-	-
	14	-	0.62374	-
	28	-	-	0.73418
	180	1.87820	1.77250	1.77550
	1000	2.88240	2.65250	2.30390

Table B.5: Slab Deflections: Test Series S5

Node number	Age (days)	Deflection (in)		
		L1	L2	L3
6	7	1.19150	-	-
	14	-	1.15190	-
	28	-	-	1.33020
	180	3.06950	2.87300	2.84650
	1000	5.50140	4.85750	4.60020
26	7	1.37640	-	-
	14	-	1.30340	-
	28	-	-	1.55940
	180	3.21860	3.02300	3.26900
	1000	6.59270	5.85750	6.52860
19	7	1.17610	-	-
	14	-	1.12990	-
	28	-	-	1.31720
	180	3.03420	2.78630	2.80530
	1000	5.45390	4.70320	4.52860
27	7	0.12020	-	-
	14	-	0.10908	-
	28	-	-	0.15234
	180	0.35616	0.31957	0.34437
	1000	0.68952	0.59172	0.60454
39	7	1.04870	-	-
	14	-	0.98896	-
	28	-	-	1.18550
	180	2.82570	2.48620	2.58930
	1000	5.19740	4.23180	4.15220

Table B.6: Slab Deflections: Test Series S6 to S10

Node number	Age (days)	Deflection (in)				
		S6	S7	S8	S9	S10
6	7	0.26083	0.17283	0.32223	0.17992	0.16660
	180	1.04560	0.72639	1.00270	0.66115	0.49282
	1000	1.64760	0.99410	1.79750	0.86134	0.79618
26	7	0.45908	0.26855	0.62808	0.38198	0.25076
	180	1.53950	1.13930	1.58500	1.35140	0.72525
	1000	2.44840	1.60300	2.77850	1.74520	1.23160
19	7	0.24155	0.16771	0.25646	0.15675	0.13003
	180	0.97035	0.70805	0.73205	0.52791	0.33264
	1000	1.54030	0.96626	1.31630	0.68480	0.55100
27	7	0.02924	0.01046	0.34974	0.21748	0.15664
	180	0.10914	0.04042	0.87045	0.71835	0.41298
	1000	0.17937	0.05350	1.54810	0.93074	0.69775
39	7	0.20666	0.15496	0.11661	0.08541	0.07871
	180	0.86861	0.65578	0.37626	0.29751	0.18293
	1000	1.39640	0.88016	0.67461	0.39325	0.28627

Appendix C

INPUT DATA FOR McNEICE SLAB EXAMPLE

```
McNEICE SLAB: TIME DEPENDENT ANALYSIS
   16    1    2    2              1    1    1
    2
   1.         10.      .001       .001
 1000.      10000.      .5         .5
   28.        365.
    1               1              1
    2                              1     9.
    3                              1    15.
    4    1                    1    1    18.
    5                              1               9.
    6                              1     9.        9.
    7                              1    15.        9.
    8    1                    1    1    18.        9.
    9                              1              15.
   10                              1     9.       15.
   11                              1    15.       15.
   12    1                    1    1    18.       15.
   13         1         1         1               18.
   14         1         1         1     9.        18.
   15         1         1         1    15.        18.
   16    1    1         1    1    1    18.        18.
    1    1         1    1
    1    1    2    2   5500.       .15                              .5
4.15E+06   5500.       550.    .0026506
                        1.75
    1  29.0E+06  60000.                  .1

    1   10
 -.875      -.7       -.525     -.35      -.175      0.        .175     .35
  .525       .7        .875
    1    2    1
    1    1   -.435     .0111     0.
    2    1   -.435     .0111    90.
    1   18

    1    1    2    5    1    1    1
    3    3    4    7    1    1    1                   1
    4    2    6    5    1    1    1
    6    4    8    7    1    1    1                   1
    7    5    6    9    1    1    1
    9    7    8   11    1    1    1                   1
   10    6   10    9    1    1    1
   12    8   12   11    1    1    1                   1
   13    9   10   13    1    1    1
   15   11   12   15    1    1    1                   1
   16   10   14   13    1    1    1
   18   12   16   15    1    1    1                   1
    3   20    1                                  3   20
   16                        -500.
4845525.   6388.      590.
    3   20    1                                  3   20
   16
```